



January 2017

Effect Of Nanomaterials On Binder And Mix Performance

Bishal Karki

Follow this and additional works at: <https://commons.und.edu/theses>

Recommended Citation

Karki, Bishal, "Effect Of Nanomaterials On Binder And Mix Performance" (2017). *Theses and Dissertations*. 2120.
<https://commons.und.edu/theses/2120>

This Thesis is brought to you for free and open access by the Theses, Dissertations, and Senior Projects at UND Scholarly Commons. It has been accepted for inclusion in Theses and Dissertations by an authorized administrator of UND Scholarly Commons. For more information, please contact zeinebyousif@library.und.edu.

EFFECT OF NANOMATERIALS ON BINDER AND MIX PERFORMANCE

by

Bishal Karki

Bachelor of Science, Tribhuvan University, 2012

A Thesis

Submitted to the Graduate Faculty

of the

University of North Dakota

in partial fulfillment of the requirements

for the degree of

Master of Science


Grand Forks, North Dakota

May


2017

Copyright 2017 Bishal Karki

This thesis, submitted by Bishal Karki in partial fulfillment of the requirements for the Degree of Master of Science in Civil Engineering from the University of North Dakota, has been read by the Faculty Advisory Committee under whom the work has been done and is hereby approved.

 5/2/2017

Dr. Daba Gedafa, P.E., Chairperson

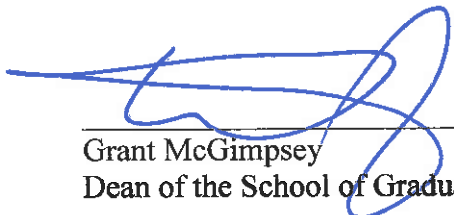
 5/2/2017

Dr. Nabil Suleiman

 5/2/2017

Mr. Bruce Dockter, P.E.

This thesis is being submitted by the appointed advisory committee as having met all of the requirements of the School of Graduate Studies at the University of North Dakota and is hereby approved.



Grant McGimpsey
Dean of the School of Graduate Studies

May 3, 2017

Date

PERMISSION

Title Effect of Nanomaterials on Binder and Mix Performance
Department Civil Engineering
Degree Master of Science

In presenting this thesis in partial fulfillment of the requirements for a graduate degree from the University of North Dakota, I agree that the library of this University shall make it freely available for inspection. I further agree that permission for extensive copying for scholarly purposes may be granted by the professor who supervised my thesis work or, in his absence, by the Chairperson of the department or the dean of the School of Graduate Studies. It is understood that any copying or publication or other use of this thesis or part thereof for financial gain shall not be allowed without my written permission. It is also understood that due recognition shall be given to me and to the University of North Dakota in any scholarly use which may be made of any material in my thesis.

Bishal Karki

Date: 05/05/2017

TABLE OF CONTENTS

LIST OF FIGURES	vi
LIST OF TABLES	xi
ACKNOWLEDGEMENTS	xiii
ABSTRACT	xiv
CHAPTER	
I. INTRODUCTION	1
II. LITERATURE REVIEW	4
III. RESEARCH METHODOLOGY	21
IV. RESULTS AND DISCUSSION	40
V. CONCLUSIONS	91
VI. LIMITATIONS AND FUTURE WORK	93
REFERENCES	95
APPENDIX	101

LIST OF FIGURES

1.	Rheological parameters of asphalt (Interactive, 2016).....	9
2.	Dynamic Shear Rheometer (DSR).....	13
3.	PG58-28 Mix Aggregates.....	25
4.	PG64-28 Mix Aggregates.....	25
5.	PG58-28 0.45-Power Gradation Chart.....	26
6.	PG64-28 0.45-Power Gradation Chart.....	27
7.	SCB Specimen Dimensions (Al-Qadi, et al., 2015).....	35
8.	SCB Loading Setup.....	35
9.	DCT Specimen Dimensions (from ASTM D7313 – 13).....	37
10.	DCT Specimen Setup.....	37
11.	Unaged PG 58-28 modified with NA.....	41
12.	RTFO-aged PG 58-28 modified with NA.....	42
13.	Unaged PG 58-28 modified with NC.....	43
14.	RTFO-aged PG 58-28 modified with NC.....	43

15.	Unaged PG 64-28 modified with NA.....	44
16.	RTFO-aged PG 64-28 modified with NA.....	45
17.	Unaged PG64-28 modified with NC.....	46
18.	RTFO-aged PG64-28 modified with NC.....	46
19.	Unaged PG 58-28 modified with NA at 64°C.....	47
20.	RTFO-aged PG 58-28 modified with NA at 64°C.....	48
21.	Unaged PG 58-28 modified with NC at 64°C.....	48
22.	RTFO-aged PG 58-28 modified with NC at 64°C.....	49
23.	Unaged PG 64-28 modified with NA at 70°C.....	50
24.	RTFO-aged PG 64-28 modified with NA at 70°C.....	50
25.	Unaged PG 64-28 modified with NC at 70°C.....	51
26.	RTFO-aged PG 64-28 modified with NC at 70°C.....	51
27.	Unaged PG 58-28 modified with 7% NC at 70°C.....	52
28.	RTFO-aged PG 58-28 modified with 7% NC at 70°C.....	52
29.	Unaged PG 64-28 modified with 7% NC at 76°C.....	53
30.	RTFO-aged PG 64-28 modified with 7% NC at 76°C.....	53
31.	PAV-aged PG58-28 modified with NA.....	54

32.	PAV-aged PG58-28 modified with NC.....	55
33.	PAV-aged PG64-28 modified with NA.....	56
34.	PAV-aged PG64-28 modified with NC.....	56
35.	PAV-aged PG58-28 modified with NA at 64°C.....	57
36.	PAV-aged PG58-28 modified with NC at 64°C.....	58
37.	PAV-aged PG64-28 modified with NA at 70°C.....	58
38.	PAV-aged PG64-28 modified with NC at 70°C.....	59
39.	PAV-aged PG58-28 modified with NC at 70°C.....	60
40.	PAV-aged PG64-28 modified with NC at 76°C.....	60
41.	Sample graph of PG+10°C and PG+20°C frequency sweeps.....	61
42.	Sample graph of $G'(\omega)$ Master curve at a reference temperature of PG+10°C.....	62
43.	Relaxation modulus master curve to determine $m_r(60s)$ and $G(60s)$	63
44.	Relaxation Modulus for Unaged PG58-28.....	65
45.	Slope for Unaged PG58-28.....	65
46.	Relaxation Modulus for RTFO-aged PG58-28.....	66
47.	Slope for RTFO-aged PG58-28.....	66
48.	Relaxation Modulus for PAV-aged PG58-28.....	67

49.	Slope for PAV-aged PG58-28.....	68
50.	Relaxation Modulus for Unaged PG64-28.....	69
51.	Slope for Unaged PG64-28.....	69
52.	Relaxation Modulus for RTFO-aged PG64-28.....	70
53.	Slope for RTFO-aged PG64-28.....	70
54.	Relaxation Modulus for PAV-aged PG64-28.....	71
55.	Slope for PAV-aged PG64-28.....	71
56.	NC Modified PG58-28 Average Rut Depth.....	74
57.	NA Modified PG58-28 Average Rut Depth.....	74
58.	NC Modified PG64-28 Average Rut Depth.....	75
59.	NA Modified PG64-28 Average Rut Depth.....	75
60.	Example of APA Specimen Prior to Test.....	76
61.	Example of APA Specimen Post-Testing.....	76
62.	NA Modified PG58-28 Rut Depth vs Air Voids.....	79
63.	NC Modified PG58-28 Rut Depth vs Air Voids.....	79
64.	NA Modified PG64-28 Rut Depth vs Air Voids.....	80
65.	NC Modified PG64-28 Rut Depth vs Air Voids.....	80

66.	Average Fracture Energies for PG58-28.....	83
67.	Average Fracture Energies for PG64-28.....	84
68.	Example energy graph of SCB specimen, load vs displacement.....	84
69.	Example of SCB Specimen Prior to Test.....	84
70.	Example of SCB Specimen Post-Testing.....	85
71.	Average Fracture Energies for PG58-28.....	88
72.	Average Fracture Energies for PG64-28.....	89
73.	Example DCT Graph of Load vs CMOD.....	89
74.	Example of DCT Specimen Prior to Test.....	90
75.	Example of DCT Specimen Post-Testing.....	90
76.	PG58-28 HMA Mix Design Summary.....	101
77.	PG64-28 HMA Mix Design Summary.....	102

LIST OF TABLES

1.	Performance Graded Asphalt Binder Specifications (AASHTO M 320).....	17
2.	PG58-28 Aggregate Gradation.....	24
3.	PG64-28 Aggregate Gradation.....	24
4.	PG58-28 and PG64-28 Mix Proportions.....	28
5.	PG58-28 HMA Specimen Volumetric Properties.....	29
6.	PG64-28 HMA Specimen Volumetric Properties.....	30
7.	Magnitude of Relaxation Modulus [G (60s)] Summary.....	64
8.	Slope (mr) of Relaxation Modulus [G (60s)] Summary.....	64
9.	APA Results Summary.....	73
10.	Effect of NM Content on Reduction in Rut Depth.....	77
11.	APA Independent T-Test Summary.....	78
12.	PG58-28 SCB Fatigue Fracture Energies.....	81
13.	PG58-28 SCB Samples Air Voids.....	82
14.	PG64-28 SCB Samples Fatigue Fracture Energies.....	82

15.	PG64-28 SCB Samples Air Voids.....	82
16.	SCB Results Summary.....	82
17.	SCB Independent T-Test Summary.....	85
18.	PG58-28 DCT Samples Fracture Energies.....	87
19.	PG58-28 DCT Samples Air Voids.....	87
20.	PG64-28 DCT Samples Fracture Energies.....	87
21.	PG64-28 DCT Samples Air Voids.....	87
22.	DCT Results Summary.....	87

ACKNOWLEDGEMENTS

I would like to thank ND EPSCoR along with the Graduate School for funding this research.

I would like to thank Flint Hills Resources, Danny Schmidt and Knife River Materials for providing the materials required for this research.

I am grateful to my committee members Dr. Nabil Suleiman and Mr. Bruce Dockter, P.E. for their advice and support. I would also like to recognize the faculty and the staff of the Civil Engineering Department for their encouragement during my master's study at UND.

Last but not the least, my sincere appreciation and thankfulness to my advisor and committee chairperson, Dr. Daba Gedafa, P.E. for giving me an opportunity to study under his guidance as well as for his continuous assistance, patience and support throughout my time at UND.

I would also like to acknowledge my friends and family for their support in my research.

ABSTRACT

Nanotechnology has been increasingly used in asphalt modification for its remarkable effect in improving the binder and mix performance. Rheological properties of binder play major roles in rutting, fatigue cracking and low-temperature cracking resistance of Hot Mix Asphalt (HMA) pavement. This study was conducted to investigate the effect of Nanomaterials (NMs) on the rheological characteristics of asphalt binders and rutting and cracking resistance of HMA mixes. NMs, Nanoclay and Nanoalumina, were mixed separately into Performance Grade (PG) 58-28 and 64-28 asphalt binder at control (0% NM), 1, 5 and 7% by binder weight. Rolling Thin Film Oven (RTFO) and Pressure Aging Vessel (PAV) were used for simulating short-term and long-term aging, respectively. Asphalt specimens (un-aged, RTFO-aged, and PAV-aged from each binder) were tested using Dynamic Shear Rheometer (DSR) to determine and compare the viscoelastic behavior of the asphalt binders at different temperatures. Hot Mix Asphalt Specimens (150mm diameter and 75mm high) were compacted with $7\pm 1\%$ air voids using Superpave Gyrotory Compactor. Asphalt Pavement Analyzer (APA), Semi-Circular Bending (SCB) and Disc-Shaped Compact Tension (DCT) were used to determine the rutting, fatigue cracking and low-temperature cracking resistance of the mixes, respectively. Cracking of mixes was measured in terms of fracture energy. The results showed that Nanomaterials increased the rutting resistance of the mixes by increasing the stiffness of the mixes, but the mixes could be more susceptible to cracking.

CHAPTER I

Introduction

Hot Mix Asphalt Pavement

Hot Mix Asphalt (HMA) is a combination of rock, sand, or gravel mixed with asphalt cement at high temperatures. HMA pavement is one of the most extensively used flexible pavement design method. It is called a flexible pavement because the entire pavement structure flexes, or deflects, under loading. Other flexible pavement design methods include warm-mix asphalt, dense and open-graded mixes etc. Asphalt cement and aggregates are heated, combined and mixed at high temperatures in a HMA plant. The resulting HMA is then transported by trucks and compacted in place by heavy rollers to form a flexible pavement (El-Korchi and Mallick, 2009).

Asphalt Pavement Failures

A typical asphalt pavement structure consists of a surface course, an underlying aggregate base course and sub-base courses. Asphalt pavement layers are organized in the order of descending load bearing capacity with the highest load bearing capacity material on the top (Interactive, 2016).

Failure of any pavement layer can occur with accumulated distresses over time. Low temperature cracking is a result of shrinkage of HMA surface and stiffening of asphalt binders at low-temperatures. Fatigue cracking occurs because of repeated traffic

loading and inadequate structural design at a wide range of temperatures. Rutting is the most common and unique failure mode for flexible pavements. It is caused by poor compaction of the HMA layers and exposure to higher ambient temperatures. In this research, additives are used to investigate the change in binder rheology and HMA mix performance.

Asphalt Binder Modification

The trend of modifying asphalt binder has been increasing for its remarkable effect in improving the binder and mix performance. Some of the different types of asphalt modifiers are resins, rubbers (Styrene-butadiene, Styrene-butadiene-styrene, and Natural etc.), plastic (polyethylene, polyvinyl chloride etc.), fibers, metal complexes and chemical agents (Yusoff et al., 2014). In this research, Nanoclay (Cloisite 20) and Nanoalumina (α -Al₂O₃) are used to modify the properties of asphalt binders.

Problem Statement

Rutting failure is the most common failure mode of a HMA pavement. Rutting resistance of the pavement can be improved by improving the binder's rheological properties. For resisting rutting, asphalt binder must be stiff enough to resist deformation and elastic enough to return to original shape after load deformation (Interactive, 2016). However, modifying high temperature rheology of an asphalt binder may affect the low and intermediate temperature rheology. The effect of Nanomaterials on low, intermediate and high temperature rheological properties were investigated.

Objectives of Study

Objectives of this research are:

1. To examine the effects of modified asphalt binder on the rheological properties of un-aged and aged binders.
2. To investigate the effect of Nanomaterials on mix performance in terms of rutting, fatigue cracking, and low-temperature cracking resistance

Organization of the Thesis

Chapter I gives a brief introduction to HMA pavements, type of pavement failures and short background information on asphalt modification. Chapter II magnifies the information in Chapter I and details the major pavement failure types. It also provides information on the rheological properties of the binder and the HMA mix design. Chapter III describes the overall procedure of selecting materials, mix designs, mixing and compaction processes, testing methods and data analysis. Chapter IV includes the results and discussions from the research. Chapter V states the conclusions and finally, limitations and future work are included in Chapter VI.

Chapter II

LITERATURE REVIEW

Asphalt Cement

Asphalt cement is a sticky, dark brown to black, highly viscous, liquid or semi-solid form of petroleum obtained naturally or produced as a byproduct of the petroleum distillation. The Federal Highway Administration (FHWA) defines asphalt as a dark brown to black cement-like material containing bitumen as the predominant constituent. It is also called asphalt binder because it is used as the binder in aggregate materials to form asphalt concrete. It is one of the world's oldest engineering materials, having been used since the beginning of civilization. In ancient days, natural asphalt was used which was formed as a black residue when crude petroleum oils drove their way up through cracks to the earth's surface. Almost all the petroleum asphalt produced nowadays is used for pavement constructions. The hot mixture of asphalt cement, sand and crushed rock, Hot Mix Asphalt (HMA), is placed on the roadbed and compacted by the heavy rollers to form asphalt pavement (El-Korchi and Mallick, 2009).

Asphalt Pavement Distresses

Pavement distresses can be evaluated by two approaches. The first approach is a functional evaluation of the effect of distress on the pavement's ability to serve traffic today. The second approach is a mechanistic evaluation of distress with an eye to finding

out the current physical condition of the pavement, the causes for this condition and its effect on the future performance of the pavement (Sargious, 1975). Pavement is said to be structurally failed when one or more components of the pavement system collapses resulting in incapability of the pavement in withstanding the load carrying capacity. The second, functional failure, may or may not be accompanied by structural failure but is such that the pavement will not serve for the intended purpose without causing discomfort to passengers or without causing high stresses in the vehicle which passes over due to its roughness (Yoder, 1959). Some of the distresses related to asphalt pavement include rutting, fatigue cracking, bleeding, pumping, low-temperature cracking etc. It is generally agreed that fatigue cracking, rutting and low-temperature cracking are the three principal types of distress to be considered for flexible pavement design (Huang, 2004).

Rutting

One of the primary reasons for premature deterioration of asphalt pavement is rutting. It is considered as the main concern of transportation agencies in the field of pavement. Rutting refers to the permanent deformation of the asphalt surface because of repeated loads at high ambient temperature. It is usually caused by consolidation or lateral movement of pavement materials due to traffic loads in any of the pavement layers or in subgrade. Generally, three factors lead to create rutting in the asphalt pavement including permanent deformation accumulation in the surface of asphalt layer, permanent deformation of the subgrade, and erosion or wear of asphalt at the wheels place due to the passing of vehicles (Shafabakhsh et al., 2014). The permanent deformation of asphalt pavements has an important impact on the performance of the pavements during their

lifetimes (Brovelli et al., 2015). Significant rutting can lead to major structural failures and a potential for hydroplaning (Huang, 2004). As the ruts get deeper, steering becomes tougher, resulting in higher safety concerns.

Rutting generally depends on the three constituents of hot-mix asphalt; asphalt cement, aggregate and air void. Excessive use of the asphalt cement makes the pavement soft, increasing its susceptibility to rutting. Modifying the properties of asphalt cement is one of the popular method for improving the performance of asphalt cement and mixture. Bitumen used in the asphalt mixtures has an important effect on the mechanical behavior of asphalt mixtures and in the presence of additives can produce asphalt mixtures with different behavior (Brovelli et al. 2015). Binder grades with varying performance temperature used for various geographic areas is also an important factor. Aggregate shape and texture play a key role in determining the interlock level of aggregate and thus influence the lateral movement of pavement (Xiao et al., 2002). Air void content of the pavement is also a significant factor in rutting. Higher air content, can also be because of poor compaction, makes asphalt pavement vulnerable to rutting. In a study done by Khan et al. (2013), the air voids were reduced by 0.4% when compared with normal surface and rutted section.

Fatigue Cracking

Fatigue cracking is one of the major distresses in HMA pavements, which is a process of accumulation of flaws in an asphalt pavement that grow under repeated loading and become densely concentrated until visible cracks develop. The mechanism of fatigue cracking can be divided into two parts: (1) the occurrence of tensile stress/tensile

strain in the asphalt mix layer, and (2) the repetitive occurrence of such tensile stress/strain under traffic repetitions (El-Korchi and Mallick, 2009). It is also called alligator cracking because the cracking pattern looks like the pattern of an alligator's skin. Fatigue cracking is made worse by inadequate pavement drainage. Roberts et al., (1996) found that the HMA layers experience high strains when the underlying layers are weakened by excess moisture and consequently fail prematurely in fatigue (as cited by Dore and Zubeck, 2009). It has been shown that low asphalt content and high air void mixes are prone to show fatigue cracking, but high asphalt content mixes tend to rut first (Nejad et al., 2010). In thin pavements, cracking starts at the bottom of the asphalt layers and propagates upward whereas in thick pavements, bending of pavement layers is reduced eventually to the level that crack initiation is restrained and no bottom up fatigue cracking occurs (Dore and Zubeck, 2009).

Different kinds of asphalt mixes with different properties show different fatigue behaviors. Semi-Circular Bending (SCB) fracture test is used for determining the fatigue cracking performance. The SCB test configuration has been favored by many researchers due to the ease of sample preparation including cores removed from the field and the quick and simple testing procedure (Elseifi et al., 2012). Fatigue cracking is a result of repetition of loading at daily temperature so average room temperature of 25°C is used for the testing (Arabani and Ferdowski, 2009, Huang et al., 2013, and Wu et al., 2005).

Low-Temperature Cracking

Low-temperature cracking, also called thermal cracking, is widely recognized in the northern regions of United States and Canada. Low-temperature cracking occurs in

two ways: (1) when the thermal stresses due to a drop-in temperature exceed the fracture strength of the material, and (2), when due to repeated thermal cycles, the strain in the asphalt layers causes thermal fatigue cracking (El-Korchi and Mallick, 2009). It is the result of continuous contraction and expansion of the surface bituminous layer under extreme temperature changes (Canestrari et al., 2015). A decrease in temperature results in the contraction of the pavement surface layer building thermally induced tensile stress, which when exceeds the tensile strength of the pavement forms a crack at the surface of the pavement. Continuous weather cycles and traffic loading causes the propagation of crack downward through the asphalt layers. Binder, as the main adhesive of material for asphalt mixture becomes brittle at low-temperatures and causes asphalt mixture brittleness at this temperature (Saeidi and Aghayan, 2016). This character of binder plays a vital role in developing cracks in asphalt pavement.

Both Disc-Shaped Compact Tension Test (DCT) and SCB test are used for testing the low-temperature fracture resistance of asphalt mix samples in lab. In a study done by Saeidi and Aghayan, (2016), the SCB results showed that the fracture behavior of asphalt at low-temperature was linear. In another study done by Hill et al., (2013), bio-modified asphalt mix with varying proportions of Reclaimed Asphalt Pavement (RAP) was studied to examine the low-temperature properties. It can be observed from the results that the mixtures displayed higher fracture energy than HMA mixtures at each RAP level, and fracture energy decreased with the increase in RAP percentage. The result is obvious because as RAP percentage is increased, the stiffness of the mix is increased thereby, making the mix susceptible to brittleness.

Binder Rheology

Rheology is the study of deformation and flow of the matter. Study of deformation and flow of asphalt is important in predicting pavement performance. HMA pavements with higher degree of flow and deformation have low rutting resistance, while those that are too stiff may be susceptible to cracking. Deformation of the pavement is occurred because of accumulation of repeated traffic loads. With each traffic loading, work is done to deform the pavement surface. A portion of this work is recovered by the elastic rebound of the HMA surface, while the rest is dissipated in the form of permanent deformation, heat, cracking, and crack propagation. To minimize pavement deformation, the amount of work dissipated per loading should be minimized (Interactive, 2016).

For rutting resistance, asphalt binder needs to be stiff but elastic enough to regain its original shape after deformation. The complex shear modulus elastic portion in Equation 1, $\left[\frac{G^*}{\sin \delta} \right]$ should be increased to decrease the work dissipation. Also, Figure 1 shows that the lower value of phase angle yields greater elastic portion.

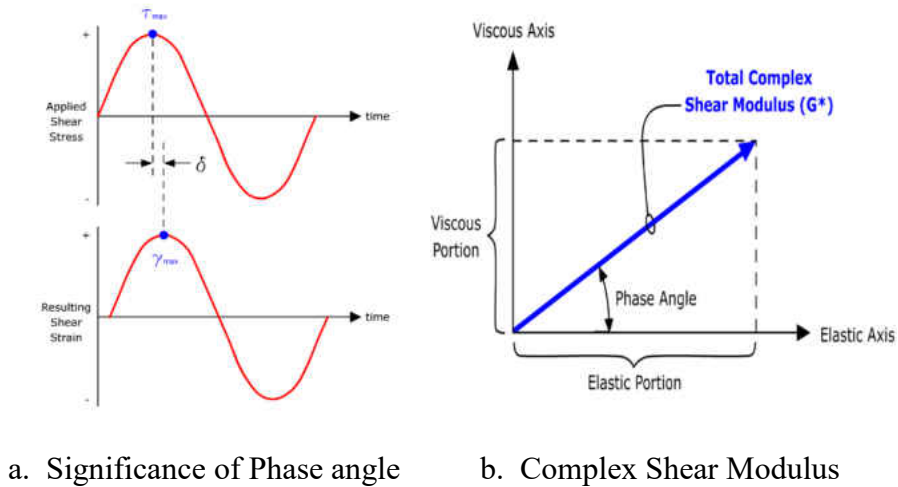


Figure 1. Rheological parameters of asphalt (Interactive, 2016)

Equation 1 is used to determine the work dissipated per loading cycle at a constant stress (Interactive, 2016).

Equation 1: Work dissipated per loading cycle at constant stress (Interactive, 2016)

$$W_c = \pi \sigma_0^2 \left[\frac{1}{G^* / \sin \delta} \right]$$

Where,

W_c = Work dissipated per load cycle

σ_0 = Stress applied during load cycle

G^* = Complex modulus

δ = Phase angle

Intuitively, it can be asserted from Equation 1 that maximized value of complex shear modulus with minimum value of phase angle results in lesser work dissipation on the pavement. To resist fatigue cracking, asphalt binder needs to be elastic but not too stiff. Since fatigue cracking is more prevalent in thin pavements, the parameter of most concern for fatigue resistance can be considered a strain-controlled one (Interactive, 2016). Equation 2 is used to express the work dissipated per loading cycle at a constant strain. From Equation 2 and Figure 1, it can be understood that minimum value of complex shear modulus viscous portion, $[(G^*)(\sin \delta)]$, minimizes the fatigue cracking.

Equation 2: Work dissipated per loading cycle at constant strain (Interactive, 2016)

$$W_c = \pi \varepsilon_0^2 [(G^*)(\sin \delta)]$$

where, all other parameters are same to Equation 1 except,

$$\varepsilon_0 = \text{Strain during load cycle}$$

In terms of low-temperature thermal cracking, the performance of an asphalt binder is predicted using a bending beam rheometer (BBR) by determining the stiffness of the binder at low-temperatures and the m-value, which is the slope of the curve of the creep stiffness versus time. Sui et al. (2011) developed a correlation to determine BBR m-value and creep stiffness, $S(t)$, from 4-mm DSR data. In this method, the slope and magnitude of the shear stress relaxation modulus $G(t)$ master curve at 2 hours and at the true low PG grading temperature are correlated with the corresponding $S(t)$ and m-values at 60 seconds and 10°C above the true low PG grading temperature from BBR measurements (Farrar et al., 2015).

Machine compliance needs to be considered too. In rheology, machine compliance is the deformation due to the compliance of instruments at low testing temperature. Equation 3 is for calculating shear modulus and Equation 4 gives the total strain in a test. At high temperatures, the deformation due to machine compliance or the second term in right hand side of Equation 4 is negligible because the test temperatures are well above the glass transition of sample, the modulus is low and is much lesser than that of instrument or measuring tool. While at low-temperatures below the glass transition temperature of sample, the modulus becomes close to that of the instrument making the machine compliance in Equation 4 significant. As a result, measured modulus is lower than its true value (Farrar et al., 2015). Sui et al., 2010 were the first to apply an

instrument compliance correction to asphalt binder low-temperature measuring equipments (-5°C to -40°C) using parallel plate geometry.

Equation 3: Shear modulus

$$G = \frac{\tau}{\gamma}$$

Equation 4: Strain measurement

$$\gamma_{\text{measured}} = \gamma_{\text{sample}} + \gamma_{\text{instrument}} = \frac{\tau}{G_{\text{sample}}} + \frac{\tau}{G_{\text{instrument}}}$$

At high temperature, the deformation due to the machine compliance i.e. the second term to the right in equation 4 is negligible but is significant in the case below glass transition temperature which increases the error factor highly (Farrar et. al, 2015).

Dynamic Shear Rheometer

Asphalt binder shows viscoelastic behavior depending on the temperature and the rate of loading. At low-temperatures and short periods of loading the response is elastic, whereas at high temperature and long periods of loading the response is viscous (El-Korchi and Mallick, 2009). The dynamic shear rheometer (DSR) is used to characterize the viscous and elastic behavior of asphalt binders over a range of temperatures, as well as evaluate its rutting and cracking potential. These behaviors can be predicted by measuring the complex shear modulus (G^*), storage modulus (G'), phase angle (δ), etc. The basic working principle of DSR applies a torque on a thin asphalt binder sample between a fixed and an oscillating plate creating a shearing action on the sample. The complex shear modulus (G^*) is the ratio of the shear stress to shear strain and phase angle

(δ) is the time lag between applied shear stress and the resulting shear strain. Figure 2 shows the type of DSR used in this research along with a test specimen.



a. Measuring Instrument

b. 25mm dia. test specimen

Figure 2. Dynamic Shear Rheometer (DSR)

DSR has been used only for high and intermediate temperatures. However, previously for low-temperature rheology test, DSR was only used to test a torsion bar for measuring dynamic shear modulus as well as phase angle under sinusoidal dynamic load (Sui et al., 2010). Bending beam rheometer (BBR) was the most commonly used reliable method among other methods like Direct Tension Test (DTT) and Torsion bar (TB). All three test methods require large amounts of materials and relatively high temperatures for testing specimens (Sui et al., 2010). Sui et al., (2010) came up with a new technique to measure low-temperature rheological properties which uses 4 mm diameter parallel plates

on a DSR with machine compliance corrections requiring only 25 mg of material. Earlier, BBR was preferred to DSR because it didn't suffer from instrument compliance error. But, the study performed by Sui et al., (2010) also confirms that, after the machine compliance corrections, the use of small parallel plates on a DSR is a reliable technique to duplicate BBR data on DSR. Also, a strong linear relationship between BBR and DSR data was observed. The low-temperature test by Farrar et al., (2015), incorporated time temperature superposition (TTS) and master curve development of storage modulus, $G'(\omega)$, from the two frequency sweeps, interconversion from $G'(\omega)$ to relaxation modulus, $G'(t)$ and estimation of slope (m_r) and relaxation modulus $G(t)$ at 60 seconds from the $G(t)$ master curve at the PG+10°C.

Superpave Mix design

There are many mix design methods used throughout the world such as Marshall mix design method, Hubbard-field mix design method, Hveem mix design method, Asphalt tri-axial method of mix design etc. But, even the most popular ones i.e. Marshall and Hveem mix design methods, had major drawbacks in performance. A Superior Performing Asphalt Pavement (Superpave) is the HMA mix design that resulted from the \$150 million, 5-year-long Strategic Highway Research Program (SHRP) in the United States between 1987 and 1993 (El-Korchi and Mallick, 2009). The Superpave mix design system is a comprehensive method of designing paving mixes tailored to the unique performance requirements dictated by the traffic, environment (climate), and structural section at a particular pavement site (Cominsky et al., 1994).

The major elements of Superpave are: Aggregate properties, Superpave mix design and Performance graded asphalt binder. The unique feature of the Superpave system is that it is a performance-based specification; that directly govern the response of pavement to load. Aggregates, having the highest composition in the HMA mix, play an integral role in overcoming pavement deformation. Two types of aggregate properties are listed in the Superpave system: consensus properties and source properties. Consensus properties are the properties that SHRP researchers considered were critical for high pavement performance like coarse aggregate angularity, fine aggregate angularity, flat and elongated particles and clay content. Source aggregate properties are toughness, soundness and deleterious materials (Interactive, 2016).

Another important element in Superpave system is the performance grade (PG) asphalt binder which is an improved technique in testing and selecting asphalt binders. For example, PG 58-28 means that the binder must meet the high-temperature physical requirements at least up to a temperature of 58°C, and low-temperature physical requirements must be met at least down to -28°C. Minimum and seven-day consecutive maximum air temperatures are collected throughout a year and converted to pavement temperature since pavement temperature is required for selecting asphalt binders. Dynamic Shear Rheometer (DSR) is used for testing the binder at both the high and low-temperatures.

After the selection of asphalt binder and aggregate, volumetric proportions of each needs to be considered. Air voids, voids in the mineral aggregate (VMA), voids filled with asphalt (VFA) and effective asphalt content provides some indication of the mixture's probable pavement service performance.

Superpave Performance Graded Binder

Superpave performance grading (PG) system is basically designed to improve the performance of HMA pavements by selecting asphalt binder with physical properties that will be able to resist tenderness of binder during laying and construction, permanent deformation and cracking after it starts aging (Kandhal and Foo, 1997). Asphalt binder contains volatile compounds and due to its exposure to oxygen, oxidative aging happens gradually resulting in reduction of adhesion and ductility of binder (Saeidi and Aghayan, 2016). This phenomenon of asphalt binder affects asphalt mixture performance making binder brittle and the asphalt mix susceptible to cracking. SHRP researcher found that Rolling thin film oven (RTFO) test could be used to simulate the aging asphalt binder in HMA undergoes during the construction and placement processes and Pressure Aging Vessel (PAV) test on RTFO-residues could be used to simulate the aging induced in pavement by heat and pressure during its service life of 7 to 10-year period (Tian et al., 2004). Superpave PG system requires constant physical properties at the specified temperature for all PG grades. For example: a PG58-28 asphalt binder meets the tenderness requirement, i.e. $\left[\frac{G^*}{\sin \delta} \right] \geq 1.0$ kPa for unconditioned asphalt binder and permanent deformation requirement, i.e. $\left[\frac{G^*}{\sin \delta} \right] \geq 2.2$ kPa for RTFO-aged binder at a high temperature of 58°C. Also, meet the requirement of low-temperature (creep stiffness value 'S' < 300 MPa and slope value '|m|' > 0.3) down to a temperature of -28°C and perform efficiently to fatigue cracking, i.e. $[(G^*)(\sin \delta)] < 5$ MPa) between service temperatures of 58°C and -28°C at an intermediate temperature of 25°C (Kandhal & Foo, 1997). Table 1 details the specifications listed on AASHTO M320 for all PG binders.

Table 1: Performance Graded Asphalt Binder Specifications (AASHTO M 320)

Material	Value	Specification	Distress Concern
Un-aged Binder	$G^*/\sin(\delta)$	≥ 1.0 kPa (0.145 psi)	Rutting
RTFO residue	$G^*/\sin(\delta)$	≥ 2.2 kPa (0.319 psi)	Rutting
PAV-residue	$G^*.\sin(\delta)$	≤ 5000 kPa (725 psi)	Fatigue Cracking
Creep Stiffness, following AASHTO 313, 'S', maximum of 300 MPa and Slope 'm' value, minimum of 0.300 @ 60 seconds			Low-Temperature Cracking

Nanomaterials as Modifiers

Nanotechnology has been discovered and used to address the problems in the design and construction of functional structures with at least one characteristic dimension measured in nanometers i.e. one billionth of a meter (Yang and Tighe, 2013).

Nanomaterials possess an extraordinary potential for improving the performance of asphalt binders and mixtures with extensive and unique properties such as the quantum effects, structural features, high surface work, spatial confinement and large fraction of surface atoms (Yao et al., 2012). There are various types of Nanomaterials used in asphalt modifications with each presenting different variable change and improvement of asphalt mixtures. Examples of the Nanomaterials that can be used in asphalt applications include Nano-tubes, Nano-fibers, polymerized powders, Nano-sized plastic powders, Nano-hydrated lime, Nano-silica and Nano-clay (Yusoff et al., 2014).

In the study performed by (You et al., 2011), two types of Montmorillonite Nanoclay were added to the original binder PG64-28. Two types of Nanoclay were added to the original binder at 2% and 4% by weight of the asphalt binder. Nanoclay was successful in improving the complex shear modulus (G^*) and viscosity, thereby reducing the strain failure rate of asphalt. But, the direct tension test results showed that the addition of Nanoclay lowered the failure strain %, making it susceptible to low-

temperature cracking. While confirming the results produced by You et al., (2011), Yao, et al., (2012) also found that although the addition of non-modified Nanoclay (NMN) increased the complex shear modulus and viscosity, but only polymer-modified Nanoclay (PMN) could significantly enhance the performance of the high temperature properties of unaged, RTFO-aged and PAV-aged asphalt binder without affecting the low-temperature and stress relaxation performance. In addition, PMN in asphalt binder increases the ability to recover, due to the polymer modification in Nanoclay, whereas NMN decreases it because of increased stiffness. Polymer-modified asphalts have increasingly been used over the last decade to minimize low-temperature cracking and high-temperature rutting while improving the fatigue cracking resistance of asphalt concrete (Chollar and Memon, 1997 and Sibal et al., 2000).

Another study performed by Jahromi and Khodaii, (2009) examined two types of Nanoclay; nanofil-15 and cloisite-15A. The rheology test done by DSR concluded that the addition of Nanoclay had significant effect on the rheological behavior and increased ageing resistances. The susceptibility to temperature of modified binder was lower than unmodified binder due to the increased shear modulus (G^*).

In another study by Golestani et al., (2015), two modifiers; Nanoclay and linear styrene-butadiene-styrene (SBS) polymer were added to binder at different proportions. Adding nanoclay, polymer and their combination increases the shear modulus and decreases phase angle. In addition, the wheel tracking test results showed that the resistance to permanent deformation of the asphalt mix was significantly improved.

Van de Ven et al., (2009) studied Nanoclay cloisite's effect on asphalt binder and mix, which was compacted using the Marshall Compaction method. Results for the binder had improved rutting resistance significantly. Cloisite Nanoclay also strongly improved the rutting resistance of the mixtures but didn't improve the fatigue resistance performance at low-temperatures.

In asphalt application, there has been increasing research on Nanoclay, Nanosilica and carbon nanotubes but very little on Nanoalumina. Ali et al., (2016) performed a study on investigating the physical as well as rheological properties of asphalt binders modified by Nano-aluminum oxide (Al_2O_3). Asphalt cement 60/70 penetration grade was modified at 3%, 5% and 7% of nano alumina by binder weight. The study showed that with addition of the Al_2O_3 nano particles, stiffness of the binder increased significantly reducing the high temperature susceptibility. The complex shear modulus increased with the addition of the Al_2O_3 particles, however, 5% of Al_2O_3 in binder was found to have greater high temperature rutting and intermediate temperature fatigue resistance than 7% content.

Shafabakhsh et al., (2015) performed a study on creep behavior of stone mastic asphalt (SMA) using Nano- Al_2O_3 Cylindrical asphalt mix samples with a diameter of 101 mm and height of 70 mm was made using 0.3%, 0.6%, 0.9% and 1.2% of Al_2O_3 by weight of binder. The results obtained from the dynamic creep tests on the samples show that asphalt binder with 0.9% of nano Al_2O_3 was found to be the optimal content for SMA mixture. Also, samples with 0.9% of Al_2O_3 had the best resistance against permanent deformation of SMA samples.

In another study performed by Lotfi-Eghlim and Karimi (2016), fatigue life of HMA mixes was investigated using Nano- Al_2O_3 modified asphalt binder. 60/70 penetration binder was modified at 0%, 2%, 5% and 8% of Al_2O_3 by binder weight using a thermodynamic driving force. The fatigue life of the samples was determined by the Indirect Tensile Method using a Universal Testing Machine (UTM) apparatus. Tests were performed at 5°C, 25°C and 40°C at two different pressure level of 250 kPa and 400 kPa. The results showed that the fatigue life of the mixtures increased significantly with the increase in the Al_2O_3 content but decreased with the increase in temperature and pressure.

Chapter III

RESEARCH METHODOLOGY

Material Selection

Two most commonly used asphalt binders in the Midwest, PG 58-28 and PG 64-28 were chosen for this study. Aggregates used in this research were pre-selected by the mix design company, Knife River Materials and their mix technician, Danny Schmidt. The mix design and aggregate source was unique to each binder. Both mix designs were from construction projects in North Dakota. PG 58-28 mix design was used in construction of North Dakota State Highway 32 whereas PG 64-28 mix design was used in Interstate 29. The aggregate blend in the mix designs used Reclaimed Asphalt Pavement (RAP). For PG 58-28 mixes, aggregate blend from the mix design for Grand Forks County by Strata Company was used whereas, for PG 64-28 mixes, aggregate blend in the original design by Knife River materials was modified to replace the RAP content by the aggregate. The unmodified asphalt binders were donated by Flint Hills Resources. Fordville donated the PG 58-28 aggregates and Deerwood Township along with Kittson Co MN donated the PG 64-28 aggregates.

In this research, Nanoclay (Cloisite 20) and Nanoalumina ($\alpha\text{-Al}_2\text{O}_3$) were chosen as modifiers to investigate their effect on the binder as well as mixes. Nanoclay, based on a natural mineral, is used widely to improve the properties of thermoplastics. Nanoclay or

the layered silicates have thickness in an order of 1 nm resulting in a very high aspect ratio. This results in a very large active surface area which makes the interaction intense between Nanoclay and binder. Studies have shown the improved engineering properties of nanoclay and nano alumina modified asphalt binders. However, using Nanoclay at large scales with little information on how they improve the rutting and fatigue parameters is not reliable. It is assumed that addition of Nanoclay and Nanoalumina strengthens the asphalt binder and mixes against permanent deformation without worsening its fatigue cracking and low-temperature cracking properties.

Modifying Asphalt Cement

The Nanomaterials were modified into the asphalt binder at a temperature of 145°C. The Nanomaterial quantities were added to PG 58-28 and PG 64-28 asphalt binders at 1%, 5% and 7% by binder weight. The binders were mixed using a high shear mixer for about 45 minutes to acquire the better dispersion of nanoparticles in the binder.

Rolling Thin Film Oven (RTFO) Test

RTFO test procedure is used to simulate short-term aging of asphalt binder i.e. aging during construction and placement. This test was completed following the standard test method in ASTM D2872-04. This test method indicates the change in rheological properties of asphalt binder because of conventional hot-mixing. The oven was pre-heated for 16 hours prior to the testing, to stabilize the testing temperature at $325 \pm 1^\circ\text{F}$. Binder was heated in a container with loose cover not to exceed 302°F . Thirty-five (35 ± 0.5) g of the binder was poured into each cylindrical glass containers, turned to a horizontal position and immediately rotated for at least one complete rotation for pre-

coating the cylindrical surface. Then, the containers filled with asphalt are cooled in a rack for 1 to 3 hours. After cooling, the testing was done in the oven, at temperature of $325 \pm 1^\circ\text{F}$ and airflow of $4000 \pm 200 \text{ mL/min}$, for 85 minutes.

Pressure Aging Vessel (PAV) Test

PAV test simulates the in-service aging of asphalt binder over a 7 to 10-year period exposing to heat and pressure. This test followed the standard test method ASTM D6521 – 08. The manufacturer’s manual was used to pre-heat the vessel to a conditioning temperature of 100°C and to apply an air pressure of $2.1 \pm 0.1 \text{ MPa}$. Temperature was selected with accordance to the specification under ASTM D6373 – 99. RTFO-aged asphalt binder samples are mixed together and poured into stainless steel pans, each with $50 \pm 0.5 \text{ g}$. The test was then run for $20 \text{ hours} \pm 10 \text{ min}$, with the temperature and pressure stabilized.

The samples from RTFO and PAV tests were tested in DSR to determine the rheological properties.

HMA Mix Design

The HMA mix design was based off AASHTO MP2 standard specification for Superpave volumetric mix design. Tables 2 and 3 show the individual aggregate and the blend gradation of PG58-28 and PG64-28, respectively. The aggregates used in the PG58-28 and PG64-28 mix designs are also shown in Figures 3 and 4, respectively.

Table 2. PG58-28 Aggregate Gradation

	Natural Fines	Rock	Washed Dust	Dirty Dust	Blend Gradation	Lower Control Pt	Upper Control Pt
Sieve Size	% Passing	% Passing	% Passing	% Passing	% Passing	% Passing	% Passing
5/8" (16mm)	100.0	100.0	100.0	100.0	100.0	100.0	100.0
1/2" (12.5mm)	100.0	92.0	100.0	100.0	97.5	90.0	100.0
3/8" (9.5mm)	99.0	62.0	100.0	100.0	88.0	-	-
#4 (4.75mm)	83.0	3.0	86.0	93.0	60.6	-	-
#8 (2.36mm)	65.0	1.0	45.0	68.0	40.2	28.0	58.0
#16 (1.18mm)	45.0	1.0	26.0	47.0	26.6	-	-
#30 (0.6mm)	23.0	1.0	14.0	33.0	15.4	-	-
#50 (0.3mm)	8.0	1.0	7.0	23.0	8.0	-	-
#100 (0.15mm)	6.0	1.0	4.0	16.0	5.5	-	-
#200 (0.075mm)	4.5	1.0	2.1	12.7	4.1	2.0	7.0
Pan	0.0	0.0	0.0	0.0	0.0	0.0	0.0

Table 3. PG 64-28 Aggregate Gradation

	Natural Fines	Rock	Washed Dust	Dirty Dust	Blend Gradation	Lower Control Pt	Upper Control Pt
Sieve Size	% Passing	% Passing	% Passing	% Passing	% Passing	% Passing	% Passing
5/8" (16mm)	100	100	100	100	100	100.0	100.0
1/2" (12.5mm)	100	100	100	100	100	90.0	100.0
3/8" (9.5mm)	100	63	100	100	91.12	-	-
#4 (4.75mm)	90	2	81	81	63.12	-	-
#8 (2.36mm)	76	1	42	53	38.77	28.0	58.0
#16 (1.18mm)	62	1	25	37	26.44	-	-
#30 (0.6mm)	47	1	13	28	17.65	-	-

Table 3. cont.

	Natural Fines	Rock	Washed Dust	Dirty Dust	Blend Gradation	Lower Control Pt	Upper Control Pt
Sieve Size	% Passing	% Passing	% Passing	% Passing	% Passing	% Passing	% Passing
#50 (0.3mm)	26	1	9	21	11.88	-	-
#100 (0.15mm)	5	1	4	13	5.47	-	-
#200 (0.075mm)	2.9	1	2.2	10.8	3.974	2.0	7.0
Pan	0	0	0	0	0	0.0	0.0



Figure 3. PG58-28 Mix Aggregates



Figure 4. PG64-28 Mix Aggregates

In Superpave mix design, 0.45-power gradation chart is used to define a permissible gradation. The important feature of the 0.45-power chart is that it can show the maximum density line for the maximum aggregate size. Figures 5 and 6 show the 0.45-power chart of the sieve analysis. For making the mix, asphalt binder is mixed with these aggregate blends. For PG58-28, binder content of 5.8% by aggregate weight was added and for PG64-28, binder content of 5.4% by aggregate weight was added to make the mix.

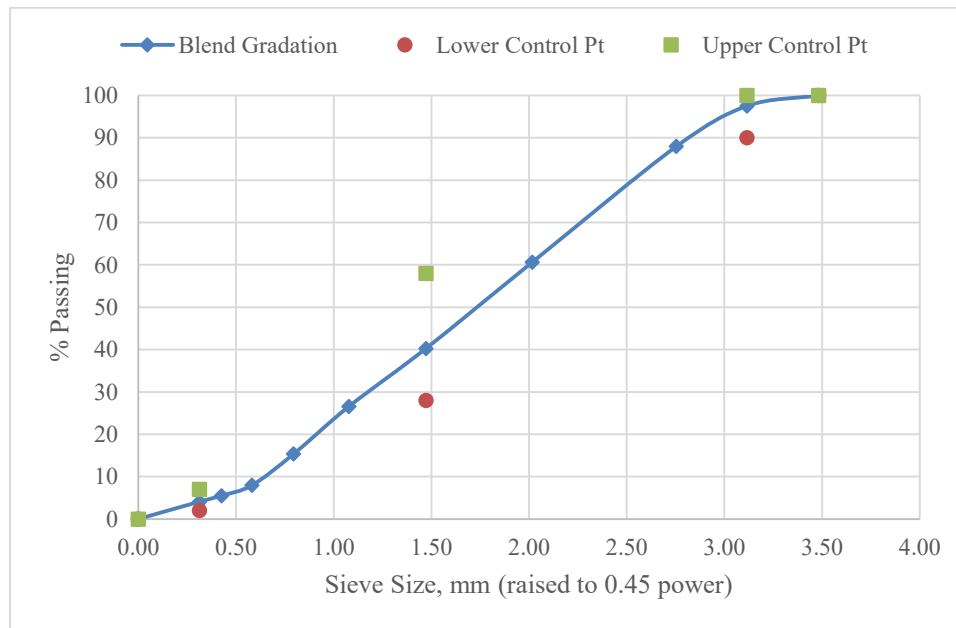


Figure 5. PG58-28 0.45-power gradation chart

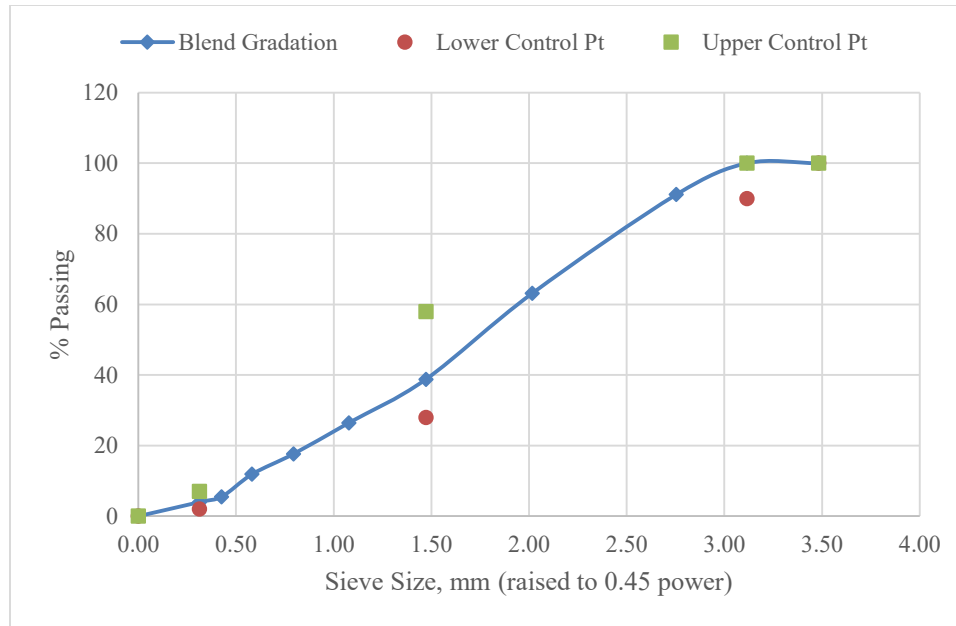


Figure 6. PG64-28 0.45-power gradation chart

HMA Compaction

The HMA mix was compacted using Superpave Gyratory Compactor (SGC) following the AASHTO standard test designated T 312. Proportions of the aggregates and binder were weighed for both PG58-28 and PG64-28 as shown in Table 4. For each specimen, a batch mix of 3100 grams was prepared. The aggregates, binder and all the components required for compaction i.e. compaction mold, pan etc. were placed and heated in an oven to a certain temperature. The aggregates were heated to 325°F for at least 3 hours, asphalt binder along with the components of compaction were heated to 290°F. The mixing and compaction temperature for this research was $285 \pm 5^\circ\text{F}$ and $275 \pm 5^\circ\text{F}$, respectively. The components of compaction were heated to the mixing temperature.

Table 4. PG58-28 and PG64-28 Mix Proportions

Material	PG58-28		PG64-28	
	Percent	Mass (g)	Percent	Mass (g)
Natural Fines	26	759.3	12	351.9
Crushed Rock	31	905.3	24	703.8
Washed Dust	16	467.2	41	1202.4
Dirty Dust	27	788.5	23	674.5
Binder	5.8	179.8	5.4	167.4

A mechanical mixer was used to mix the asphalt binder and aggregate quickly and thoroughly for uniform binder distribution. After mixing, the HMA mix was put into oven for 2 hours \pm 10 min to simulate short-term aging. After aging, samples were compacted using SGC at the compaction temperature. Compaction mold, pre-heated to mixing temperature, was taken out of the oven and a paper disc was placed inside the bottom before pouring the mix in. The heated and conditioned HMA mix was then poured into the mold in one lift to avoid segregation. Another paper disc was placed on the top. Paper discs were used to prevent the mix from sticking to the mold. The mold was then loaded into the SGC. The machine lowers the compaction ram, with the pressure pre-adjusted to 600 ± 60 kPa, and an angle of $1.25 \pm 0.02^\circ$ was applied. Compaction continued until a desired height of the specimen was achieved. The specimen was then extruded from the SGC mold and paper disc were immediately removed. The specimen height, %G_{mm}, and the number of gyrations were recorded.

The height of the HMA specimen used in this research was 75mm and the target air void percentage was $7 \pm 1\%$. A trial and error method was carried out prior to the tests

to achieve the desired weight of the mixture. It was found that a mixture weight of about 2950 grams was enough to achieve the desired properties. There were two different mix designs used in this research, one for PG58-28 and the other for PG64-28. The comparison between these two mix designs may not be appropriate because of the difference in mix design. The HMA was then tested for determining volumetric properties. The bulk specific gravity (G_{mb}), from AASHTO T166-13, was computed after recording the dry weight, saturated surface dry (SSD) weight and water submerged weight. With maximum specific gravity (G_{mm}) from the mix design and computed G_{mb} , the air voids were calculated. Tables 5 and 6 show the summary of the specimens with the weights and calculated air voids. Figures 72 and 73 in Appendix show the mix design and volumetrics provided for this research.

Table 5. PG58-28 Specimen volumetric properties

Binder Type	Mass (g)	Height (mm)	Gmm (%)	Dry (g)	Wet (g)	SSD (g)	Gmb	Air Voids (%)
0%	2920	74.97	91.1	2920.4	1626.2	2927.0	2.25	7.50
	2940	74.97	91.7	2939.9	1640.1	2945.7	2.25	7.22
	2940	74.97	91.7	2928.0	1628.7	2934.8	2.24	7.63
	2940	74.97	91.7	2927.8	1625.1	2935.3	2.23	7.93
	2940	74.97	91.7	2947.0	1646.4	2954.3	2.25	7.16
	2940	74.97	91.7	2937.5	1634.2	2945.1	2.24	7.67
1% NA	2940	74.91	91.8	2939.9	1635.0	2946.1	2.24	7.61
	2960	74.97	92.3	2956.1	1657.6	2963.4	2.26	6.72
	2950	74.91	92.1	2947.0	1644.9	2953.1	2.25	7.18
	2940	74.97	92.0	2939.9	1639.2	2944.6	2.25	7.21
5% NA	2950	74.91	92.1	2946.6	1646.4	2953.8	2.25	7.14
	2950	74.86	92.2	2941.3	1637.0	2946.4	2.25	7.45
	2950	74.97	92.0	2953.3	1652.6	2960.3	2.26	6.95
	2940	74.97	91.4	2941.1	1633.6	2947.5	2.24	7.77
7% NA	2940	74.91	91.8	2938.2	1639.4	2945.0	2.25	7.27
	2940	74.97	91.7	2944.3	1640.7	2950.4	2.25	7.37

Table 5. cont.

Binder Type	Mass (g)	Height (mm)	Gmm (%)	Dry (g)	Wet (g)	SSD (g)	Gmb	Air Voids (%)
7% NA	2940	74.97	91.7	2937.4	1633.3	2943.4	2.24	7.62
	2940	74.97	91.7	2941.3	1644.0	2947.6	2.26	7.03
	2940	74.97	91.7	2942.2	1648.4	2949.3	2.26	6.81
	2940	74.91	91.8	2938.3	1639.7	2946.4	2.25	7.35
1% NC	2915	74.97	91.1	2916.7	1625.3	2924.7	2.24	7.51
	2930	74.97	91.4	2927.6	1627.8	2933.8	2.24	7.64
	2930	74.97	91.4	2928.7	1639.8	2937.3	2.26	7.00
	2925	74.97	91.2	2916.4	1621.4	2925.8	2.24	7.88
5% NC	2921	74.91	91.2	2909.3	1612.7	2916.8	2.23	8.00
	2930	74.97	91.4	2920.2	1626.5	2932.8	2.24	7.89
	2945	74.97	91.9	2945.6	1647.9	2953.0	2.26	7.00
	2940	74.97	91.7	2932.3	1631.6	2939.3	2.24	7.61
7% NC	2935	74.97	92.6	2935.4	1638.8	2942.2	2.25	7.21
	2935	74.97	91.6	2927.5	1628.1	2934.2	2.24	7.65
	2935	74.97	91.6	2925.5	1623.7	2931.6	2.24	7.84
	2930	74.97	91.4	2934.0	1637.4	2944.1	2.25	7.48
	2930	74.97	91.4	2932.1	1629.5	2939.0	2.24	7.74
	2935	74.97	91.4	2941.7	1633.2	2947.1	2.24	7.75

Table 6. PG64-28 Specimen volumetric properties

Binder Type	Mass (g)	Height (mm)	Gmm (%)	Dry (g)	Wet (g)	SSD (g)	Gmb	Air Voids (%)
0%	2990	74.81	91.1	2982.2	1701.2	2990.8	2.31	7.09
	2990	74.86	91.1	2988.1	1703.7	2998.8	2.31	7.30
	2990	74.97	90.9	2985.3	1703.3	2993.0	2.32	7.00
	2990	74.86	91.1	2982.1	1704.4	2990.6	2.32	6.85
	2990	74.97	90.9	2977.4	1700.3	2989.7	2.31	7.23
	2990	74.86	91.1	2986.2	1697.4	2993.9	2.30	7.46
	2990	74.91	91.0	2982.9	1701.0	2993.5	2.31	7.28
	2990	74.86	91.1	2991.2	1705.3	3003.4	2.30	7.42
	2990	74.97	90.9	2977.6	1697.4	2988.2	2.31	7.32
	2990	74.76	91.2	2998.2	1715.2	3004.8	2.33	6.59
1% NA	2990	74.91	91.0	2982.3	1710.1	2995.9	2.32	6.81
	2985	74.91	90.9	2986.4	1703.5	2995.9	2.31	7.16

Table 6. cont.

Binder Type	Mass (g)	Height (mm)	Gmm (%)	Dry (g)	Wet (g)	SSD (g)	Gmb	Air Voids (%)
1% NA	2985	74.91	90.9	2983.1	1696.6	2997.4	2.29	7.86
	2985	74.81	91.0	2980.4	1696.5	2994.9	2.30	7.78
5% NA	2990	74.91	91.0	2988.7	1707.0	3005.1	2.30	7.50
	3000	74.91	91.3	2998.6	1712.2	3007.9	2.31	7.02
	3000	74.91	91.3	2991.9	1711.1	3003.8	2.31	7.01
	3000	74.97	91.3	2995.9	1715.1	3004.4	2.32	6.64
7% NA	2990	74.91	91.0	2988.4	1711.0	3004.5	2.31	7.18
	2990	74.91	91.0	2980.7	1701.7	2995.6	2.30	7.45
	2990	74.86	91.1	2989.2	1711.1	3001.2	2.32	6.91
	2990	74.97	90.9	2997.0	1709.6	3008.4	2.31	7.29
	2990	74.91	91.0	2988.0	1700.1	3001.8	2.30	7.78
	2990	74.97	90.9	2986.9	1706.4	2997.1	2.31	7.02
1% NC	3000	74.97	91.3	3000.2	1712.9	3011.5	2.31	7.18
	3000	74.86	91.4	2991.1	1699.4	3000.5	2.30	7.64
	3000	74.97	91.3	2991.5	1714.0	3004.6	2.32	6.87
	3000	74.97	91.3	2999.9	1716.7	3009.6	2.32	6.78
5% NC	2990	74.97	90.9	2992.2	1714.4	3005.7	2.32	6.90
	2990	74.87	91.1	2983.1	1701.9	2996.7	2.30	7.44
	2990	74.91	91.0	2994.2	1709.8	3005.6	2.31	7.16
	2990	74.81	91.4	2995.6	1714.5	3006.9	2.32	6.88
7% NC	2990	74.76	91.2	2990.9	1716.8	3004.6	2.32	6.69
	2985	74.91	90.9	2987.6	1710.6	3001.2	2.31	7.00
	2985	74.97	90.8	2983.8	1705.3	2994.9	2.31	7.04
	2985	74.97	90.8	2992.2	1712.1	3005.4	2.31	7.05
	2985	74.81	91.0	2992.3	1722.6	3008.8	2.33	6.53
	2985	74.81	93.4	2986.7	1713.7	3001.1	2.32	6.79

Data Collection

Binder Tests

DSR was used for determining the rheological parameters of binder i.e. complex shear modulus (G^*), phase angle (δ), storage modulus (G') etc. 25mm diameter plates

were used for high temperature rutting and fatigue cracking, while 4mm diameter plates for low-temperature cracking. The results were collected from the rheometer software.

Dynamic Shear Rheometer (DSR) Test

The DSR test followed AASHTO T 315 standard method for determining the rutting and fatigue cracking resistance of the binder. The test specimens were made using a 25mm diameter silicon mold, loaded in between the parallel plates and trimmed to remove the excess binder. The binder was subjected to a shear stress at the higher temperature of the PG grade, e.g. 58°C for PG 58-28. This test determined the complex shear modulus (G^*) and phase angle (δ). Amplitude sweep at a 10% strain rate and a frequency of 10rad/sec was assigned for this test. For every test, the values of G^* and δ are recorded by the Rheocompass software at 25 points. The rutting parameter $\left[\frac{G^*}{\sin \delta} \right]$ along with fatigue parameter $[(G^*)(\sin \delta)]$ are also calculated by the software itself. However, the DSR doesn't have a standard test for determining the low-temperature rheological properties. The proposed standard in Technical White paper by Farrar et al., (2015) at Western Research Institute prepared for Federal Highway Administration was used to determine the low-temperature performance properties of binder. This test determines the complex shear modulus (G^*), phase angle (δ) and Storage modulus (G'). The binder specimens are loaded into the DSR using the same procedure as above but, using 4mm diameter silicon mold in this case. The specimen was then conditioned at 30°C for 20 minutes. The temperature was again cooled to target testing temperature and stabilized for additional 20 minutes. A strain sweep test was then performed on the specimen to determine the linear viscoelastic region. The Rheometer then performed two

frequency sweeps, one at 10°C and another at 20°C above the low-temperature of PG grade, from 0.1 to 50 radians per second using the linear strain determined from the strain sweep.

Mix Tests

Asphalt Pavement Analyzer (APA) was used for understanding the rutting behavior of the HMA mixes at higher PG temperature. Semi-Circular Bending (SCB) test was done to determine the fatigue cracking potential while Disk-shaped Compact Tension (DCT) test was done to determine the low temperature cracking potential of the HMA mixes. Both, SCB and DCT, were carried out using the same equipment with inter-changeable fixtures.

Asphalt Pavement Analyzer (APA)

The APA machine was used to evaluate the performance of HMA mixes against rutting. AASHTO T340 standard method was used for determining the rutting susceptibility of Hot Mix Asphalt (HMA). The specimens compacted in the SGC were loaded into the cylindrical polyethylene molds at 150 ± 2 mm diameter and height of 75 ± 2 mm. The molds were placed in the machine under pre-pressurized hose reading of 100 ± 5 psi (695 ± 35 kPa) and load cylinder pressure under each wheel to achieve a load of 100 ± 5 lbf (445 ± 22 N). Since pavement rutting occurs at higher temperatures, test was carried out at the highest pavement temperature which is the upper temperature in the PG grade. Prior to beginning the test, the specimens were conditioned and stabilized at the testing temperature for 5 to 6 hours. During the test, loaded wheel moves back and forth on the top of pressurized linear hoses, hoses being placed over the molds. The APA test

was set to stop after it reached the preset counter of 8000 cycles. The APA computer records rut depth at each cycle and plots a graph of rut depth vs cycle. The failure criterion was 12.5mm rut depth.

Semi-Circular Bending (SCB) Test

SCB test method was used to determine the fatigue cracking potential of HMA mix by means of the semi-circular bend (SCB) geometry. Although there are many types of test procedures used by several researchers, there is not a single standard test until date. The test procedures vary mainly on dimensions of specimen and the testing temperature. In this research, Illinois Flexibility Index Test (I-FIT) was used because Illinois represented the closest pavement and environment condition to the North Dakota. The SCB specimen is a half disc with a notch that is 15mm long as shown in Figure 7. Samples used in I-FIT are required to be a height of 50mm; however, due to limited availability of materials 25 ± 2 mm samples were used. The specimen was positioned in the fixture with the notch side centered to two rollers as show in Figure 8. The specimen was conditioned for 2 hours and tested at 25°C (77°F). The test was done using Load Line Displacement (LLD) control at a rate of 50 m/min after reaching a contact load of 0.1 kN and stopped when the load dropped below 0.1 kN. The test equipment provided a software which was used as a post processing software to get the fracture energy in J/m^2 (in.-lbf/in²).

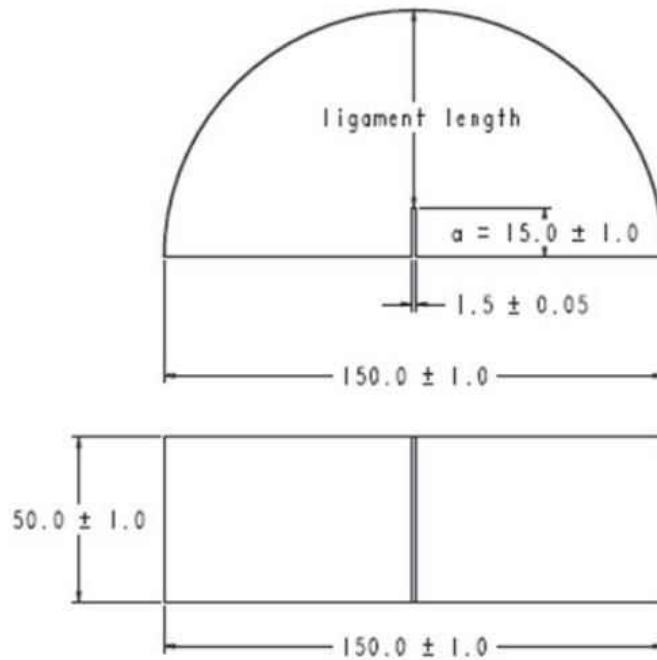


Figure 7. SCB Specimen Dimensions (Al-Qadi, et al., 2015)

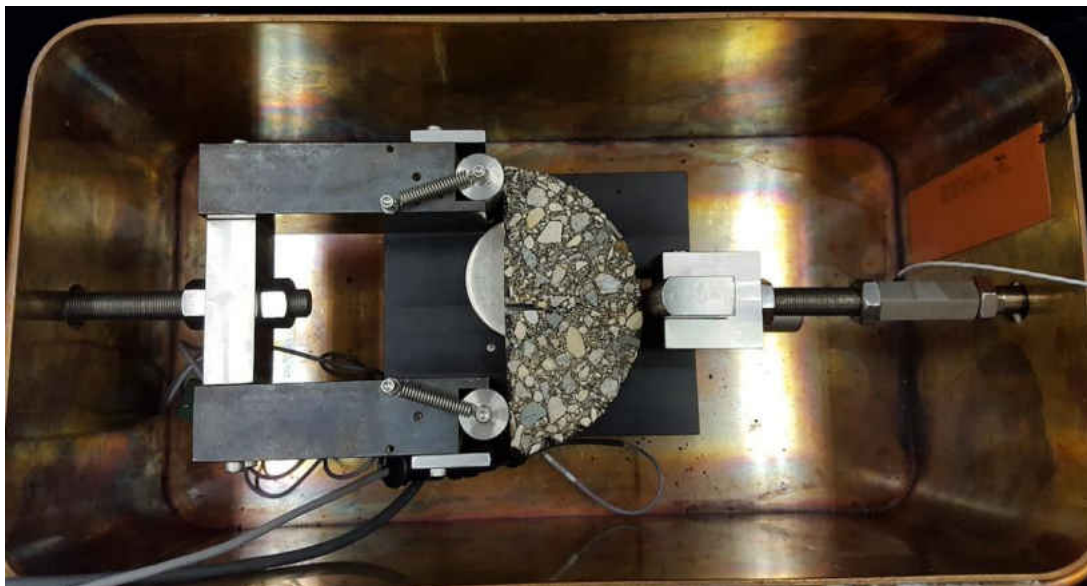


Figure 8. SCB Loading Setup

Disk-Shaped Compact Tension (DCT) Test

DCT test followed standard method under ASTM D7313 – 13. This test is generally used for determining the cracking susceptibility of the HMA mixes at lower

temperatures. HMA specimen's dimensions required in this test is shown in Figure 9. In this research, compacted HMA specimens from SGC were fabricated to achieve the desired dimensions. A circular saw was used to cut the 75mm specimens from SGC down to 50 ± 3 mm. A lateral flat face of length 50mm was cut along the thickness of the specimen. Then, a notch, as shown in Figure 9, perpendicular to the face was cut from along the diameter of the specimen within ± 1.5 mm (± 0.06 in.). The 25mm diameter loading holes were then drilled on either side of the notch with the center of the hole at 25mm distance from the notch. After creating the specimen, the specimen was loaded into the machine for temperature conditioning as shown in Figure 10. The testing temperature was specified at 10°C higher than the low-temperature performance grade of the binder. After conditioning the specimens from 8 to 16 hours, the test was ready to start. Figure 10 shows the setup of the specimen prior to testing. A small seating load of 0.1 kN was applied to pre-load the specimen before beginning the test. The test is complete when the loading reaches to a peak load with a constant mouth opening displacement (CMOD) rate of 0.017 mm/s and reduces back to the pre-load. The software that comes with the DCT equipment plots a graph of CMOD versus load. The area under the graph divided by the product of specimen thickness and the initial ligament length gives the fracture energy of the specimen. Fracture energy is commonly accepted parameter to interpret the low-temperature properties of HMA. The DCT program does the calculation and provides the fracture energy in J/m^2 (in.-lbf/in²).

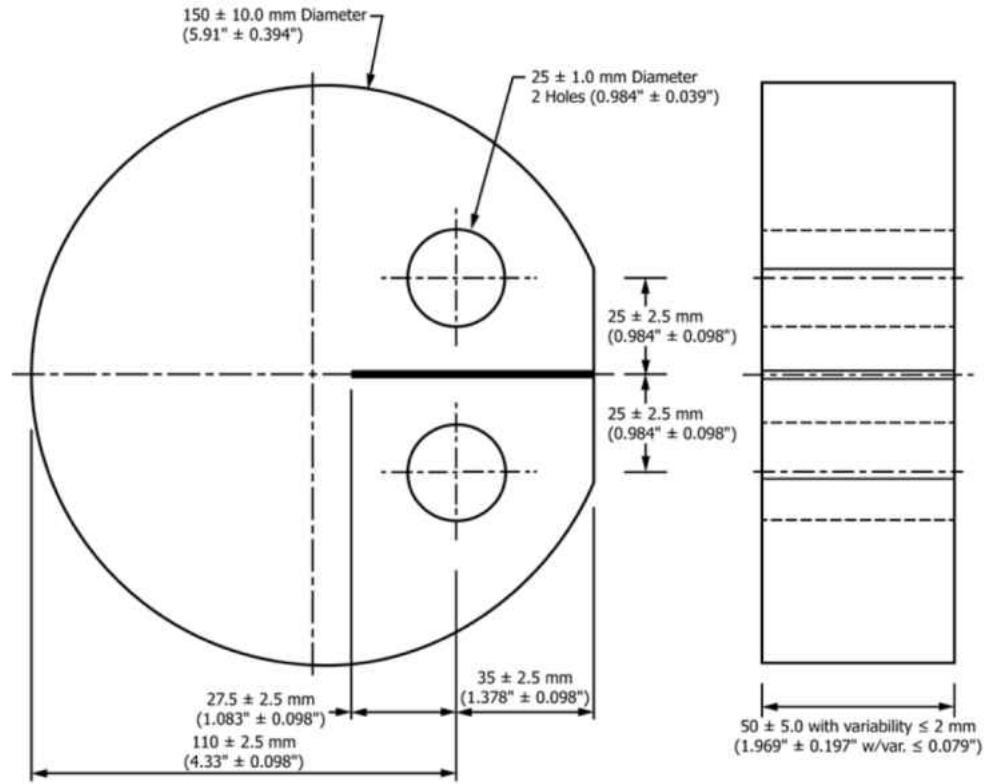


Figure 9. DCT Specimen Dimensions (from ASTM D7313 – 13)

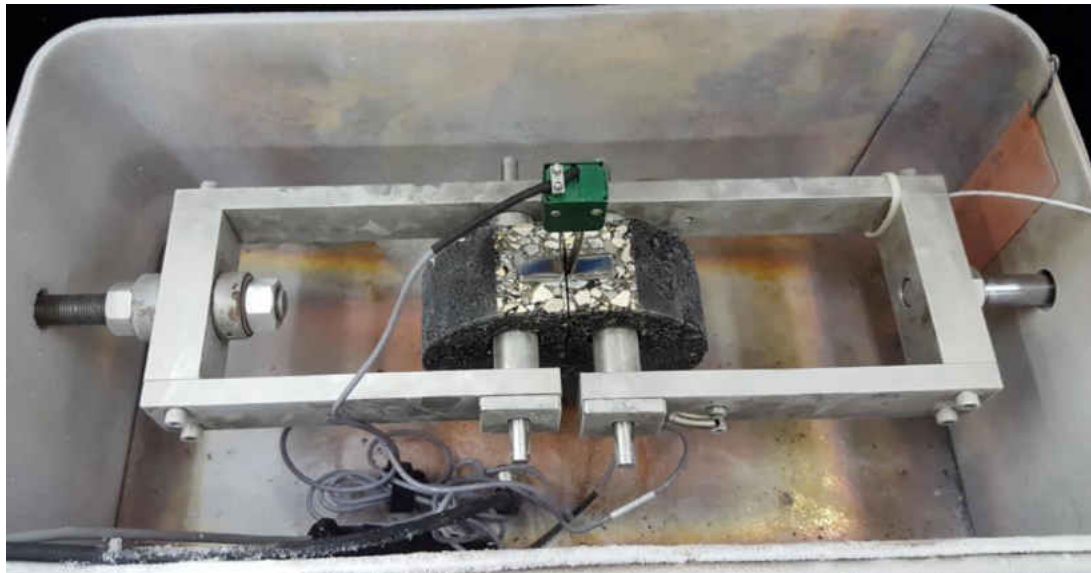


Figure 10. DCT Specimen Setup

Data Analysis

For binder's rutting and fatigue cracking resistance, the complex shear modulus (G^*) and phase angle (δ) values from the DSR were recorded at a frequency rate of 10rad/sec. The graphical view of the results shows the change in the elastic and viscous portion of the binder caused by varying contents of Nanoclay and Nanoalumina.

The results for the low-temperature rheology was recorded by the DSR in the graphical form of storage modulus master curve. The slope and magnitude of the relaxation modulus were manually calculated from the master curve of storage modulus obtained by time-temperature superposition (TTS) method. Tabular results and graphical images for slope and magnitude were investigated to determine the effect of Nanoclay and Nanoalumina on the low-temperature rheology.

APA results showed the rut depth of specimen at each pass for all the specimen loaded. The average rut depths of the specimens loaded were calculated, then standard deviation and coefficient of variation was calculated where possible. Rut depths at 2000, 4000, 6000 and 8000 passes were analyzed to determine the progression of rutting. Finally, independent t-tests were performed to find out the statistical difference between the samples at 0.05 significance level.

The analysis of the DCT and SCB were almost the same. The results for DCT were given directly by the machine in terms of fracture energies whereas for SCB, I-FIT's post processing software was used to calculate the fracture energy of the samples. For both SCB and DCT tests, average fracture energies were calculated and displayed in a graph for ease of analysis. Table of air voids for each specimen was made to relate the

air voids and fracture energies. However, t-test was possible only on SCB due to limited number of DCT specimens.

Chapter IV

RESULTS AND DISCUSSION

The purpose of this study was to investigate the effect of Nano-materials on binder and mix performance. DSR was used for finding the resistance of binder at different temperatures whereas APA for determining rutting, SCB for fatigue cracking and DCT for low-temperature (thermal) cracking. Modified binders were mixed and tested along with virgin (0% Nanomaterials) to compare the performance of both binder and mixes with the latter. This section is further divided into results of binders and HMA mixes.

a. Effect on Binder Performance

Rutting Resistance

Un-aged, RTFO-aged and PAV-aged binders at control (0%), 1%, 5% and 7% contents of both Nanoclay and Nanoalumina were poured into a silicon mold to produce 25mm diameter specimens. Superpave specifications demands short term aged asphalt binder to be tested at high temperature to determine rutting resistance, so specimens were tested in DSR measuring instrument at their corresponding higher temperature of PG grade to calculate the complex shear modulus (G^*) and phase angle (δ).

Figures 11 and 12 show the graph of $\left[\frac{G^*}{\sin \delta} \right]$ versus Strain (%) for unaged and RTFO-aged asphalt binder at different Nanoalumina (NA) content in PG58-28, respectively. The binders are stiffer than the unmodified binder which results in the higher value of elastic component of complex shear modulus, $\left[\frac{G^*}{\sin \delta} \right]$ as expected. Higher values in the Y-axis increases the binder's resistance to pre-mature permanent deformation. Addition of more than 1% NA didn't make much difference. The difference in NA content does show a significant difference after the binder was aged as shown in Figure 12. Also, RTFO-aged binder at 5% and 7% NA have almost the same rutting resistance but higher than 1%, which is expected. All binders passed the AASHTO M320 PG binder specifications as shown in both figures denoted by critical line.

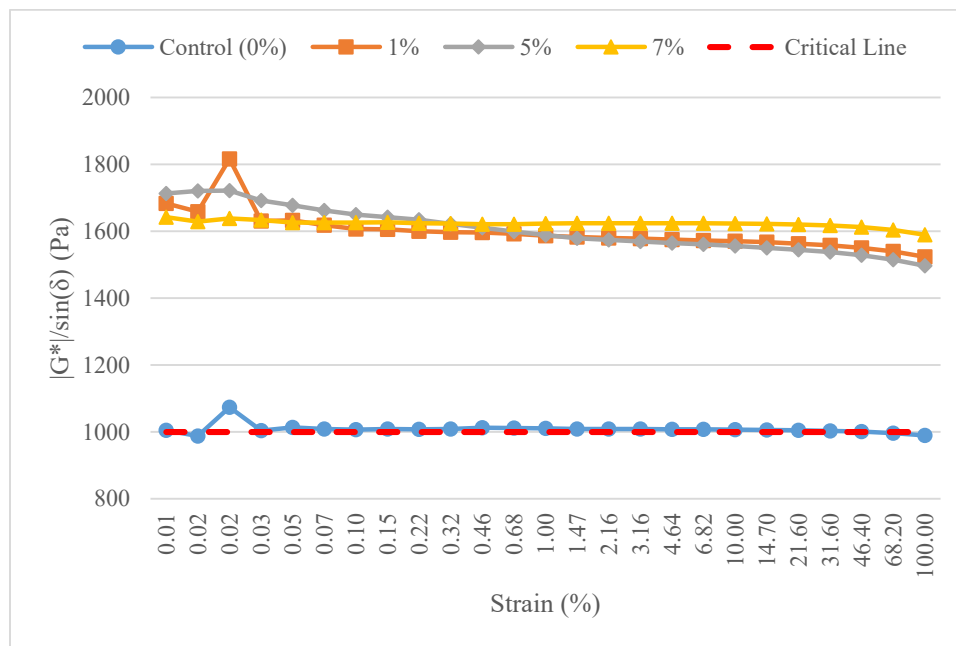


Figure 11. Unaged PG 58-28 modified with NA

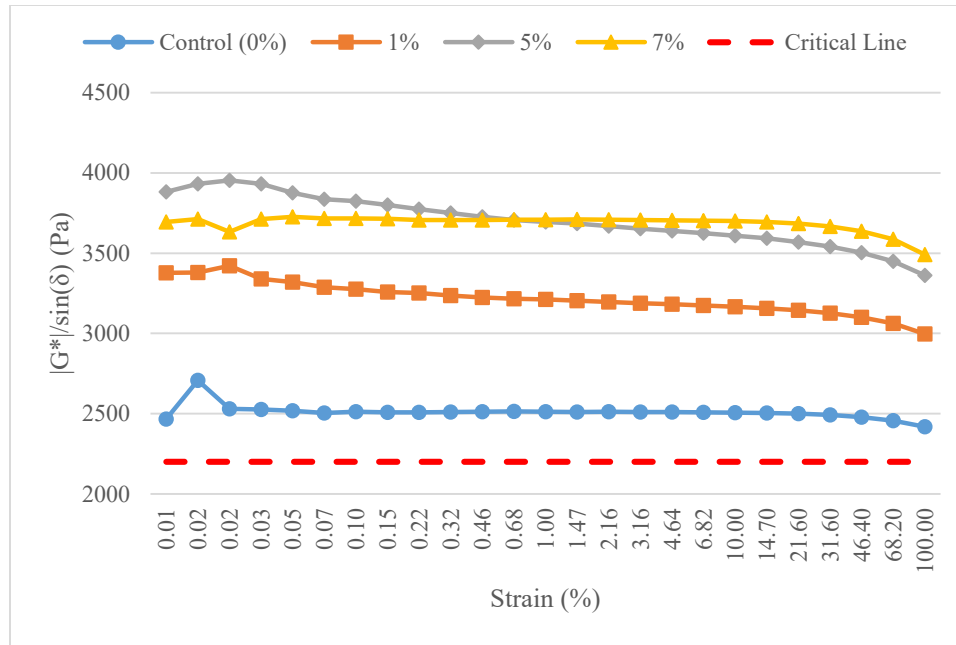


Figure 12. RTFO-aged PG 58-28 modified with NA

Addition of Nanoclay (NC) performed to as expected as shown in Figures 13 and 14. Both Figures 13 and 14 show that the stiffness of the binder has increased significantly for both unaged and RTFO-aged binder, with the addition of NC. The increase in rutting resistance is directly proportional to the content of NC. 7% has the highest stiffness and then decreases from 5% to 1% NC content. The change in value of phase angle (δ) is insignificant which explains the significant increase in shear modulus (G^*).

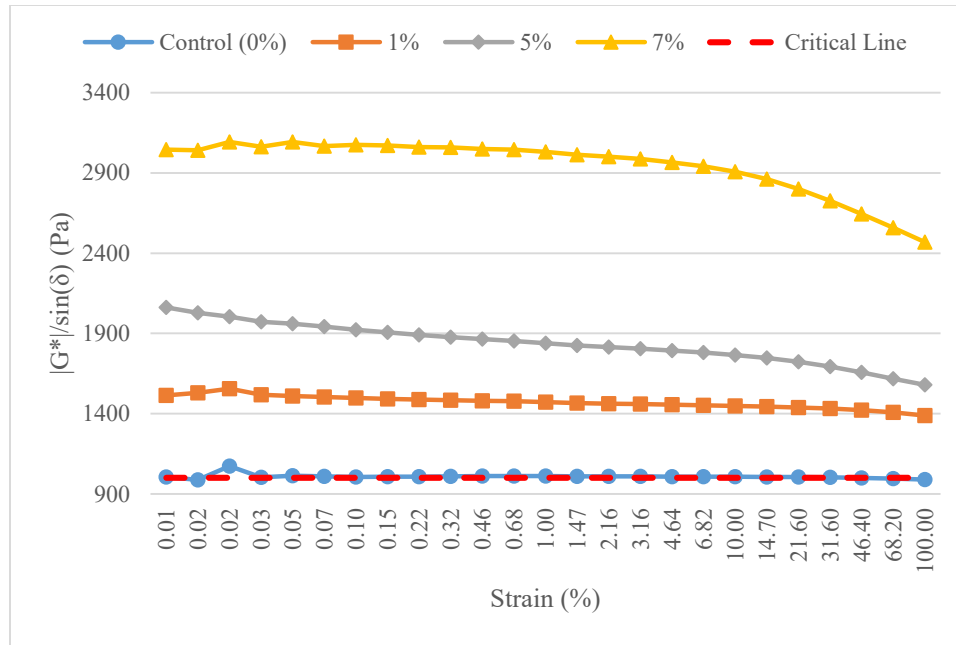


Figure 13. Unaged PG 58-28 modified with NC

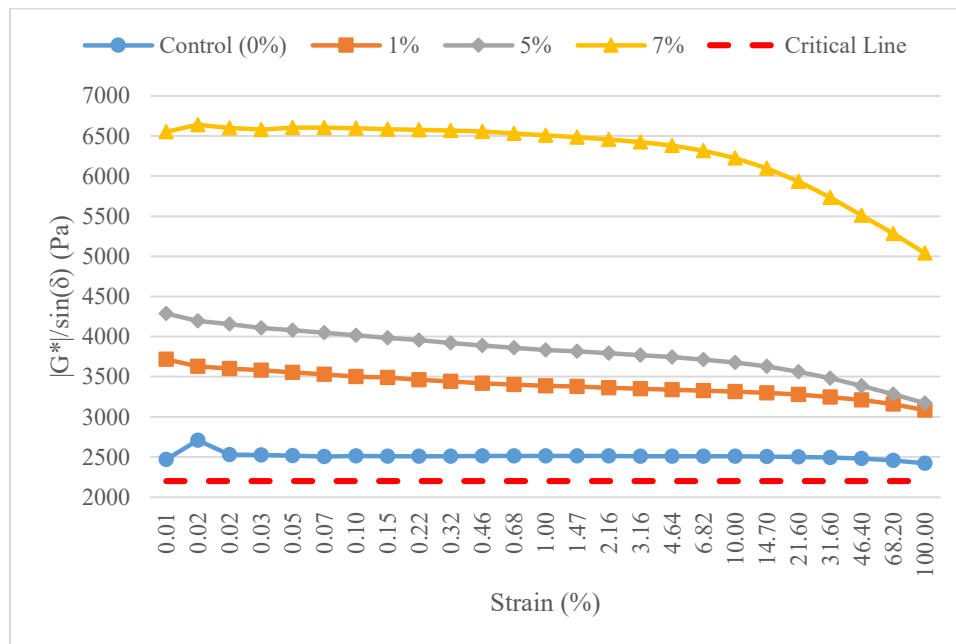


Figure 14. RTFO-aged PG 58-28 modified with NC

Figures 15 and 16 show the effect of NA on unaged and RTFO-aged binders for PG64-28. In Figure 15, the value of elastic component of shear modulus was higher for the control than modified binders at the beginning of the test. But as, the test progressed

the value went below all the modified binders. This result of PG64-28 can be compared to the result in Figure 11 of PG58-28. In both cases, for unaged binders, increasing the NA content in binder does little or no difference to the stiffness. However, the addition of NA did have an effect in increasing the stiffness in PG58-28 but was insignificant in PG64-28. From Figure 16, 1% NA has the highest rutting resistance. All the binders, as shown in both Figures 15 and 16, are well above the critical line passing the specifications.

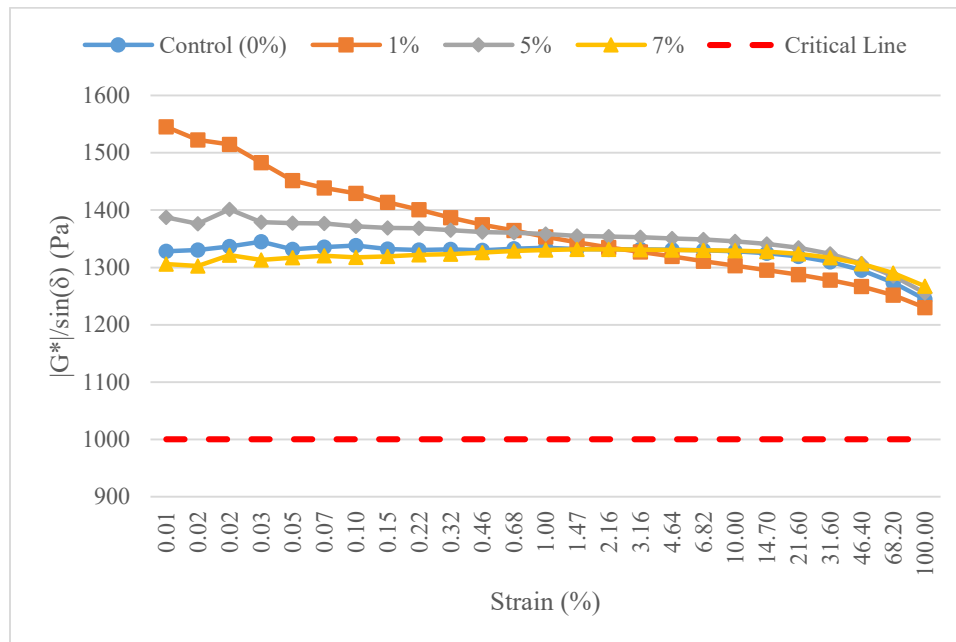


Figure 15. Unaged PG 64-28 modified with NA

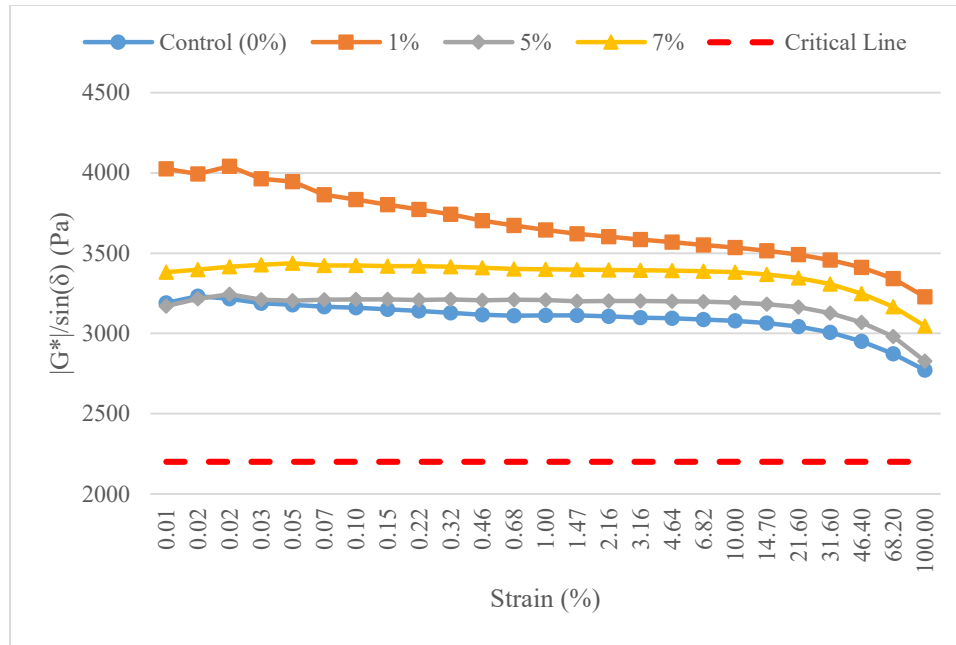


Figure 16. RTFO-aged PG 64-28 modified with NA

Like the effect in PG58-28, rutting resistance of unaged and RTFO-aged binder was increased in PG64-28 as the NC content increased as shown in Figures 17 and 18. From both Figures 17 and 18, it can be said that the stiffness of the binder has increased as the NC content increased, but increased tremendously from 5% to 7% NC. In both the Figures, the values of the elastic component of the complex shear modulus is well above the specifications for all the binder types. In both cases, the 1% NC content has the lowest stiffness value. This can be a result of low amount of NC which didn't disperse uniformly in the binder. PG64-28 is also stiffer than PG58-28, making the mixing of NC with the binder challenging.

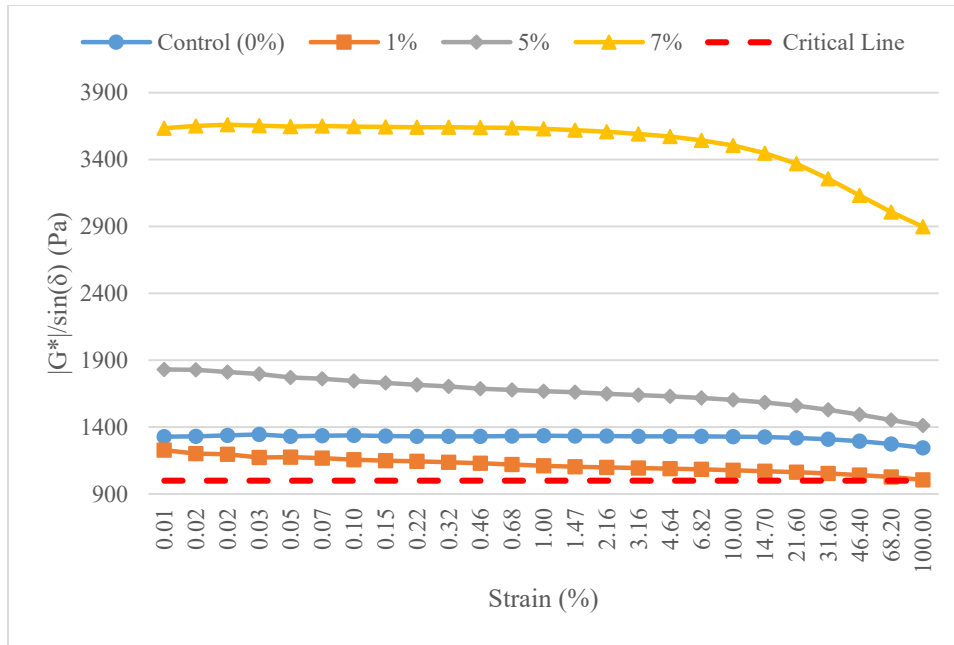


Figure 17. Unaged PG64-28 modified with NC

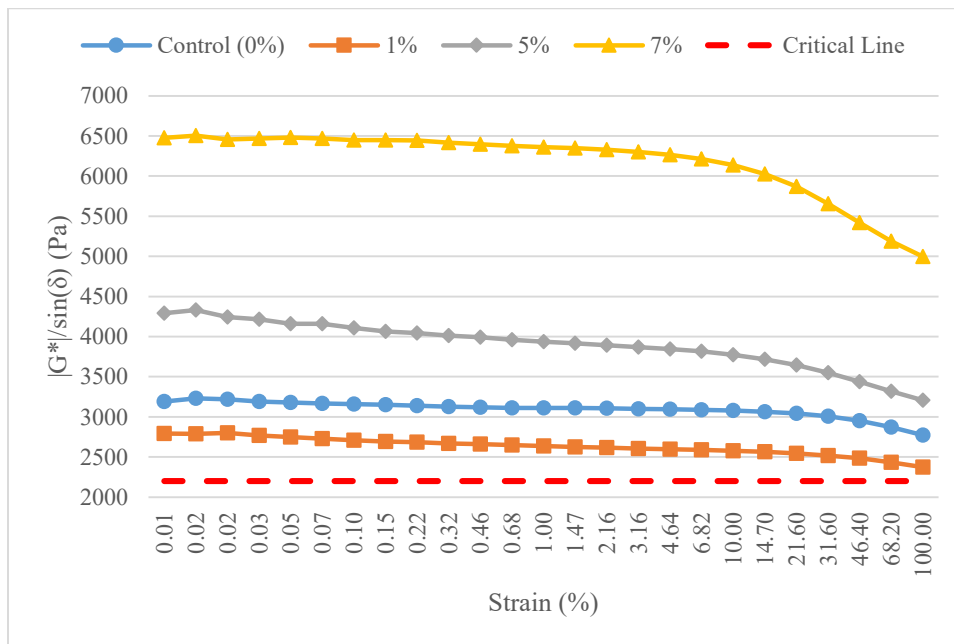


Figure 18. RTFO-aged PG64-28 modified with NC

In all the rutting results, most of the values for elastic portion of the complex shear modulus are extremely higher than the specifications. Further investigation was

done to check at what content of Nanomaterials the PG grade binder can move up by a grade i.e. pass the specifications at higher temperature of PG +6°C.

Figures 19-22 show the effect on the modified PG58-28 binders when tested at PG +6°C i.e. 64°C. The increase in temperature decreases the stiffness of the binder. The values of $\left[\frac{G^*}{\sin \delta} \right]$ has reduced significantly as expected. It was also found that only 7% NC was stiff enough to pass the higher-grade binder's PG specifications in both unaged and RTFO-aged binders. The optimum content of NC must be between 5% and 7% to move the binder's specification by a grade i.e. 6°C.

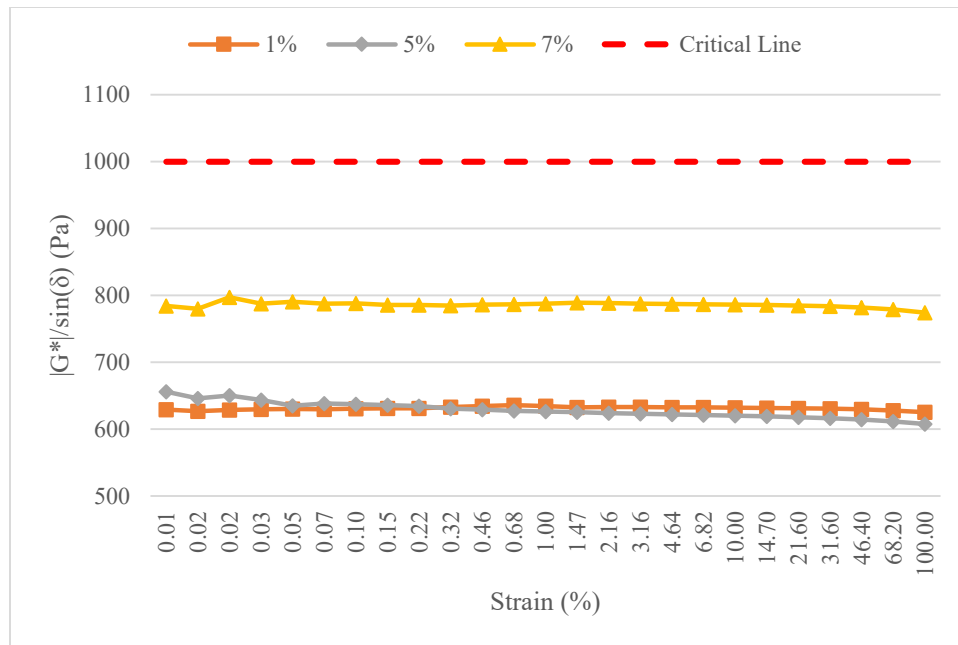


Figure 19. Unaged PG 58-28 modified with NA at 64°C

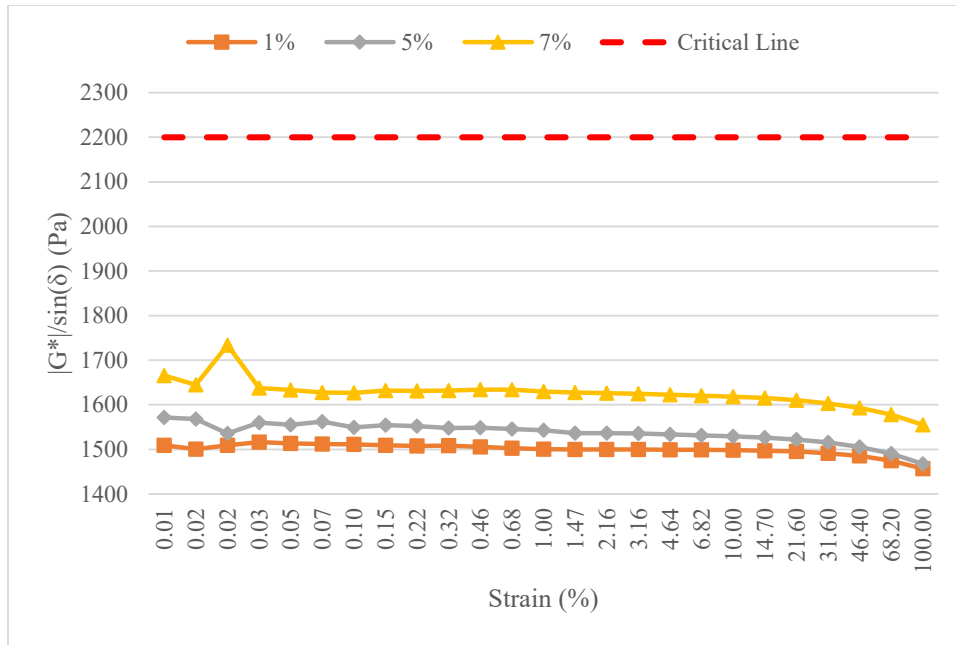


Figure 20. RTFO-aged PG 58-28 modified with NA at 64°C

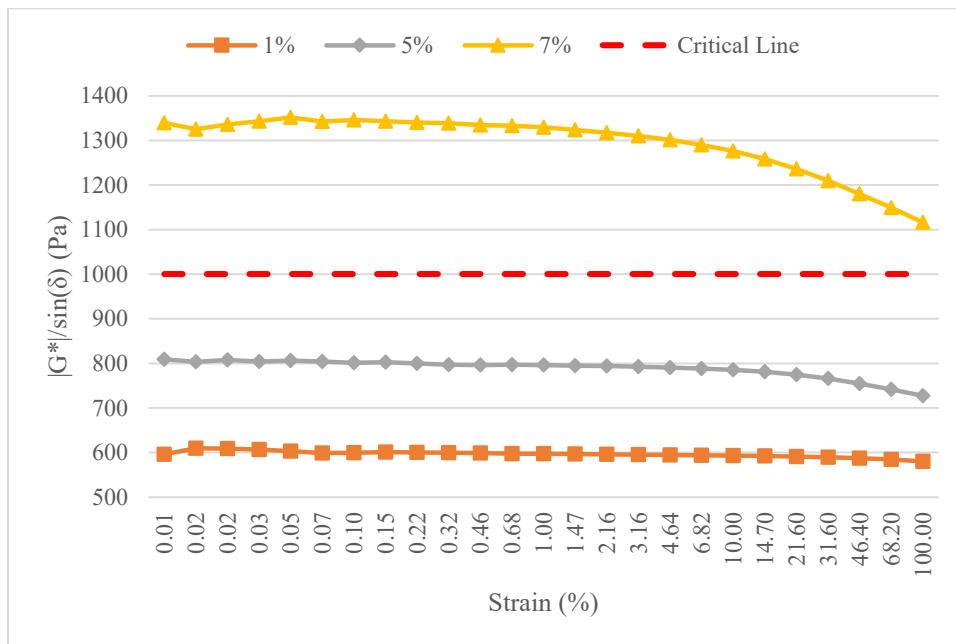


Figure 21. Unaged PG 58-28 modified with NC at 64°C

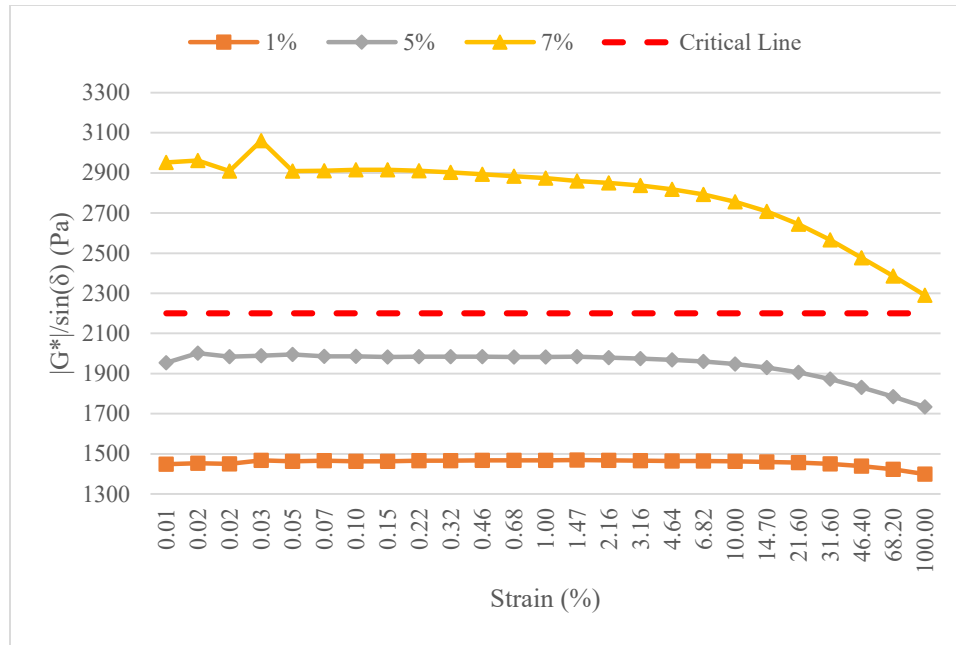


Figure 22. RTFO-aged PG 58-28 modified with NC at 64°C

Figures 23-26 show the effect of Nanomaterials on PG64-28 binders when tested at PG+6°C i.e. 70°C. It can be seen that similar results were found for both NA and NC. None of the binder content passed the PG specifications for NA content, and only 7% NC content could pass the specifications at higher binder grade in both unaged and RTFO-aged binders. It can be asserted that like in PG58-28, 7% NC content brings an enormous increase in the stiffness of the binders compared to 5%. Therefore, the optimum content of NC must be between 5% and 7% to move the binder's PG by a grade higher i.e. 6°C.

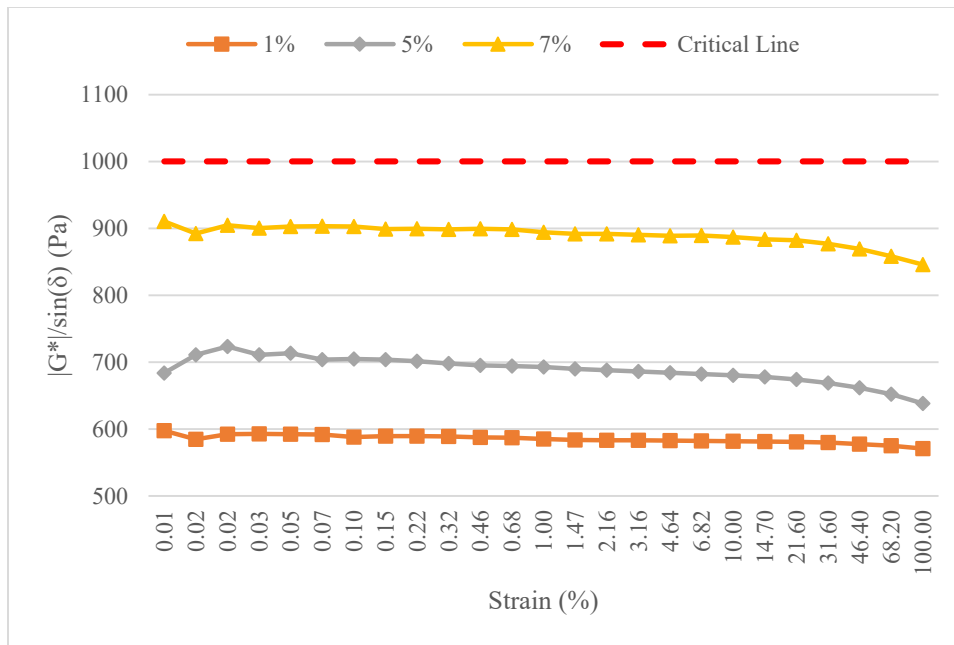


Figure 23. Unaged PG 64-28 modified with NA at 70°C

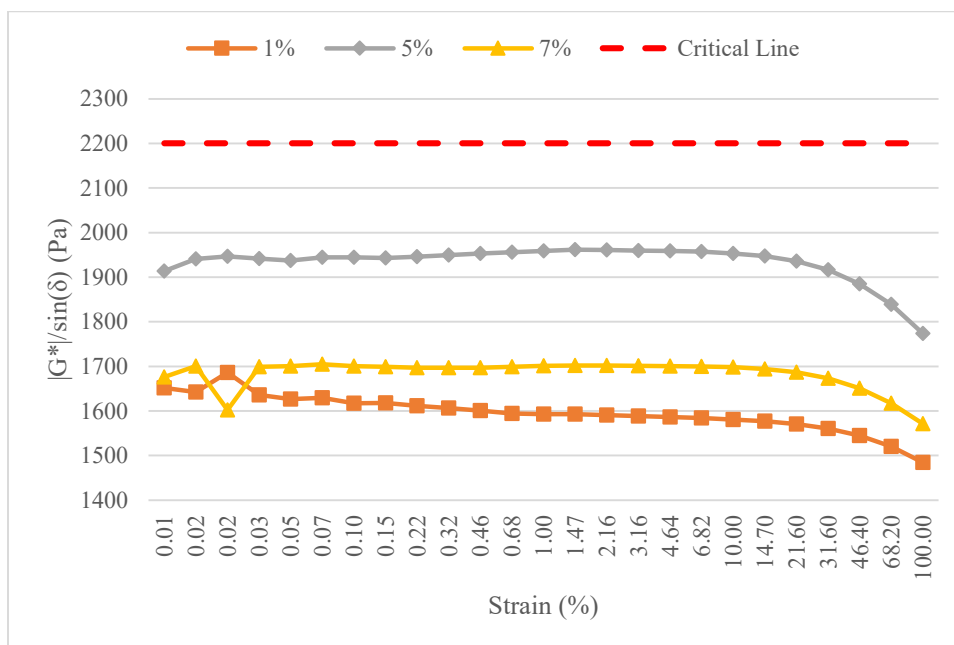


Figure 24. RTFO-aged PG 64-28 modified with NA at 70°C

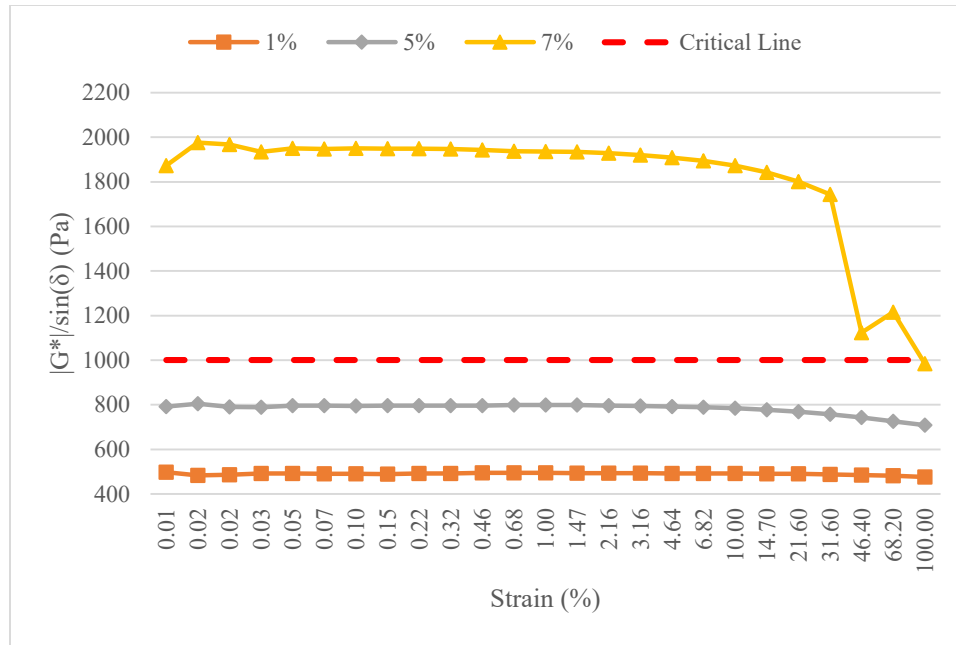


Figure 25. Unaged PG 64-28 modified with NC at 70°C

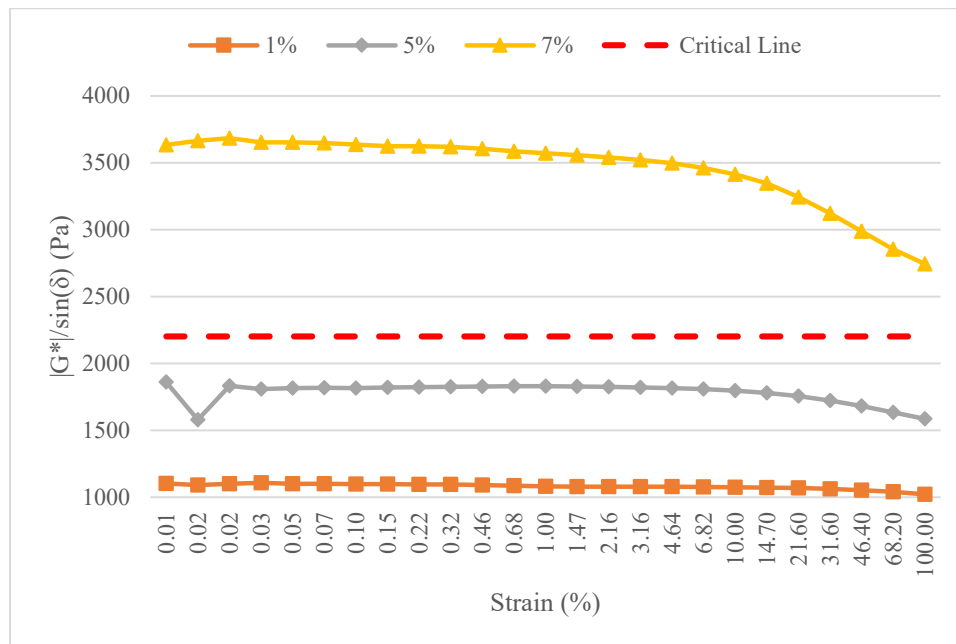


Figure 26. RTFO-aged PG 64-28 modified with NC at 70°C

Figures 19-26 show that only 7% NC could pass the specifications for both the binder grades, PG58-28 and PG64-28. But the results of the tests on 7% NC was very high compared to the specifications. Further testing was done to make sure the 7% NC is

stiff enough to pass 2 higher binder grades, i.e. PG +12°C. Figures 27-30 show the graphs of $\left[\frac{G^*}{\sin \delta} \right]$ versus strain (%) for both unaged and RTFO-aged binders at 7% NC content at PG +12°C for both binders, i.e. 70°C for PG58-28 and 76°C for PG64-28.

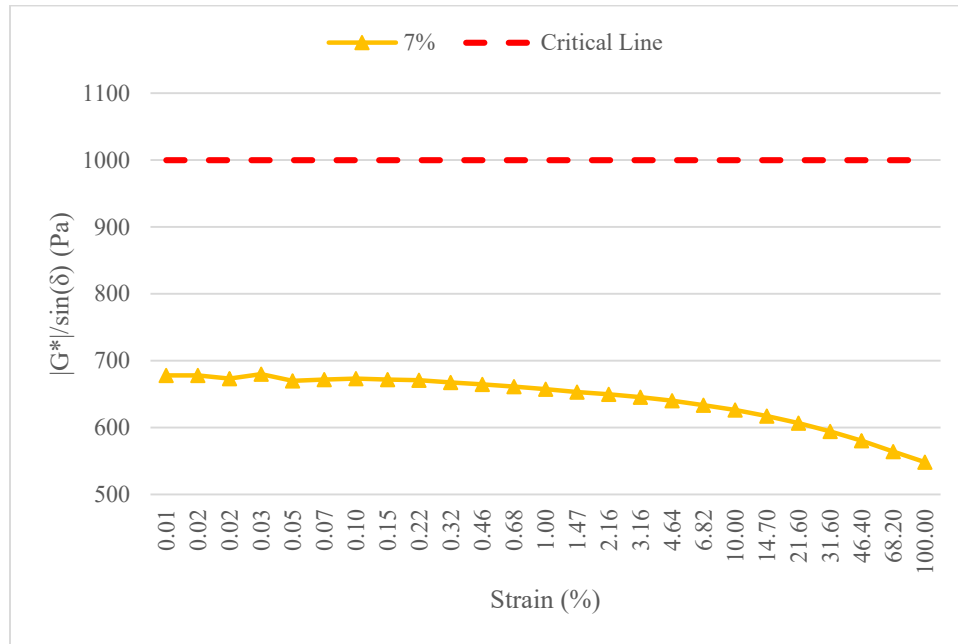


Figure 27. Unaged PG 58-28 modified with 7% NC at 70°C



Figure 28. RTFO-aged PG 58-28 modified with 7% NC at 70°C

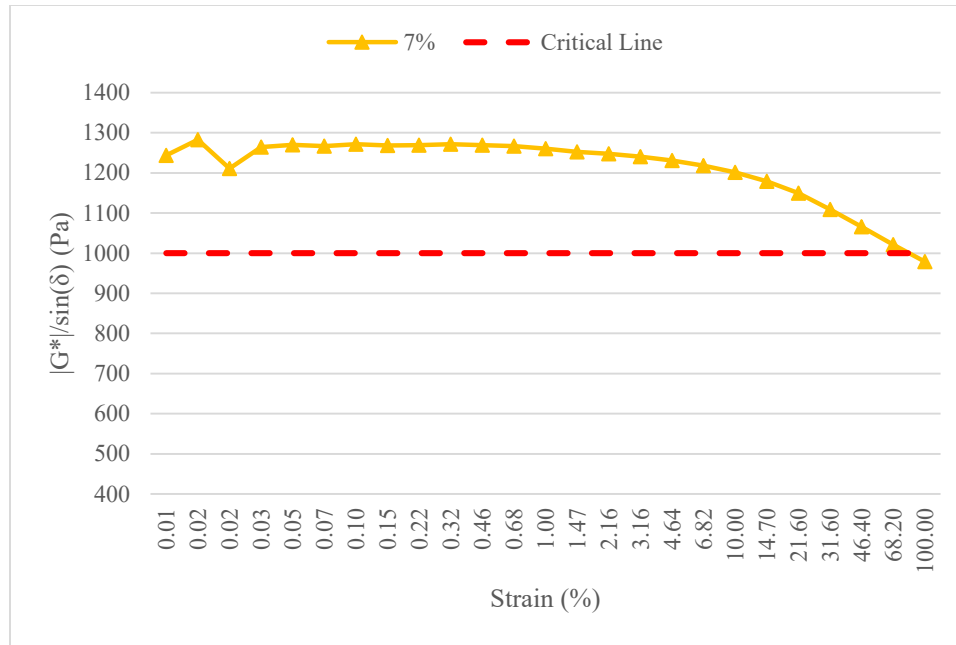


Figure 29. Unaged PG 64-28 modified with 7% NC at 76°C

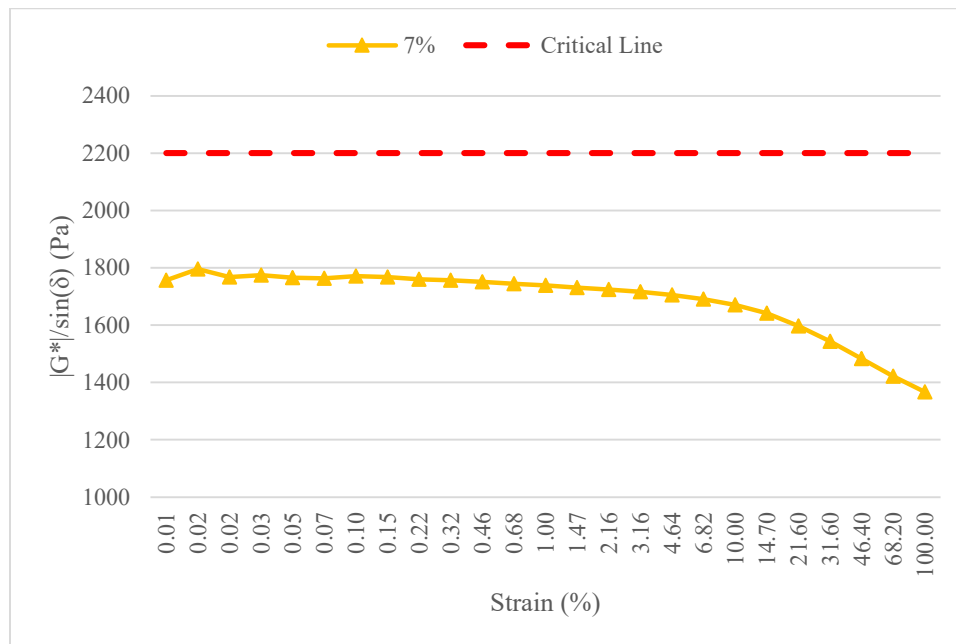


Figure 30. RTFO-aged PG 64-28 modified with 7% NC at 76°C

It can be seen in Figures 27 and 28, the binder did not pass the specification for 70°C. The binder passed at unaged test for PG64-28 binder at 24 out of 25 points, but it failed at RTFO-aging which is the binder's aging at mixing and placement. It can be

concluded that the optimal content to move the high temperature grade to resist rutting of a binder, PG58-28 or PG64-28, is between 5% and 7%.

Fatigue Resistance

The specifications for the PAV-aged PG binder calls for the value of $[(G^*)(\sin \delta)]$ to be lower than 5000kPa. All the values recorded in the test for fatigue resistance were much lower than the critical value. Figure 31 shows the graph of $[(G^*)(\sin \delta)]$ versus the applied strain (%) for PAV-aged PG58-28 modified with NA. As expected highest NA content, 7% NA, has the highest stiffness value although 1% NA is stiffer than 5%.

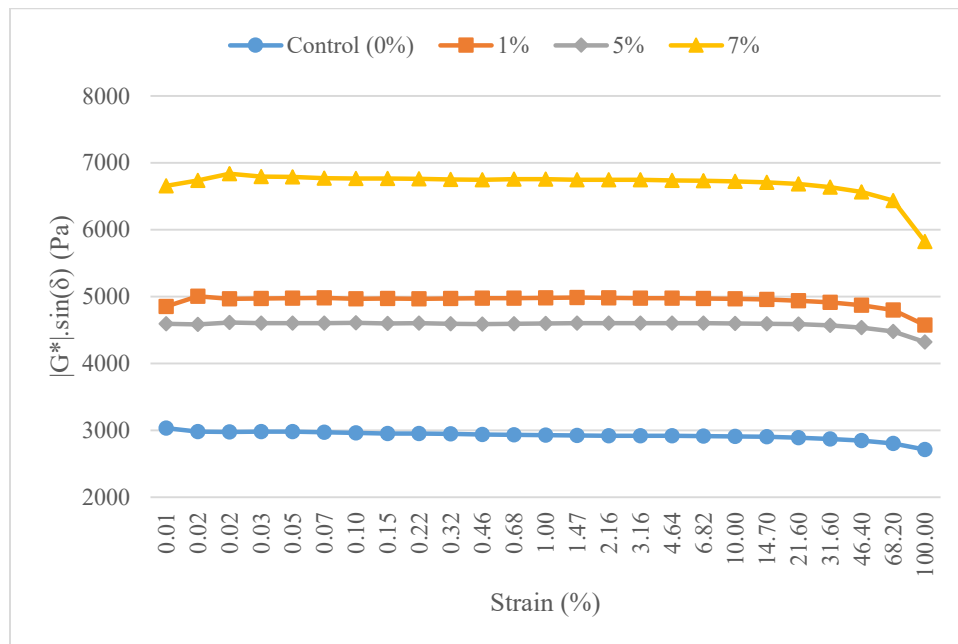


Figure 31. PAV-aged PG58-28 modified with NA

Lower value of viscous component of complex shear modulus is desired to prevent fatigue cracking. In Figure 31, 5% NA modification has the lowest stiffness

increasing the fatigue resistance of the binder at PG58-28. The optimum NA content for PG58-28 is 5%.

The effect of NC on the binder performance is consistent regardless of aging. It can be seen in Figure 32, the binder's stiffness increases as the NC content increases. The higher value of viscous portion of shear modulus may increase the binder's susceptibility to fatigue cracking.

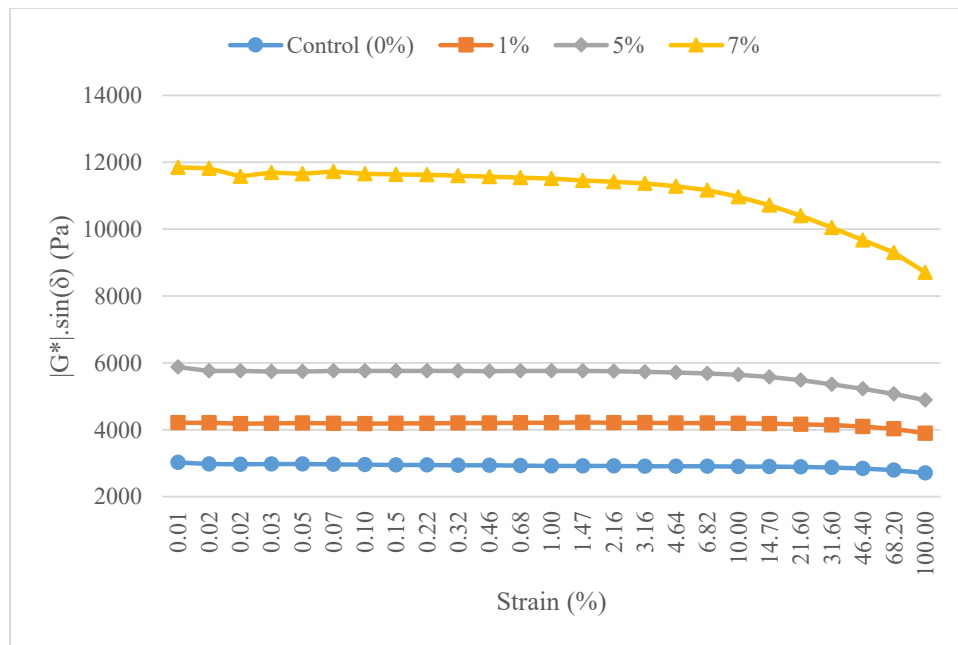


Figure 32. PAV-aged PG58-28 modified with NC

Figure 33 shows the graph of $[(G^*)(\sin \delta)]$ versus strain in PAV-aged PG64-28 binder modified with NA. 1% NA has the lowest viscous portion of the shear modulus compared to the other % contents of NA making it the best binder against fatigue cracking. Combining with the results from un-aged and RTFO-aged results in Figures 15 and 16, 1% NA could increase the binder's elastic portion of shear modulus in both un-aged and RTFO-aged binders making 1% NA the optimal proportion for PG64-28 to both rutting and fatigue cracking resistance.

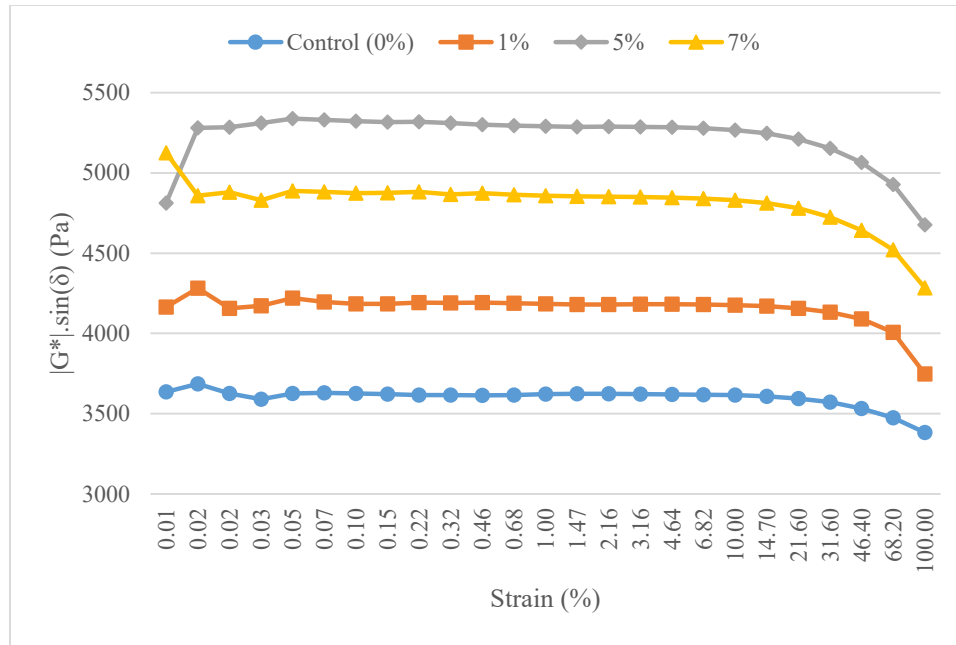


Figure 33. PAV-aged PG64-28 modified with NA

The stiffness significantly increases with an increase in NC content regardless of aging or the binder grade as shown in Figure 34. 7% NC has the highest value for viscous portion of shear modulus. The value of 1% NC is lower than the control.

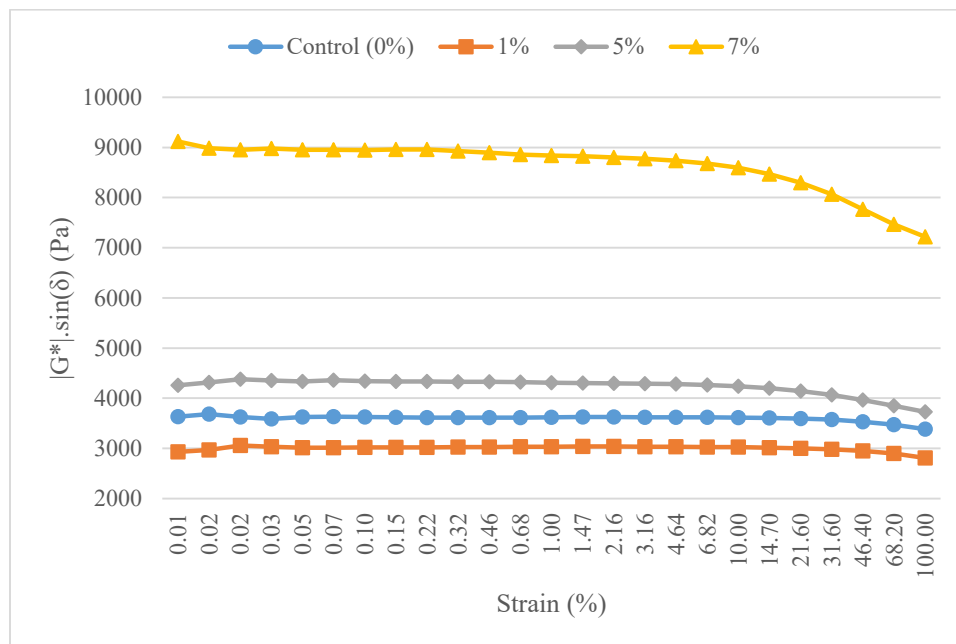


Figure 34. PAV-aged PG64-28 modified with NC

All the PAV-aged tests were well under the specifications but, addition of NC significantly increased the shear modulus making it susceptible to cracking as compared to NA.

Since tests were done to study the rutting performance of binder at higher temperature, i.e. PG +6°C, respective tests were performed to study the fatigue performance. Figures 35-38 show the effect on the viscous portion of the shear modulus, $[(G^*)(\sin \delta)]$ at PG +6°C. For PG58-28, both for NA and NC, the stiffness parameter was maximum at 7% content. In Figure 35 for PG58-28, 5% NA is the best content because of its minimum value compared to other content and 1% NA for PG64-28, as shown in Figure 37. In Figures 36 and 38, 1% and 5% have minimum values of complex shear modulus compared to 7% NC. Although the NA content values from Figures 35 and 37 are appropriate to prevent fatigue cracking, those didn't pass the specifications for unaged and RTFO-aged binders in Figures 19-20 and 23-24.

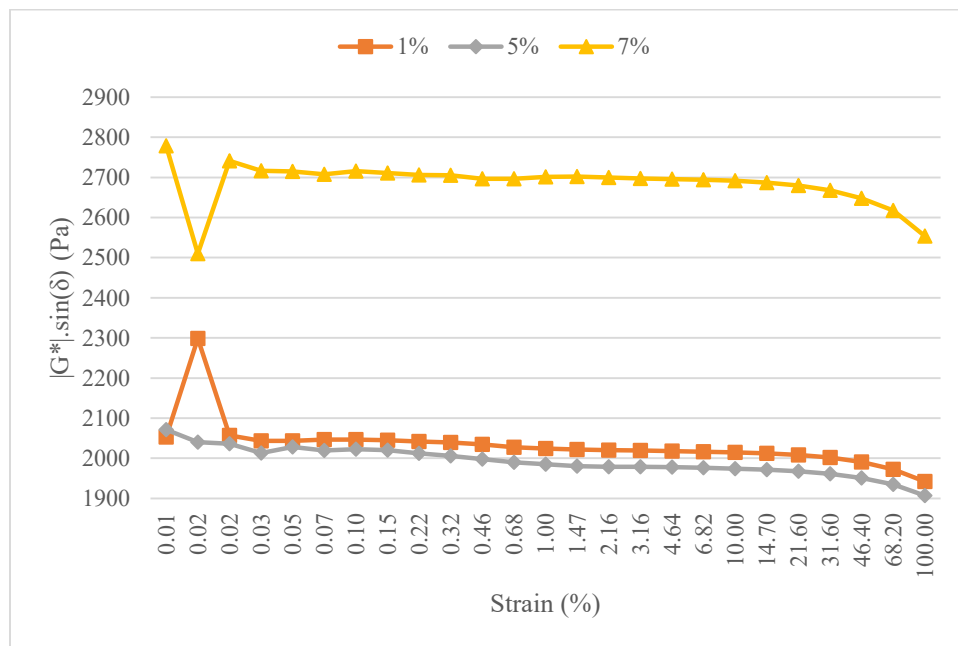


Figure 35. PAV-aged PG58-28 modified with NA at 64°C

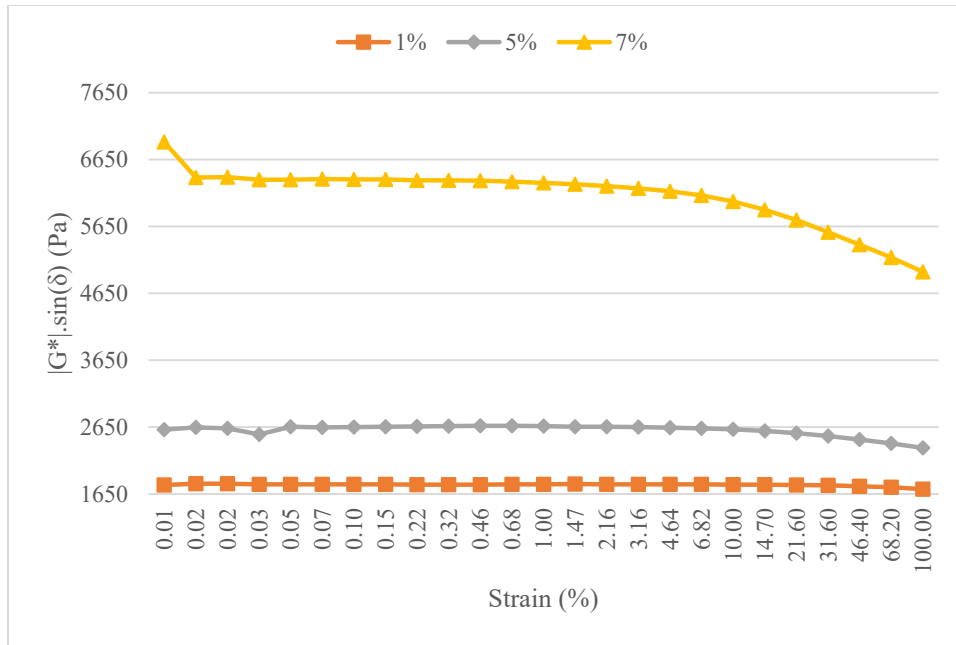


Figure 36. PAV-aged PG58-28 modified with NC at 64°C

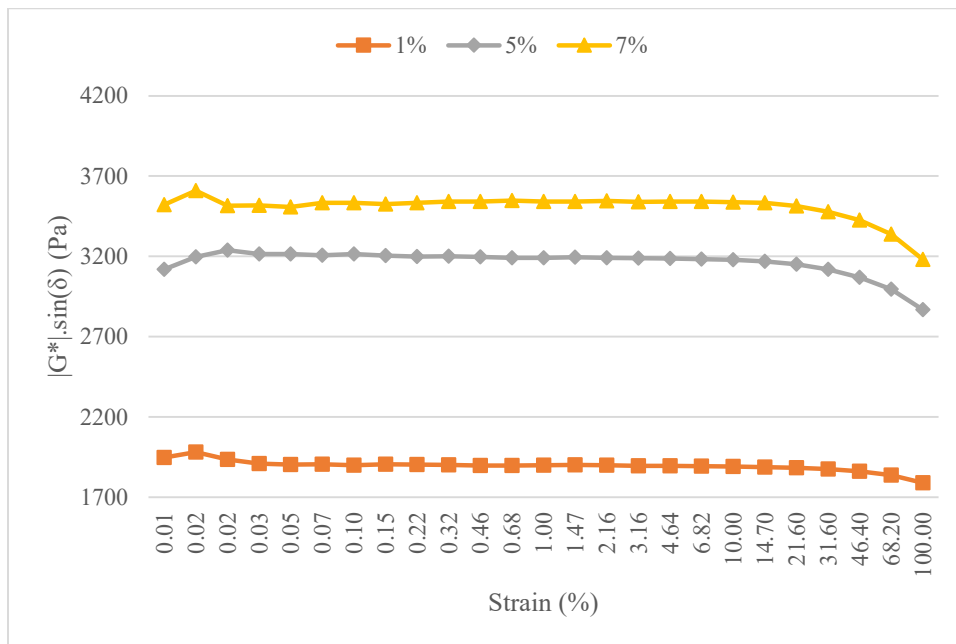


Figure 37. PAV-aged PG64-28 modified with NA at 70°C

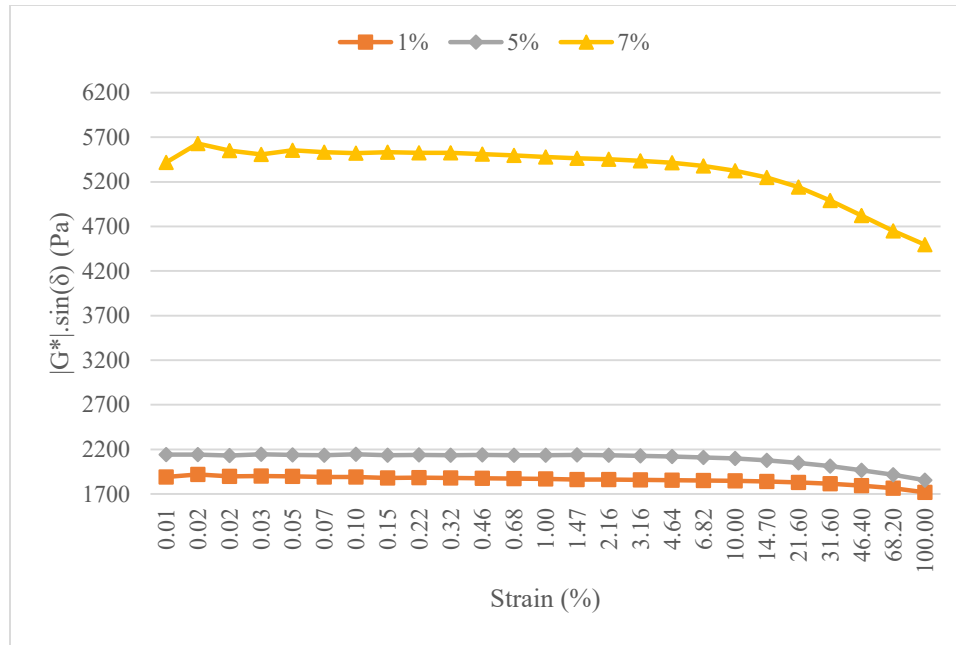


Figure 38. PAV-aged PG64-28 modified with NC at 70°C

Only the 7% NC content passed the unaged and RTFO-aged specifications for both PG58-28 and PG64-28 although 7% NC didn't perform well against fatigue cracking of the binder. Further testing was done to see how the 7% NC performs at PG +12°C to compare it with the results of rutting resistance. Figures 39 and 40 show the graph of $[(G^*)(\sin \delta)]$ versus strain at PG +12°C. The stiffness of the binder is reduced greatly as expected at higher temperature. Figures show that the binder has high fatigue resistance but it failed the specifications for both PG58-28 and PG64-28 in unaged and RTFO-aged binder tests.

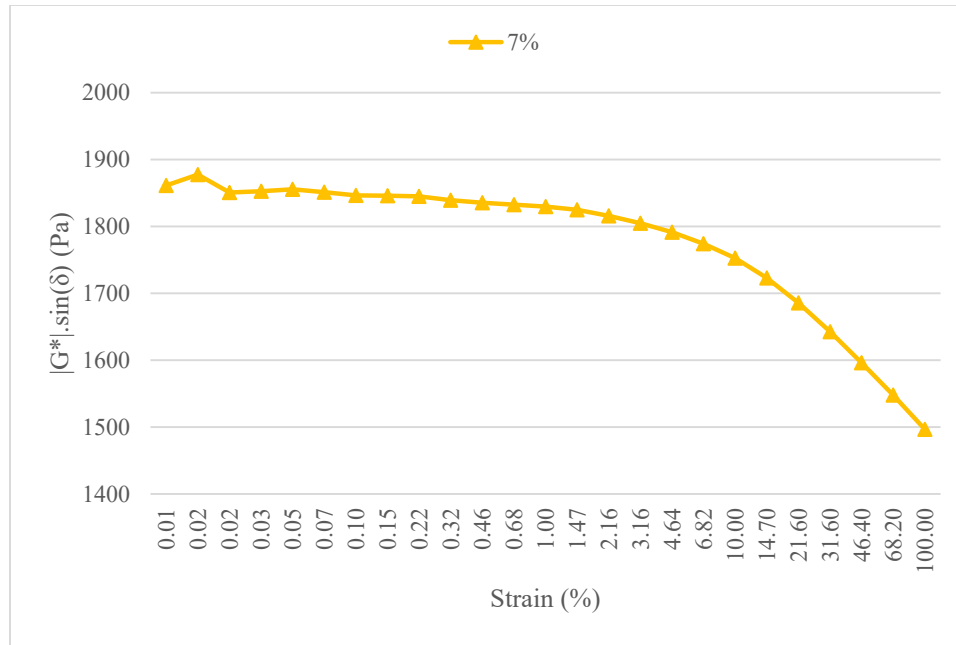


Figure 39. PAV-aged PG58-28 modified with NC at 70°C

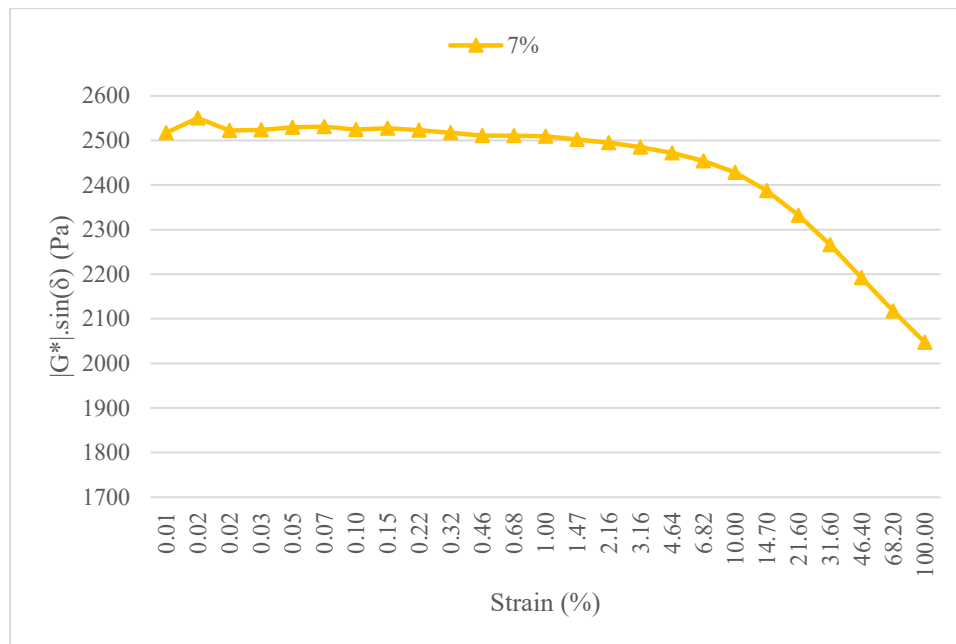


Figure 40. PAV-aged PG64-28 modified with NC at 76°C

Low-Temperature (Thermal) Cracking Resistance

The testing of low-temperature properties of binder was completed using the DSR following the method mentioned in Technical White Paper by Farrar et al. (2015). For

this test, 4mm diameter specimens were used at all contents of NA and NC and for all unaged, RTFO-aged and PAV-aged binders. Superpave classifies PG binders at low-temperature with their respective slope (m_r) and magnitude of the relaxation modulus, $G(t)$ as shown in Table 1. A series of steps are involved to calculate these variables. Two frequency sweeps were taken in each test, one at the lower temperature of PG +10°C and the other at PG +20°C as shown in Figure 41.

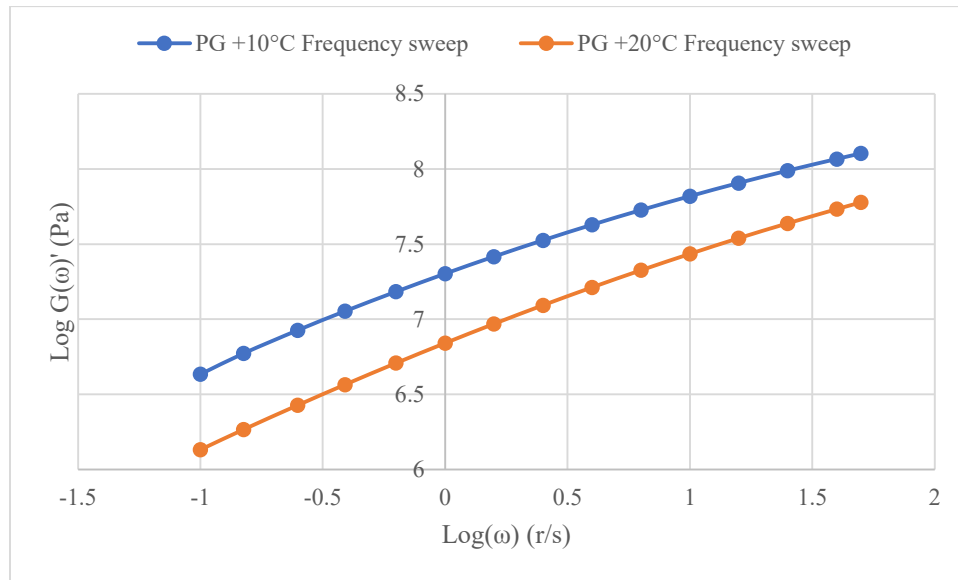


Figure 41. Sample graph of PG+10°C and PG+20°C frequency sweeps

Then, horizontal shift of PG +20°C frequency sweep is carried out along the abscissa to overlap the PG +10°C frequency sweep by time-temperature superposition (TTS) method. The resulting graph is storage modulus [$G'(\omega)$] master curve at reference temperature of PG +10°C as shown in Figure 42.

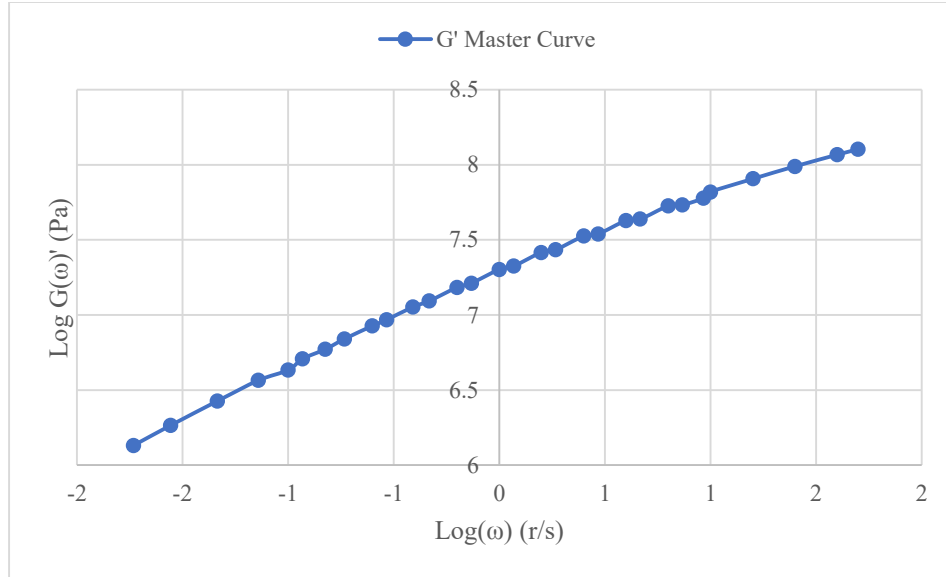


Figure 42. Sample graph of $G'(\omega)$ Master curve at a reference temperature of PG+10°C

The relaxation modulus $G(t)$ is then determined thru interconversion of the storage modulus $G'(\omega)$ by the approximate expression in Equation 5 developed by Christensen (1982).

Equation 5: Conversion of Storage modulus master curve to relaxation modulus (Farrar et al., 2015)

$$G(t) \approx G'(\omega)|_{\omega=2\pi/t}$$

Figure 43 shows the relaxation modulus determined from Figure 42 using the Equation 5 mentioned above. The relaxation modulus is then fit with a 2nd order polynomial using the time points that bracket 60 seconds to generate the polynomial in Figure 43. The slope of the relaxation modulus is determined by taking the first derivative of the 2nd order polynomial equation in Figure 42. Solving the polynomial equation at 60 seconds gives the value of $G(60)$ while solving the first derivative of polynomial at 60 seconds gives the value of slope, $m(60)$.

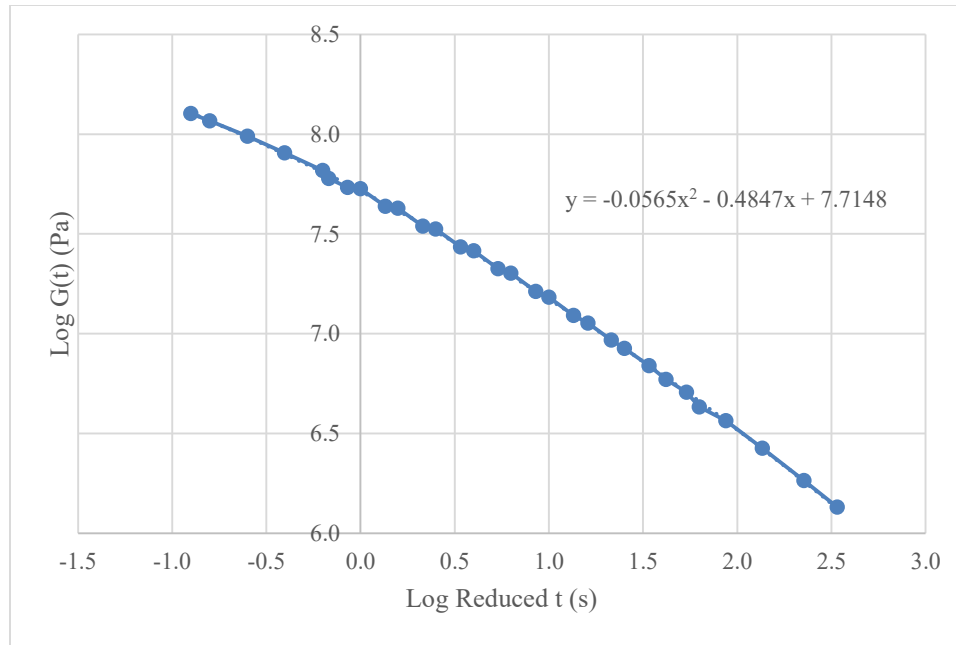


Figure 43. Relaxation modulus master curve to determine $m_r(60s)$ and $G(60s)$

The steps listed above are used to calculate the slope (m_r) and magnitude of the relaxation modulus, $G(60s)$ for each type of binder and respective binder content as shown in Tables 7 and 8. Creep stiffness value, $[G(60s)]$, is a measure of thermal stresses in the binder which is the result from thermal contraction. AASHTO M320 specifies a maximum value for the creep stiffness because a higher creep stiffness value represents higher thermal stresses. If these stresses are too large, thermal cracking will occur. The slope of the relaxation modulus, $m_r(60s)$, is a measure of the rate at which the asphalt binder relieves stress through plastic flow (Pavement Interactive, 2016). AASHTO M320 specifies a minimum value for the slope because lower value represents lower ability to relax stresses. The value of creep stiffness for all types of binder is much below the maximum value i.e. 300MPa, specified by AASHTO M320. The slope values are relatively closer to the critical value of 0.3 as shown in Figures 44-55.

Table 7. Magnitude of Relaxation Modulus [G (60s)] Summary

PG	Type of Binder	0%	1% NC	5% NC	7% NC	1% NA	5% NA	7% NA
58-28	Unaged	5.988	1.175	8.189	12.455	6.575	7.376	4.923
	RTFO-aged	4.634	14.787	23.531	30.539	13.263	23.738	2.048
	PAV-aged	10.832	19.646	31.389	39.714	18.606	31.663	29.505
64-28	Unaged	6.054	3.999	4.724	6.234	8.710	2.270	6.269
	RTFO-aged	17.628	9.479	12.606	10.834	21.983	10.455	26.722
	PAV-aged	16.820	19.117	12.662	26.384	29.728	15.661	30.471

Table 8. Slope (m_r) of Relaxation Modulus [G (60s)] Summary

PG	Type of Binder	0%	1% NC	5% NC	7% NC	1% NA	5% NA	7% NA
58-28	Unaged	0.736	0.835	0.675	0.648	0.674	0.684	0.722
	RTFO-aged	0.638	0.633	0.562	0.522	0.579	0.541	0.570
	PAV-aged	0.495	0.559	0.490	0.452	0.524	0.494	0.492
64-28	Unaged	0.676	0.722	0.686	0.650	0.672	0.761	0.670
	RTFO-aged	0.576	0.624	0.597	0.581	0.535	0.590	0.534
	PAV-aged	0.482	0.524	0.535	0.482	0.448	0.541	0.448

Figures 44-49 show the change in slope (m_r) and magnitude of the relaxation modulus, G(60s) at different stages of aging for all nanomaterial content in PG58-28 binder. Figures 44-45 show that at 1% NC the binder displays low-temperature cracking resistance higher than the rest of the Nanomaterial contents including virgin binder before aging. For unaged binder creep stiffness value is the lowest and the value of slope is highest at 1% NC, which defines the binder with the lowest thermal stresses and the highest ability to relax stresses. As the NC content increases, the binder's stiffness increases and slope value decreases, increasing the binder's susceptibility to thermal cracking.

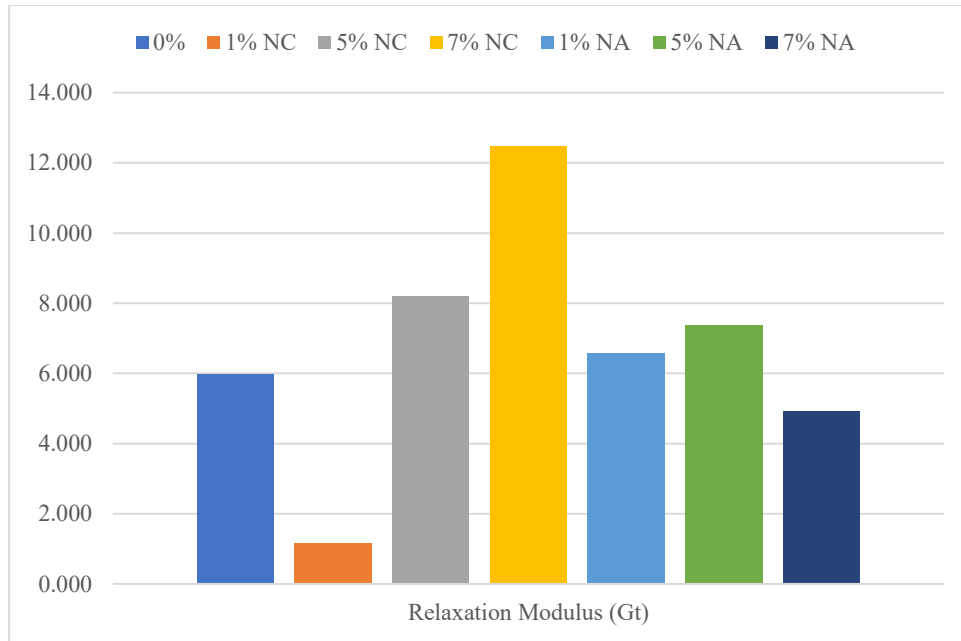


Figure 44. Relaxation Modulus for Unaged PG58-28

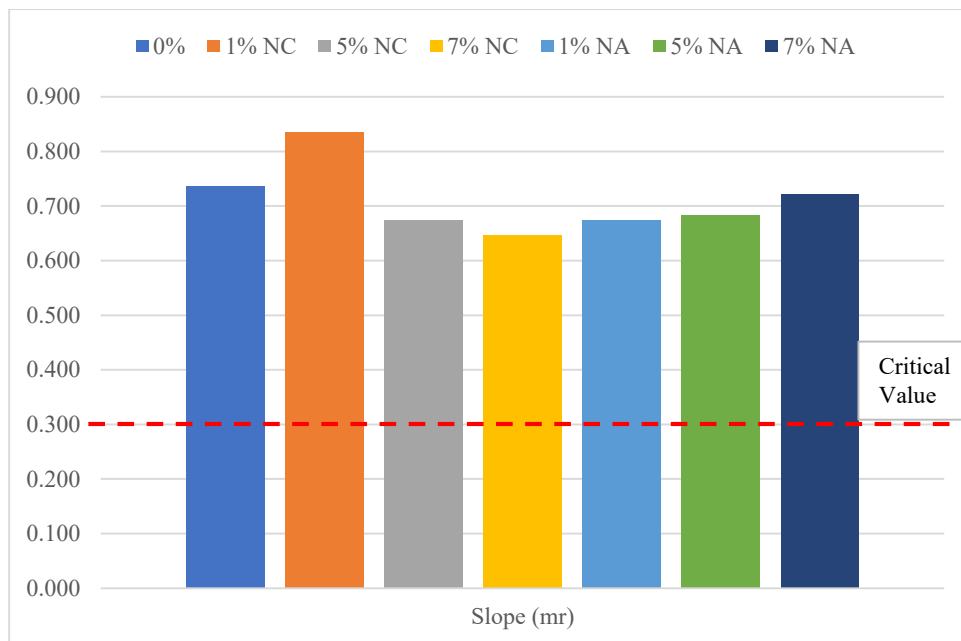


Figure 45. Slope for Unaged PG58-28

Figures 46-47 show that the stiffness of NC modified binders is increased due to short-term aging. The increase in NC content increased the creep stiffness of the binder and thereby reduced the ability to relax stresses. With the increase in NA content, the

binder's ability to resist thermal cracking reduced from 1% to 5% but increased as the content was increased to 7%. The Nanomaterials content in binder reduced the performance of binder after short-term aging.

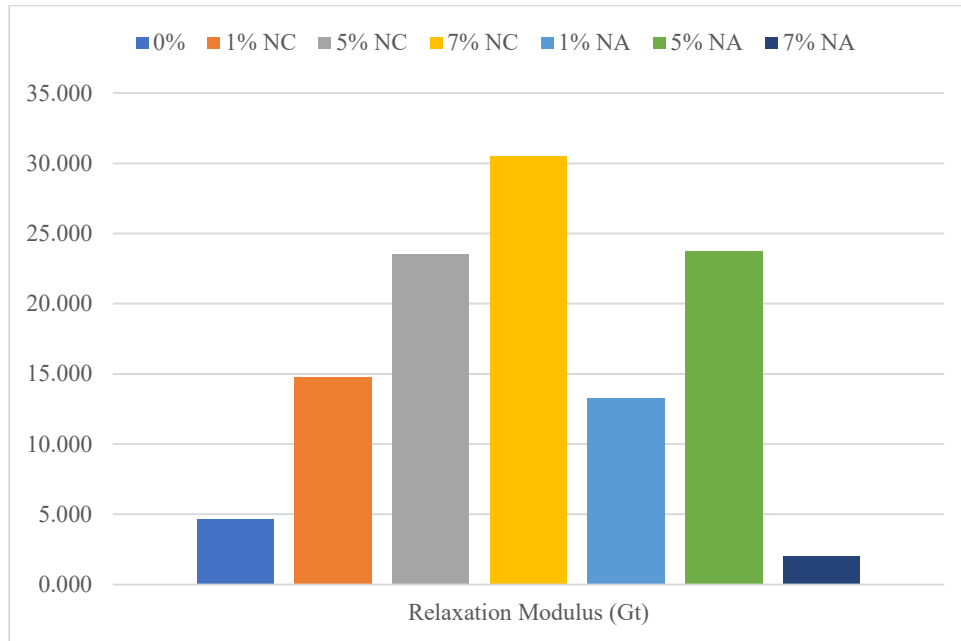


Figure 46. Relaxation Modulus for RTFO-aged PG58-28

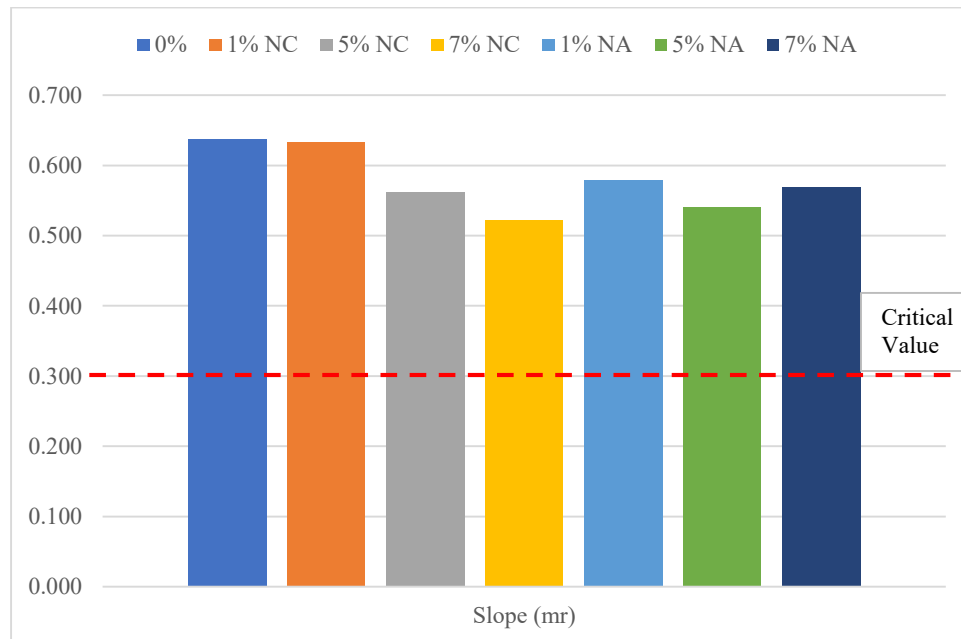


Figure 47. Slope for RTFO-aged PG58-28

The increase in NC results in an increase in stiffness and a decrease in slope of the PAV-aged binder as shown in Figures 48 and 49. The NA modification doesn't make too much difference on the slope but increases the stiffness as the content increases. PAV-aged binder shows susceptibility to cracking is increased mainly because of the stiffness of the binder at low-temperatures as compared to the control.

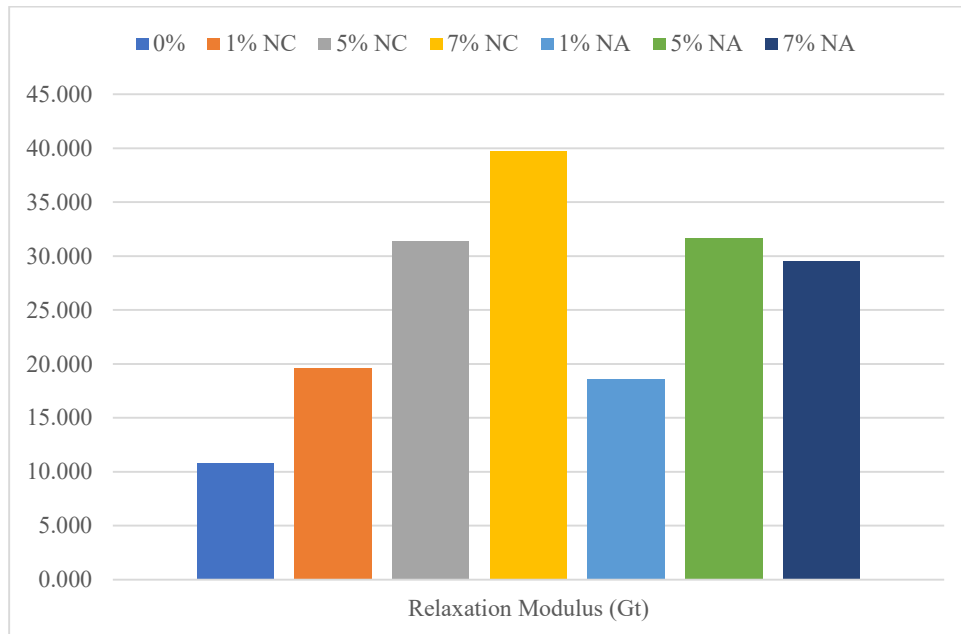


Figure 48. Relaxation Modulus for PAV-aged PG58-28

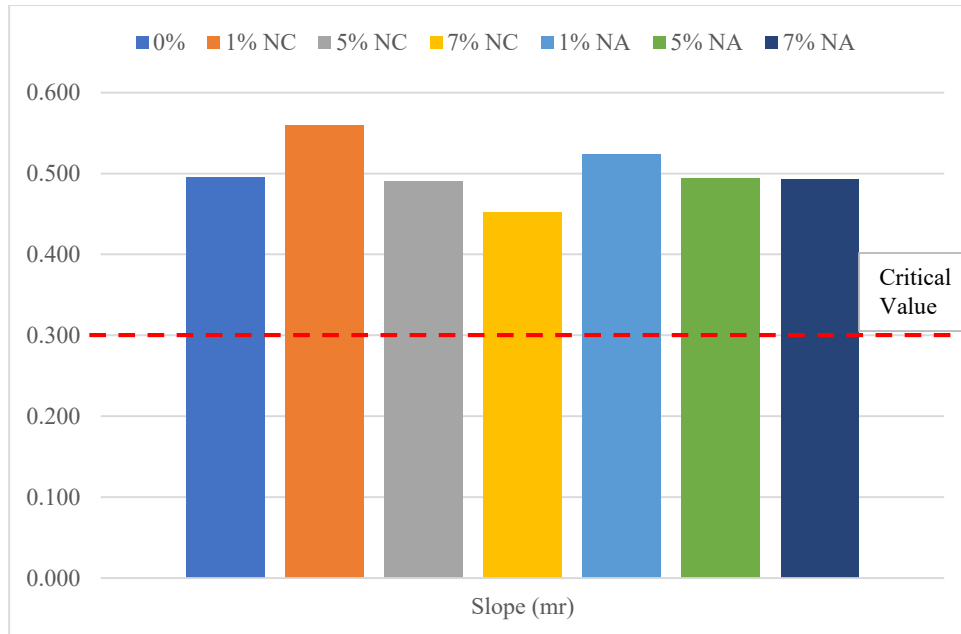


Figure 49. Slope for PAV-aged PG58-28

Figures 50-55 show the effect of NC and NA on low-temperature characteristics at different aging stages of PG64-28 binder. For unaged PG64-28 binder, the 5% NA modification is the optimum Nanomaterial content as shown in Figures 50 and 51. It performed better than the virgin binder by reducing the stiffness and increasing the stress relaxation of the binder. Addition of NC increased the thermal cracking susceptibility at higher content.

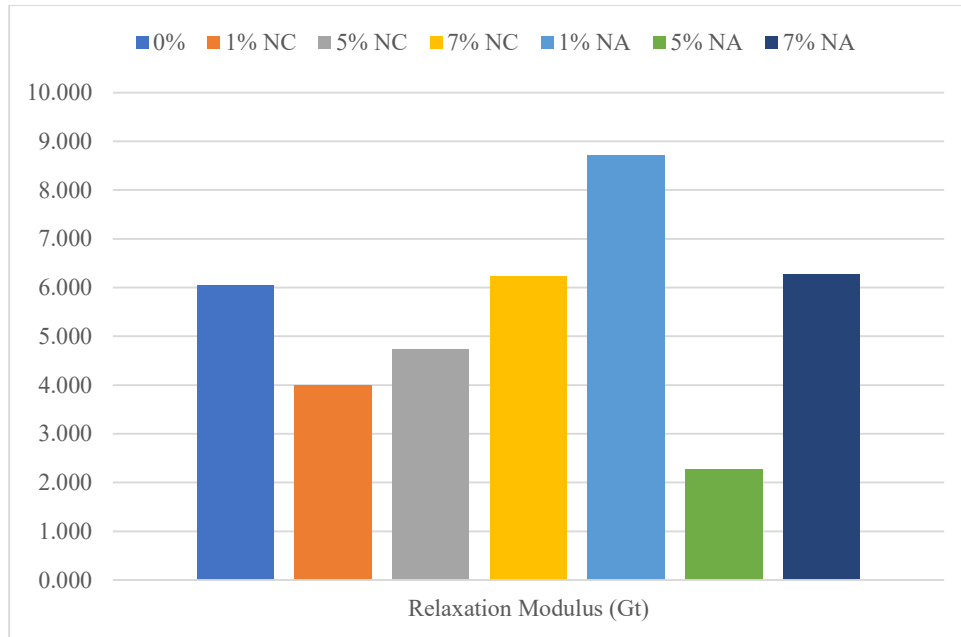


Figure 50. Relaxation Modulus for Unaged PG64-28

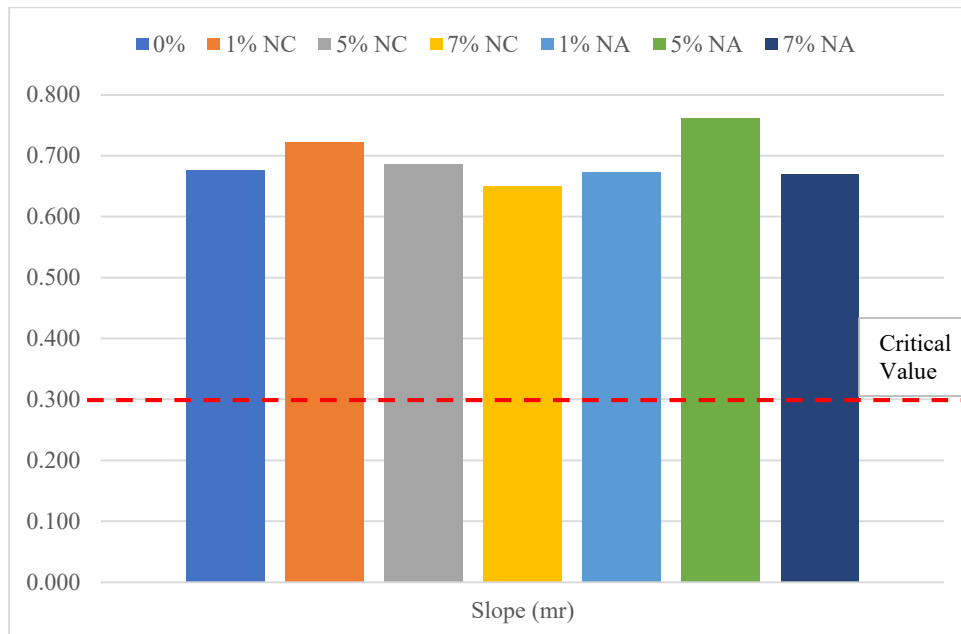


Figure 51. Slope for Unaged PG64-28

Figures 52-53 show that addition of NC to the RTFO-aged PG64-28 binder decreased the creep stiffness and increased the value of slope as compared to the virgin binder. Increasing NC from 1% to 7% made only a slight difference to the creep stiffness

in RTFO-aged PG64-28 binder. 5% NA showed the thermal cracking performance of the binder close to 5% NC.

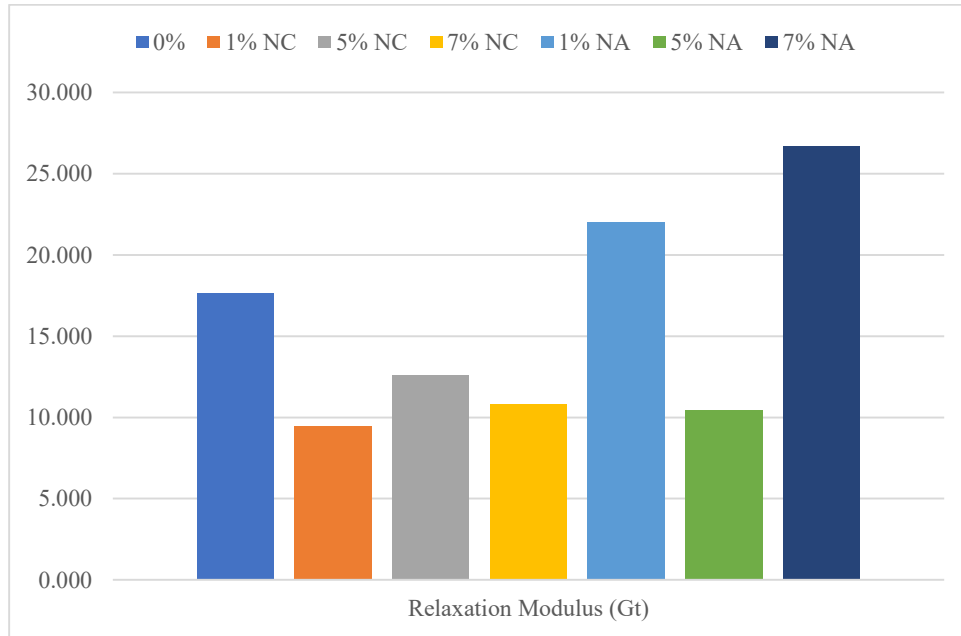


Figure 52. Relaxation Modulus for RTFO-aged PG64-28

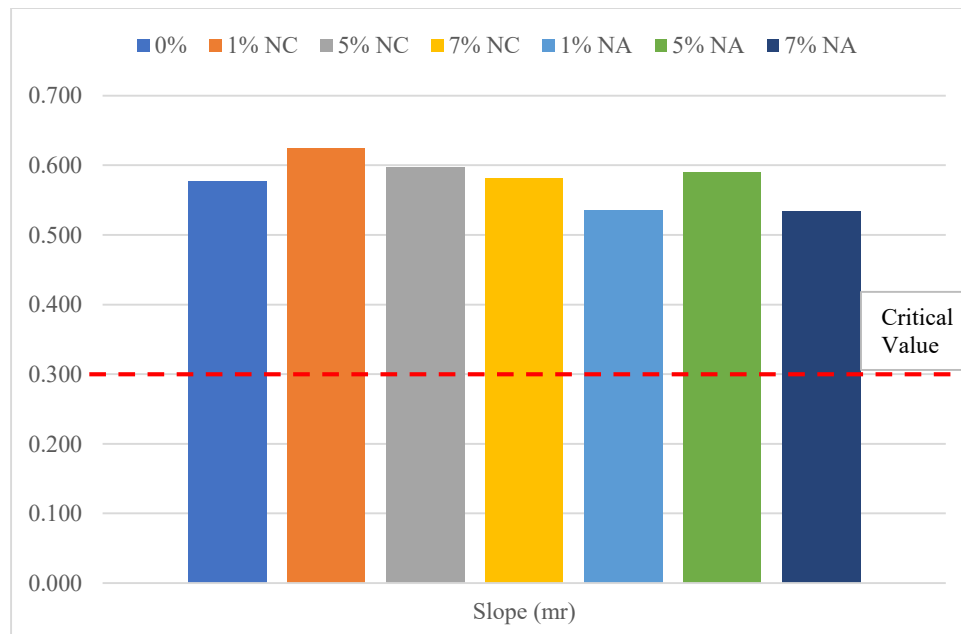


Figure 53. Slope for RTFO-aged PG64-28

For PAV-aged 64-28, Figures 54-55 shows the effect of NM on the thermal cracking of the binder. For both NA and NC modification, 5% content performed the best among all the types of binder used including the virgin binder.

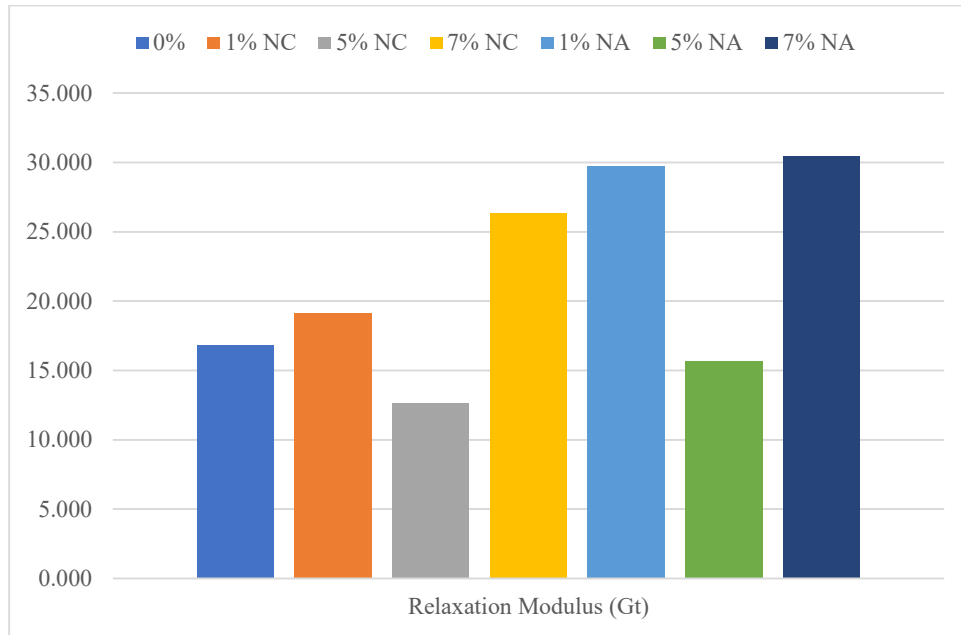


Figure 54. Relaxation Modulus for PAV-aged PG64-28

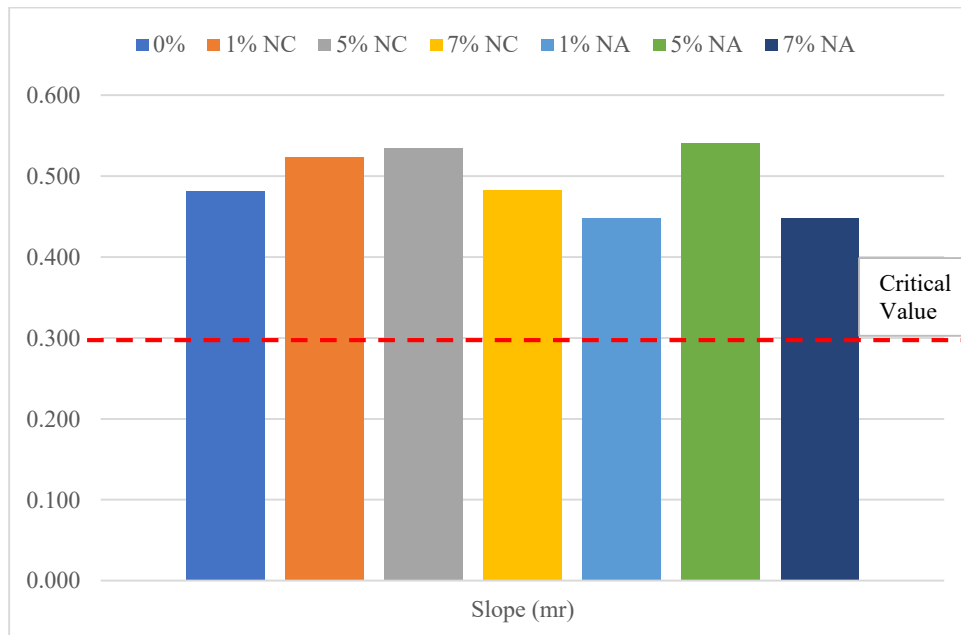


Figure 55. Slope for PAV-aged PG64-28

b. Effect on HMA Mix Performance

Rutting Resistance

APA was used to understand the effect of modifying asphalt binders on the rutting potential of the HMA mixes. All the mixes were prepared by mixing in the lab. Table 9 shows the summary of the average rut depth, standard deviation and coefficient of variation at each quarter for both PG grades and different Nanomaterial content. Due to limited amount of materials available, 4 specimens were prepared for each of virgin and 7% modified binder but for binders with 1% and 5% modified binder, only 2 specimens each was prepared.

From Table 9, NC modification performed as expected in increasing the rutting resistance of the HMA mixes. For both PG58-28 and PG64-28, the rut depth decreased as the NC content increased throughout the test at 2000, 4000, 6000 and 8000 cycles. The trend for NA is different from NC. At 2000 passes, the rut depth decreased as the NA content increased from 1% to 5%, but increased on further increasing the content to 7%. It followed the same progression till the end of the test i.e. 8000 passes. The increase in rut depth as NA increases was not expected. This could have happened either by the uneven mixing of the inadequate Nanomaterials at 1% content or uneven finish of the compaction. The standard deviation and coefficient of variation couldn't be calculated for in Table 9, marked '*', because of the lack of specimens because of limitation on the materials. Figures 56 and 57 display the progression of average rut depth from the opening to the end of the test at 8000 passes for PG58-28 modified with NC and NA

respectively. Figures 58 and 59 show the average rut depth for PG64-28. Figures 60 and 61 show the effect of rutting on the APA specimens before and after the test.

Table 9. APA Results Summary

Binder Grade (PG)	Nano-materials (%)	2000			4000			6000			8000			
		Avg (mm)	St.D. (mm)	COV (%)	Avg (mm)	St.D. (mm)	COV (%)	Avg (mm)	St.D. (mm)	COV (%)	Avg (mm)	St.D. (mm)	COV (%)	
58-28	0	1.065	0.091	8.545	1.197	0.188	15.742	1.250	0.139	11.152	1.302	0.148	11.332	
	%NC	1	1.167	*	*	1.324	*	*	1.417	*	*	1.511	*	*
		5	0.854	*	*	0.964	*	*	1.019	*	*	1.046	*	*
		7	0.718	0.068	9.430	0.742	0.093	12.518	0.823	0.148	17.972	0.833	0.117	14.093
	%NA	1	1.140	*	*	1.312	*	*	1.456	*	*	1.604	*	*
		5	0.841	*	*	0.874	*	*	0.886	*	*	0.888	*	*
		7	0.900	0.063	6.949	0.933	0.013	1.393	0.987	0.102	10.360	1.033	0.036	3.504
64-28	0	3.515	0.994	28.264	4.563	1.316	28.832	5.146	1.406	27.326	5.596	1.384	24.729	
	%NC	1	4.058	*	*	4.922	*	*	5.367	*	*	5.661	*	*
		5	2.598	*	*	3.333	*	*	3.790	*	*	4.093	*	*
		7	1.860	0.048	2.564	2.282	0.007	0.309	2.592	0.061	2.365	2.757	0.051	1.848
	%NA	1	3.701	*	*	4.712	*	*	5.297	*	*	5.709	*	*
		5	1.729	*	*	2.418	*	*	2.857	*	*	3.149	*	*
		7	1.879	0.058	3.069	2.487	0.168	6.758	2.937	0.051	1.744	3.247	0.084	2.579

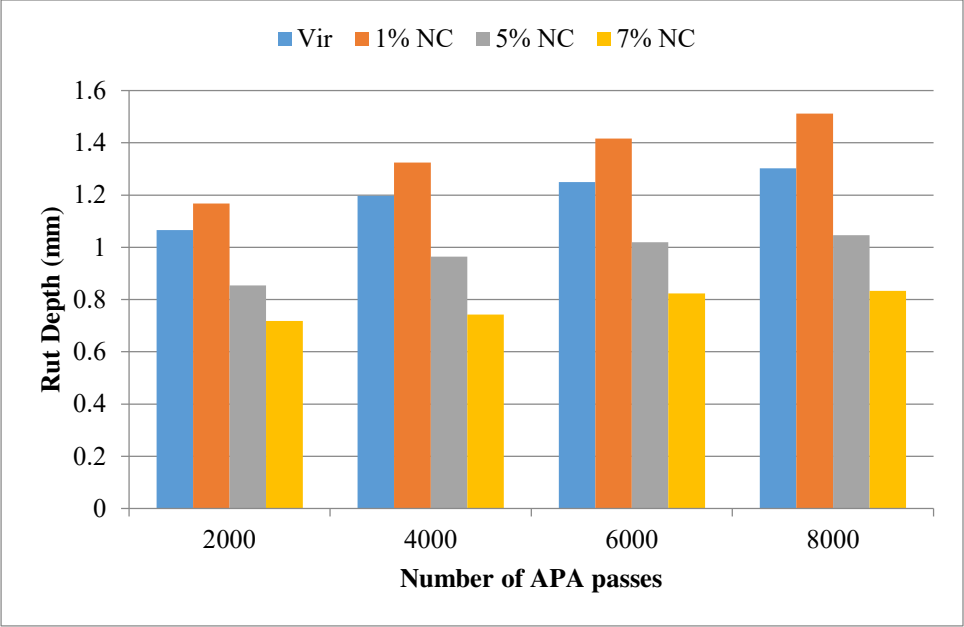


Figure 56. NC Modified PG58-28 Average Rut Depth

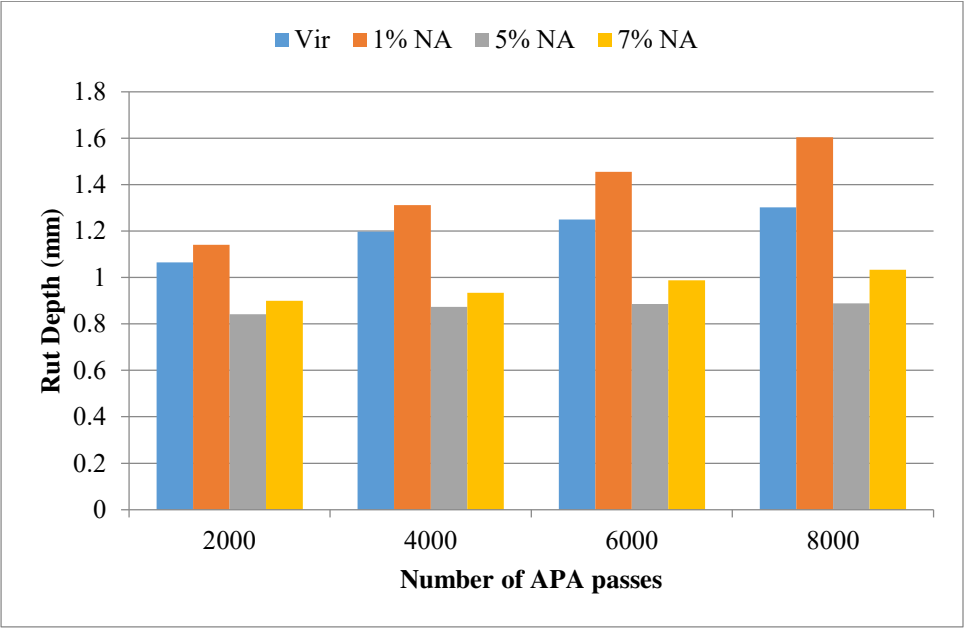


Figure 57. NA Modified PG58-28 Average Rut Depth

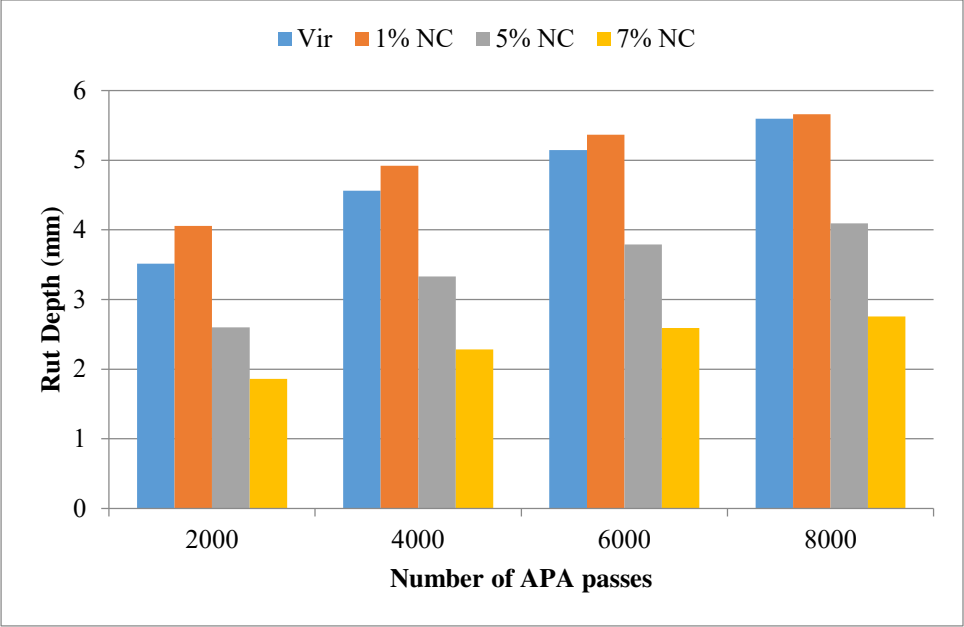


Figure 58. NC Modified PG64-28 Average Rut Depth

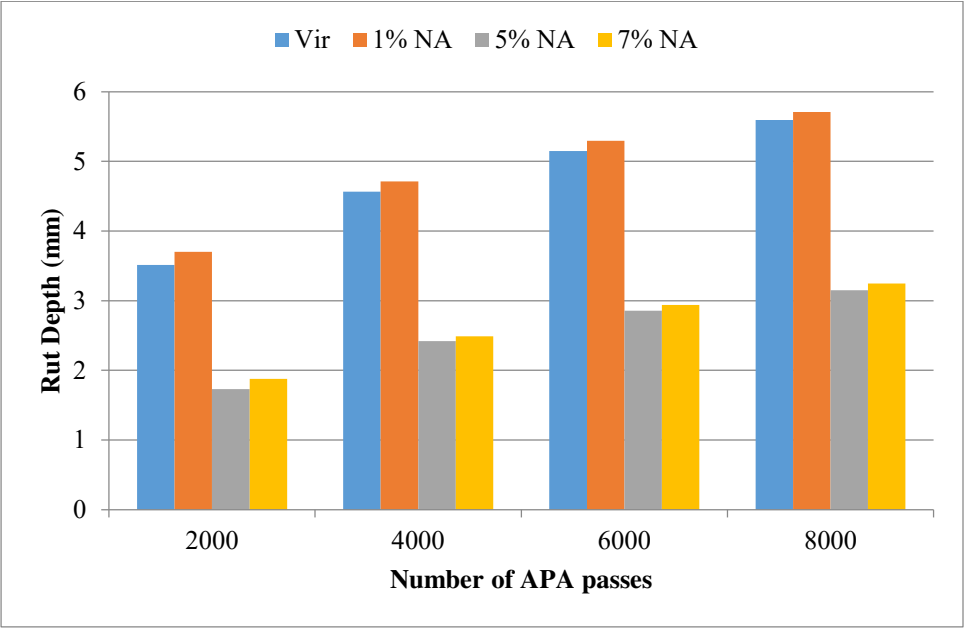


Figure 59. NA Modified PG64-28 Average Rut Depth



Figure 60. Example of APA Specimen Prior to Test



Figure 61. Example of APA Specimen Post-Testing

Average rut depth at each quarter for individual specimens gives an idea about each type of specimen, but to compare the effect of content of Nanomaterial (NM) in each binder type, reduction in rut depth as content is varied is the best alternative. Table 10 shows the reduction in rut depth as both NC and NA content is increased in each type of binder. The reduction in rut depth is higher for 1% to 7% than 0% to 7% due to the increase in rut depth even though the NC was introduced at 1% to virgin binder. Values are highlighted where it was expected for a decrease in rut depth, but results show the opposite. In both PG grades, intervals at 1% to 7% NC and 1% to 5% NA has the highest decrease in rut depth.

Table 10. Effect of NM Content on Reduction in Rut Depth

Nano-material (%)	Interval	58-28				64-28			
		Nanoclay		Nanoalumina		Nanoclay		Nanoalumina	
		Red. In Rut (mm)	% Red.	Red. In Rut (mm)	% Red.	Red. In Rut (mm)	% Red.	Red. In Rut (mm)	% Red.
1	0 to 1	0.209	16.082	0.302	23.196	0.065	1.165	0.113	2.022
2	5 to 7	-0.213	-20.381	0.145	16.340	-1.336	-32.642	0.098	3.126
4	1 to 5	-0.465	-30.788	-0.716	-44.648	-1.568	-27.700	-2.561	-44.853
5	0 to 5	-0.256	-19.658	-0.414	-31.809	-1.503	-26.858	-2.448	-43.738
6	1 to 7	-0.679	-44.894	-0.571	-35.604	-2.904	-51.898	-2.462	-43.129
7	0 to 7	-0.469	-36.032	-0.269	-20.667	-2.839	-50.732	-2.349	-41.979

Further analysis of the rut results was done using independent t-test to determine if there was any significant difference between the mixes. The results from the independent t-tests are shown in Table 11. All the tests were done at 0.05 significance level. The ‘Y’ indicates that there is a significant difference and ‘N’ indicates there is no significant difference between the mixes performance. For both PG grades, there is no significant difference between 0% and 1% content of both NC and NA. There is significant difference in the performance of mix between all other contents of NC for both PG grades besides 0% NC and 5% NC for PG64-28. For both PG grades modified with NA, there is no significant difference between 0% and 1% modified mixes. Similar result is found between 5% NA and 7% NA for PG64-28. For both binder grades, there is no significant difference in the performance of the mixes between the modification of either NA or NC at 1% and 5%, but there is significant difference at 7% modification.

Table 11. APA Independent T-Test Summary

Binder Grade	Mix	At 8000 APA passes						
		0%	1% NC	5% NC	7% NC	1% NA	5% NA	7% NA
PG 58-28	0%	x	N	Y	Y	N	Y	Y
	1% NC	x	x	Y	Y	N	x	x
	5% NC	x	x	x	Y	x	N	x
	7% NC	x	x	x	x	x	x	Y
	1% NA	x	x	x	x	x	Y	Y
	5% NA	x	x	x	x	x	x	Y
	7% NA	x	x	x	x	x	x	x
PG 64-28	0%	x	N	N	Y	N	Y	Y
	1% NC	x	x	Y	Y	N	x	x
	5% NC	x	x	x	Y	x	N	x
	7% NC	x	x	x	x	x	x	Y
	1% NA	x	x	x	x	x	Y	Y
	5% NA	x	x	x	x	x	x	N
	7% NA	x	x	x	x	x	x	x

The air void content and rut depth for each APA sample for both PG58-28 and PG64-28 binder type are correlated in Figures 62 through 65. The correlation in the figures are given by R^2 . Figures 62 and 64 show that NA modification in both PG58-28 and PG64-28 specimens have no correlation between the rut depth and air voids. PG58-28 specimens modified with NC show a weak correlation between rut depth and air voids in Figure 63. Rut depth increases with the decrease in air voids. PG64-28 specimens modified with NC show a strong correlation between rut depth and air voids in Figure 65. Rut depth increases with an increase in air voids.

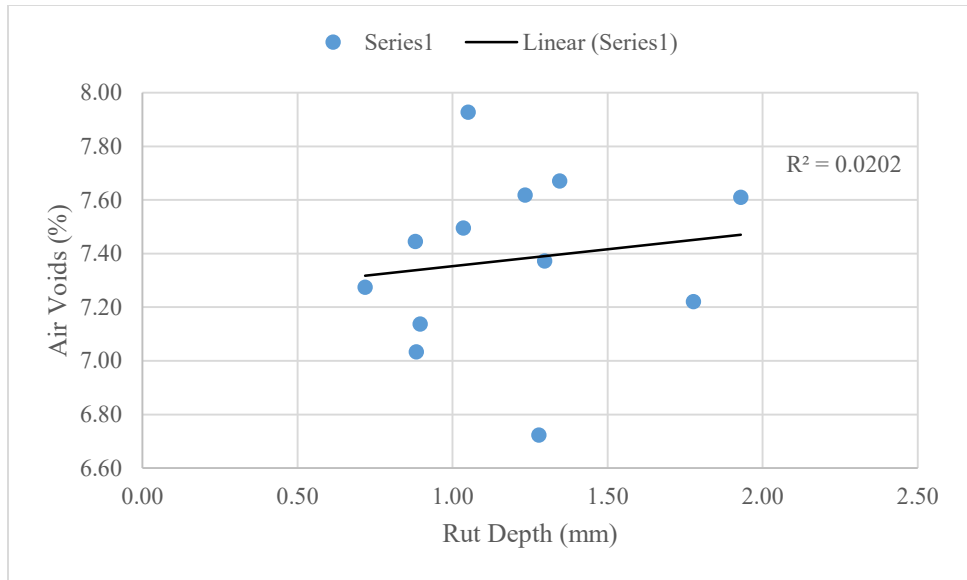


Figure 62. NA Modified PG58-28 Rut Depth vs Air Voids

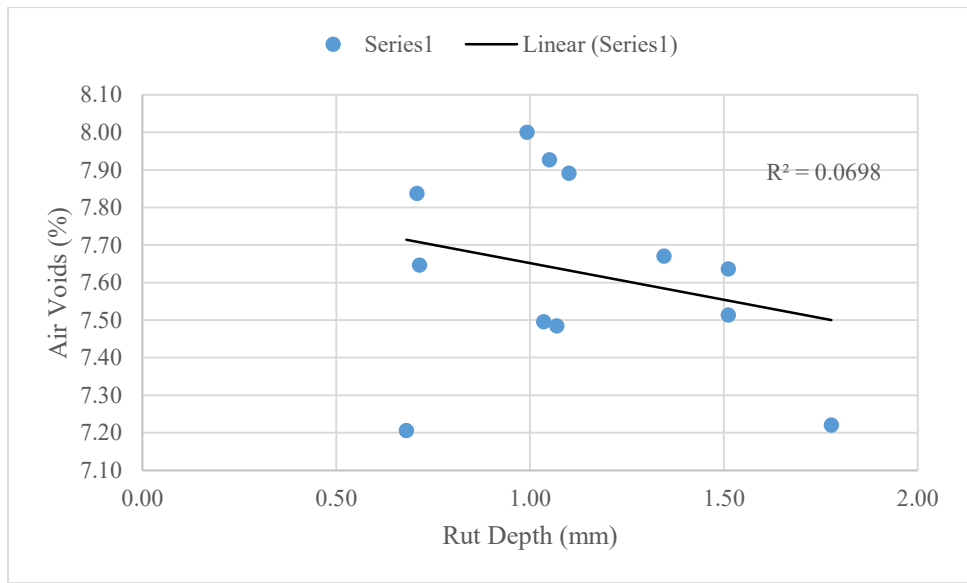


Figure 63. NC Modified PG58-28 Rut Depth vs Air Voids

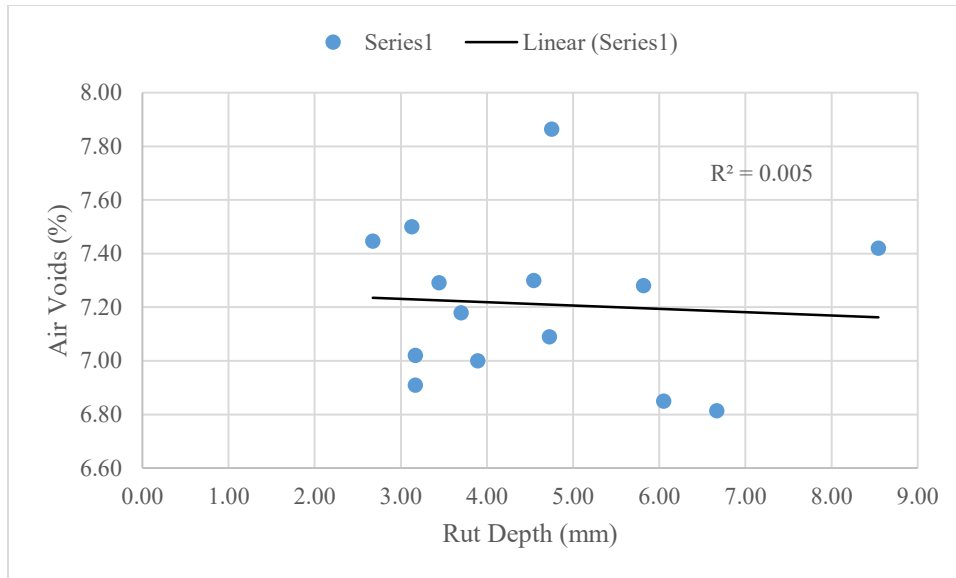


Figure 64. NA Modified PG64-28 Rut Depth vs Air Voids

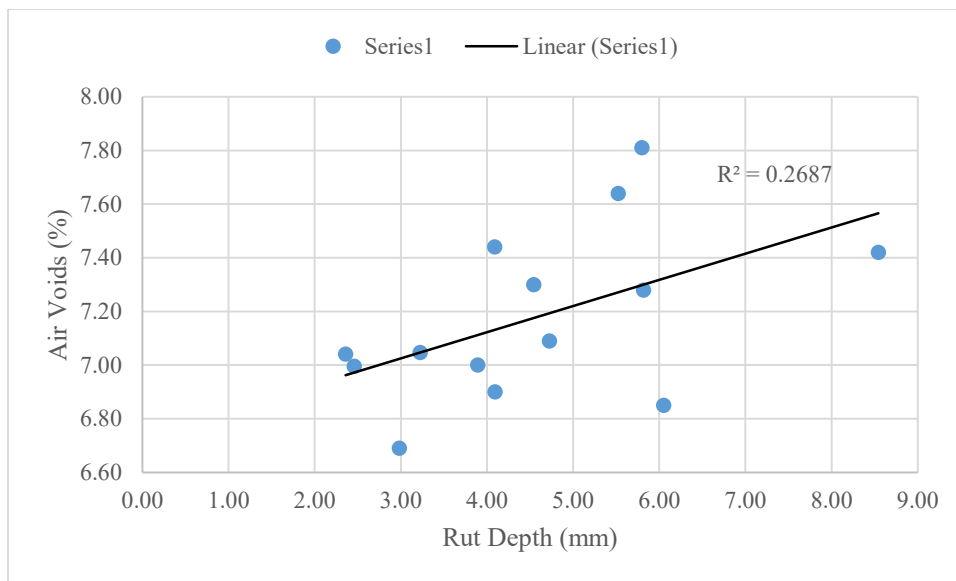


Figure 65. NC Modified PG64-28 Rut Depth vs Air Voids

Fatigue Cracking Resistance

SCB test was used for this analysis in determining fatigue cracking resistance of the mixes. Fracture energy is the variable that is most commonly used in comparing and predicting the performance of the mixes. The measure of fracture energy is calculated as

the area under the curve of load versus displacement as shown in Figure 68. Due to the limited availability of materials, test samples were created in limited amount. The size of the test specimen used was only the half i.e. 25mm instead of commonly used 50mm. Tables 12 and 13 are the results of the fracture energies from I-FIT test and calculated air voids for each sample in PG58-28 while Tables 14 and 15 for PG64-28. Table 16 shows the summary of the results from SCB tests. The average fracture energy decreased with the increase in NMs content in PG58-28 but increased for PG64-28. Inconsistency of the results is explained by the higher coefficient of variation (COV). Air voids are included in the tables to see if there is any correlation with the fracture energies. The fracture energies for the mix is not consistent even for the same mix. This can be a result of using the smaller-size specimen. Figures 66 and 67 show the average fracture energies at varying NM content for PG58-28 and PG64-28 respectively. From Figure 66 the fracture energy of the PG58-28 samples wasn't highly affected by the addition of NC up to 5%. The fracture energy of 7% NC was lower than that of unmodified mix. Addition of 1% NA improved the fracture energy of the mix. The fracture energy decreases as the stiffness of the mix increases, but the samples display the highest average fracture energy for PG64-28 at 7% NC. Figure 69 shows a sample SCB specimen and Figure 70 shows the progression of crack in a sample.

Table 12. PG58-28 SCB Fatigue Fracture Energies

Binder	0%	1%	5%	7%	1% NC	5%	7%
Fracture Energy (J/m²)	741.26	842.17	608.69	822.58	723.53	841.44	592.55
	834.37	958.70	934.41		731.82	649.70	500.37
	716.51		704.09		1166.39	796.29	769.26
					677.95		

Table 13. PG58-28 SCB Samples Air Voids

Binder	0%	1% NA	5% NA	7% NA	1% NC	5% NC	7% NC
Air Voids (%)	7.63	7.18	7.77	6.81	7.00	7.00	7.74
	7.63	7.18	7.77		7.00	7.00	7.75
	7.16		6.95		7.88	7.61	7.75
					7.88		

Table 14. PG64-28 SCB Samples Fatigue Fracture Energies

Binder	0%	1% NA	5% NA	7% NA	1% NC	5% NC	7% NC
Fracture Energy (J/m ²)	1219.60	1632.79	1315.55	1575.48	1079.29	1815.10	1808.87
	1305.77	1574.40	1613.45	1441.28	1553.04	1539.50	1598.24
	1454.15	1163.95	1801.89	1817.91	1643.85	1468.40	1500.32
	1861.16		1622.13		1647.15	1062.57	1819.09
	1892.95						
	1565.42						
	1418.82						
	1606.62						

Table 15. PG64-28 SCB Samples Air Voids

Binder	0%	1% NA	5% NA	7% NA	1% NC	5% NC	7% NC
Air Voids (%)	7.23	7.78	7.01	7.78	6.87	7.16	6.53
	7.23	7.78	7.01	7.02	6.87	7.16	6.53
	7.46	7.16	6.64	7.02	6.78	6.88	6.792
	7.46		6.64		6.78	6.88	6.792
	7.32						
	7.32						
	6.59						
	6.59						

Table 16. SCB Results Summary

Binder	Mix	Average Energy (J/m ²)	St. Dev. (J/m ²)	COV (%)
PG58-28	0%	764.05	62.15	8.13
	1% NA	900.43	82.40	9.15
	5% NA	749.07	167.45	22.35
	7% NA	*	*	*

Table 16. cont.

Binder	Mix	Average Energy (J/m ²)	St. Dev. (J/m ²)	COV (%)
PG58-28	1% NC	824.92	228.87	27.74
	5% NC	762.48	100.24	13.15
	7% NC	620.73	136.64	22.01
PG64-28	0%	1540.56	242.71	15.75
	1% NA	1457.04	255.50	17.54
	5% NA	1588.25	201.49	12.69
	7% NA	1611.56	190.89	11.84
	1% NC	1480.83	271.22	18.32
	5% NC	1471.39	310.87	21.13
	7% NC	1681.63	158.02	9.40

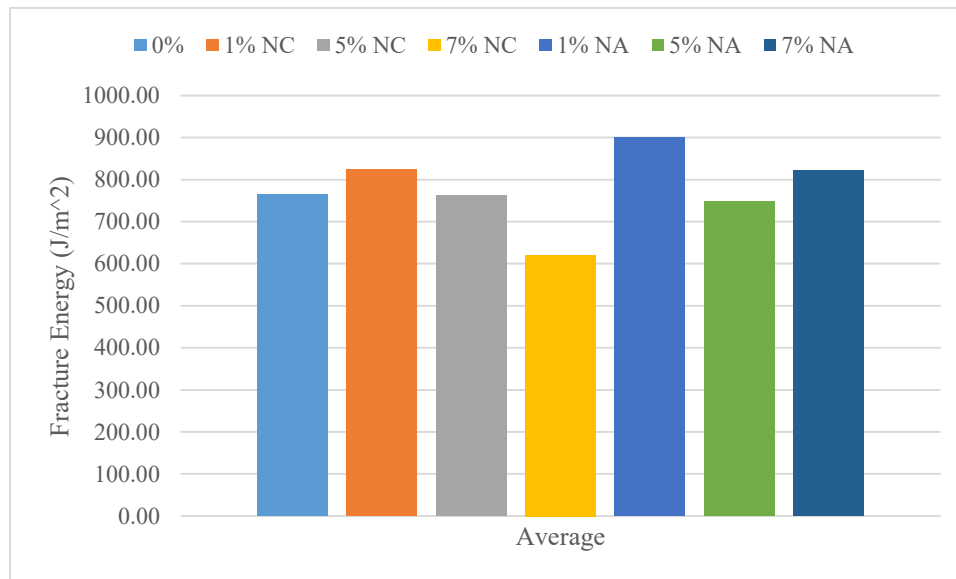


Figure 66. Average Fracture Energies for PG58-28

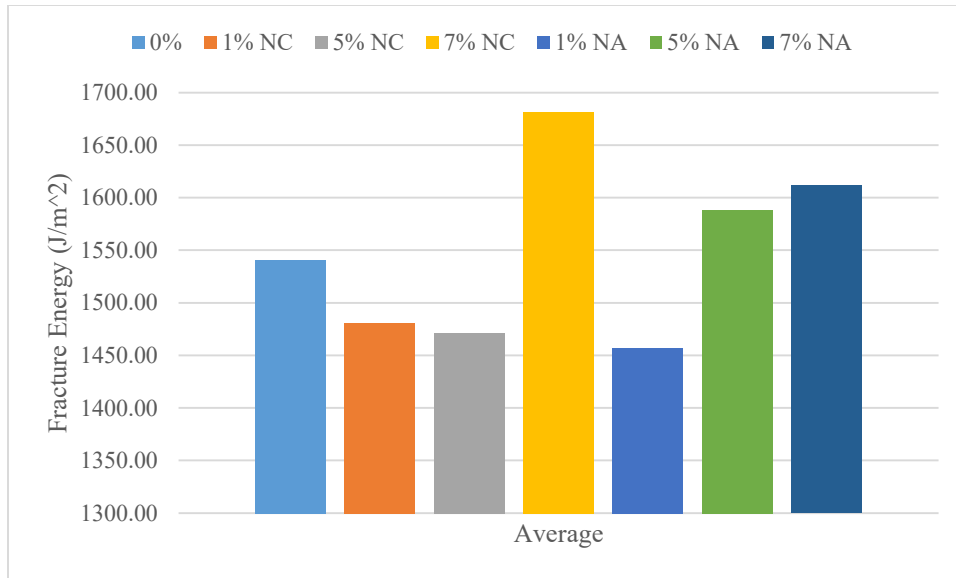


Figure 67. Average Fracture Energies for PG64-28

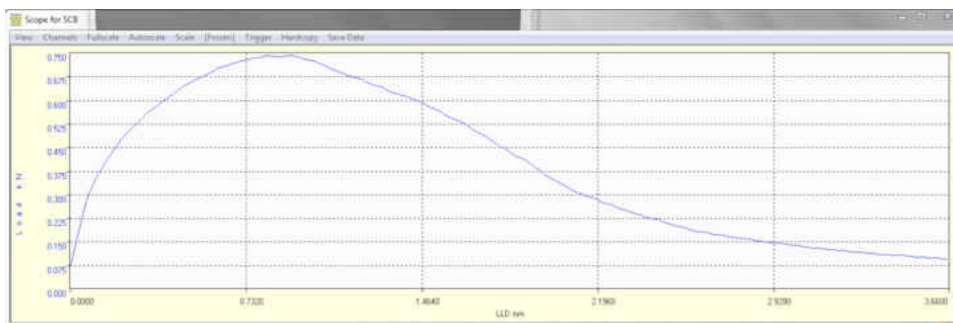


Figure 68. Example energy graph of SCB specimen, load vs displacement



Figure 69. Example of SCB Specimen Prior to Test



Figure 70. Example of SCB Specimen Post-Testing

Independent t-tests were performed on the SCB results to determine if there is any significant difference. Table 17 shows the summary of the result of t-tests. The test couldn't be performed to analyze with 7% NA because a sample failed during the SCB test and the test required at least three samples. For both PG grades, the results show there is no significant difference between any of the mixes tested. These results are inconclusive and the reasons behind the results could be the limited number of samples prepared, unusual specimen height, test temperature, etc.

Table 17. SCB Independent T-Test Summary

Binder Grade	Mix	Binder Mix						
		0%	1% NC	5% NC	7% NC	1% NA	5% NA	7% NA
PG58-28	0%	x	N	N	N	N	N	x
	1% NC	x	x	N	N	N	x	x
	5% NC	x	x	x	N	x	N	x
	7% NC	x	x	x	x	x	x	x
	1% NA	x	x	x	x	x	N	x
	5% NA	x	x	x	x	x	x	x
	7% NA	x	x	x	x	x	x	x
PG64-28	0%	x	N	N	N	N	N	N
	1% NC	x	x	N	N	N	x	x
	5% NC	x	x	x	N	x	N	x
	7% NC	x	x	x	x	x	x	N

Table 17. cont.

Binder Grade	Mix	Binder Mix						
		0%	1% NC	5% NC	7% NC	1% NA	5% NA	7% NA
PG64-28	1% NA	x	x	x	x	x	N	N
	5% NA	x	x	x	x	x	x	N
	7% NA	x	x	x	x	x	x	x

Low Temperature Cracking Performance

The low-temperature cracking test for the mixes were completed using the DCT test. Fracture energy is used to predict the performance of the mix against low-temperature cracking. Fracture energy is calculated as the area under the curve of load versus Crack Mouth Opening Displacement (CMOD). Figure 73 shows an example of graph plotted by the program within DCT machine. Tables 18 and 19 display the results of DCT test for mixes in terms of fracture energy and their respective air voids while Tables 20 and 21 display similar results for PG64-28. Summary statistics of the DCT results can be found in Table 22. Due to limited availability of mixes, only two samples were produced for each binder type. Figures 71 and 72 portray the graphs of average fracture energies of the mixes for PG58-28 and PG64-28, respectively. All modified PG58-28 samples performed better than the unmodified mix samples. From Figure 71, 5% NC modified and 1% NA modified samples have similar and the highest average fracture energies. At 7% NC, the fracture energy reduces significantly in Figure 71. Nanoclay modified samples performed better than Nanoalumina modified samples as shown in Figure 72. The progression of average fracture energy can be seen to increase from 1% NC to 7% NC modified samples. Individual t-tests were not performed for this

test because of insufficient number of samples. Figures 74 and 75 show an example of specimen before and after the test for understanding the progression of crack.

Table 18. PG58-28 DCT Samples Fracture Energies

Binder	0%	1% NA	5% NA	7% NA	1% NC	5% NC	7% NC
Fracture Energy (J/m ²)	249	266	300	243	311	266	244
	250	263	285	274	267	*	276

Table 19. PG58-28 DCT Samples Air Voids

Binder	0%	1% NA	5% NA	7% NA	1% NC	5% NC	7% NC
Air Voids (%)	7.62	7.18	7.77	6.81	7.00	7.00	7.74
	7.15	7.21	6.95	7.35	7.88	7.61	7.75

Table 20. PG64-28 DCT Samples Fracture Energies

Binder	0%	1% NA	5% NA	7% NA	1% NC	5% NC	7% NC
Fracture Energy (J/m ²)	519	433	383	519	487	665	695
	530	351	387	485	452	456	465
	525						
	512						

Table 21. PG64-28 DCT Samples Air Voids

Binder	0%	1% NA	5% NA	7% NA	1% NC	5% NC	7% NC
Air Voids (%)	7.28	7.78	7.01	7.78	6.87	7.16	6.53
	7.42	7.16	6.64	7.02	6.78	6.88	6.79
	7.32						
	6.59						

Table 22. DCT Results Summary

Binder	Mix	Average Energy (J/m ²)	St. Dev. (J/m ²)	COV (%)
PG58-28	0%	249.5	0.71	0.28
	1% NA	264.5	2.12	0.80
	5% NA	292.5	10.61	3.63

Table 22. cont.

Binder	Mix	Average Energy (J/m ²)	St. Dev. (J/m ²)	COV (%)
PG58-28	7% NA	258.5	21.92	8.48
	1% NC	289.0	31.11	10.77
	5% NC	266.0	*	*
	7% NC	260.0	22.63	8.70
PG64-28	0%	521.5	7.77	1.49
	1% NA	392.0	57.98	14.79
	5% NA	385.0	2.83	0.73
	7% NA	502.0	24.04	4.79
	1% NC	469.5	24.75	5.27
	5% NC	560.5	147.79	26.37
	7% NC	580.0	162.63	28.04

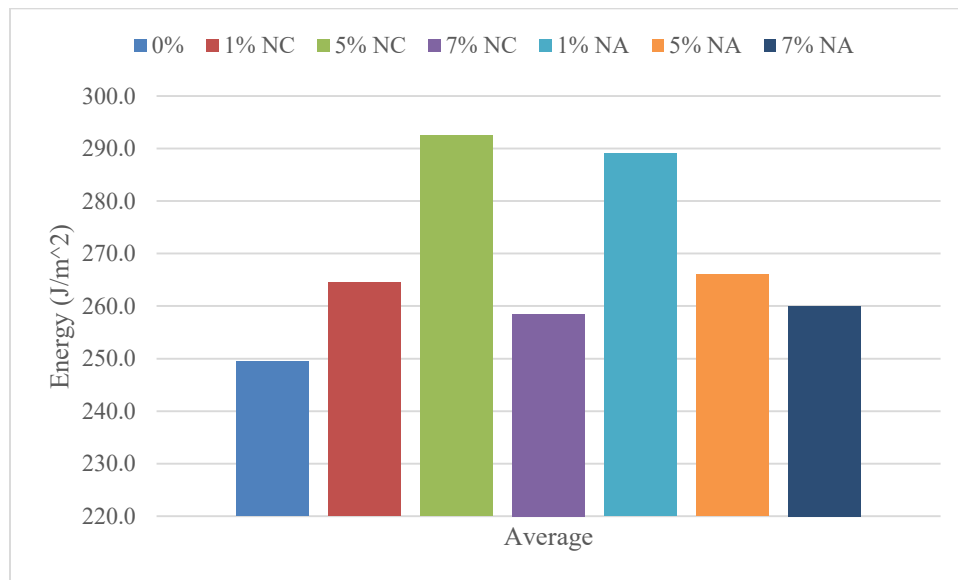


Figure 71. Average Fracture Energies for PG58-28

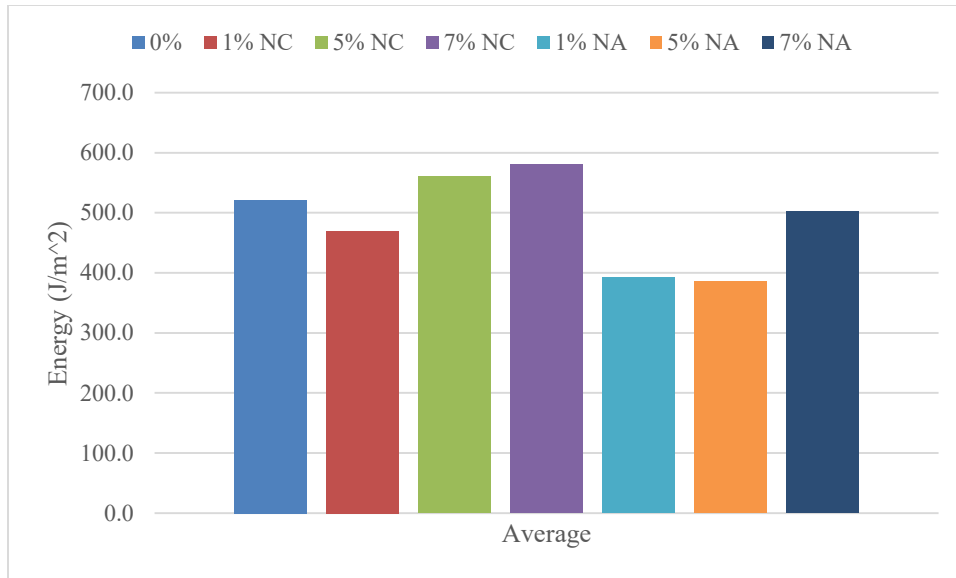


Figure 72. Average Fracture Energies for PG64-28

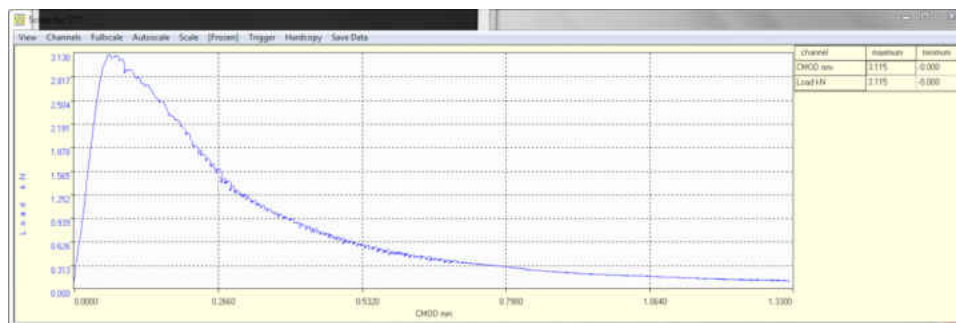


Figure 73. Example DCT Graph of Load vs CMOD



Figure 74. Example of DCT Specimen Prior to Test



Figure 75. Example of DCT Specimen Post-Testing

Chapter V

CONCLUSIONS

Nanoclay and Nanoalumina Improved the Rutting Resistance

The analysis of the results obtained from the binder's high performance grade temperature test performed in the DSR showed addition of Nanoclay and Nanoalumina improved the rutting resistance. Nanoclay is more effective than Nanoalumina in increasing the rutting resistance. For higher Nanomaterial content, the binder's high temperature grade could increase by one or more grade.

The APA results showed that the addition of Nanoclay and Nanoalumina increases the rutting resistance of the pavement specimens. The rutting resistance of the specimens is increased with the increase in Nanoclay content. The resistance increased up to 5% content but started to drop on further increase of Nanoalumina. The statistical analysis of the mixes in this research was inconclusive.

Fatigue Resistance Declined by the Addition of Nanoalumina and Nanoclay

Addition of Nanomaterials results in higher susceptibility of binder to fatigue cracking in general. Binder modification and the simulated long-term aging increased the stiffness of the binder significantly making the modified binder more vulnerable to fatigue cracking.

The SCB results did not show any specific progression as Nanomaterial content increases for both binder grades. A statistical analysis did not show any significant difference in all the mixes. One reason for such variation in results can be the use of non-standard sized specimen.

Susceptibility to Thermal Cracking Increases with Nanoclay content, Nanoalumina Results Vary with the Binder Grade

The analysis of results from the DSR at the low-temperature of performance grade reveal that with the increase in Nanoclay, the stiffness of the binder increases resulting in higher thermal stresses and lower ability of the binder to relax stresses. Results are not consistent with the Nanoalumina, 7% Nanoalumina for PG58-28 and 5% Nanoalumina for PG64-28 performed the best among other Nanoalumina contents.

The DCT results were inconclusive possibly because due to limited number of specimens and statistical analysis couldn't be conducted.

Nanoalumina is Significant Only After Aging

Based on the results from the DSR, the effect of Nanoalumina is more significant after aging. The performance of the modified binder after a certain content is not affected by any further addition of Nanoalumina.

CHAPTER VI

LIMITATIONS AND FUTURE WORK

LIMITATIONS

During this research, there were a few limitations on mixes which could have influenced the results. The value of maximum specific gravity (G_{mm}) is the key factor for the calculation of air voids in the mix specimens. But it was assumed to be as provided in the field mix design due to time and material constraints. The specimen sizes used in the SCB test were not the standard size recommended by the I-FIT due to limited materials. Limited materials led to limited specimen preparation for the DCT and SCB tests which could be a reason for inconclusive results.

FUTURE WORK

Further investigation into the effect of Nanoalumina on binder needs to be done to validate the data collected in this study. Additional tests for the Nanoalumina modified binder should be done at all temperature range to confirm the results presented in this research. Detail analysis of DSR results at all temperatures should be done to find the optimum content of Nanoalumina and Nanoclay to enhance the performance of binder.

A few maximum specific gravity tests should be done in the lab before producing any mix specimens. Additional mix specimens for APA, SCB and DCT must be created after estimating the maximum specific gravity. Standard sized specimens should be used

for all types of tests to compare the results with other researchers. Sufficient samples need to be created to increase the accuracy of each test performed.

REFERENCES

- Ali, S. I., Ismail, A., Mohammed, N. I., Hassan, Y. N., & Ibrahim, A. N. (2016). Characterization of the Performance of Aluminum Oxide Nanoparticles Modified Asphalt Binder. *Jurnal Teknologi*, 91-96.
- Al-Qadi, I., Ozer, H., Lambros, J., Khatib, A. E., Singhvi, P., Khan, T., . . . Doll, B. (2015). *Testing Protocols to Ensure Performance of High Asphalt Binder Replacement Mixes Using RAP and RAS*. Urbana: Illinois Department of Transportation.
- Arabani, M., & Ferdowski, B. (2009). Evaluating the Semi-Circular Bending Test for HMA Mixtures. *International Journal of Engineering A: Basics*, 47-58.
- Brovelli, C., Crispino, M., Pais, J., & Pereira, P. (2015). Using polymers to improve the rutting resistance of asphalt concrete. *Construction and Building Materials*, 117-123.
- Canestrari, F., Stimilli, A., Bahia, H. U., & Virgili, A. (2015). Canestrari, F., Stimilli, A., Bahia, H. U., & Virgili, A. (2015). Pseudo-variables method to calculate HMA relaxation modulus through low-temperature induced stress and strain. *Materials and Design*, 141-149.
- Chollar, B., & Memon, M. (1997). *Where the tire meets the road*. Washington: Federal Highway Administration.

- Cominsky, R. J., Huber, G. A., Kennedy, T. W., & Anderson, M. (1994). *The Superpave Mix Design Manual for New Construction and Overlays*. Washington, DC: National Research Council.
- Dore, G., & Zubeck, H. K. (2009). *Cold Regions Pavement Engineering*. Quebec City: ASCE Press.
- El-Korchi, T., & Mallick, R. B. (2009). *Pavement Engineering - Principles and Practice*. Boca Raton, FL: CRC Press.
- Elseifi, M. A., Mohammad, L. N., Ying, H., & Cooper III, S. (2012). Modeling and evaluation of the cracking resistance of asphalt mixtures using the semi-circular bending test at intermediate temperatures. *Road Materials and Pavement Design*, 124-139.
- Farrar, M., Sui, C., Salmans, S., & Qin, Q. (2015). Determining the low-temperature rheological properties of asphalt binder using a dynamic shear rheometer (DSR). *Western Research Institute*, 1-62.
- Golestani, B., Nam, B. H., Nejad, F. M., & Fallah, S. (2015). Nanoclay application to asphalt concrete: Characterization of polymer and linear nanocomposite-modified asphalt binder and mixture. *Construction and Building Materials*, 32-38.
- Hill, B., Oldham, D., Behnia, B., Fini, E., Buttlar, W., & Reis, H. (2013). Low-temperature performance characterization of biomodified asphalt mixtures that contain reclaimed asphalt pavement. *Transportation Research Record: Journal of the Transportation Research Board*, 49-57.

- Huang, B., Shu, X., & Zuo, G. (2013). Using notched semi circular bending fatigue test to characterize fracture resistance of asphalt mixtures. *Engineering Fracture Mechanics*, 78-88.
- Huang, Y. H. (2004). *Pavement Analysis and Design*. Upper Saddle River, NJ: Pearson Education, Inc.
- Interactive, P. (2016, October 10). *Dynamic Shear Rheometer*. Retrieved from Pavement Interactive: <http://www.pavementinteractive.org/dynamic-shear-rheometer/>
- Jahromi, S. G., & Khodaii, A. (2009). Effects of nanoclay on rheological properties of bitumen binder. *Construction and Building Materials*, 2894-2904.
- Kandhal, P. S., & Foo, K. Y. (1997). Designing recycled hot mix asphalt mixtures using Superpave technology. *Progress of Superpave (Superior Performing Asphalt Pavement): Evaluation and Implementation*, 1-18.
- Khan, S., Nagabhushana, M., Tiwari, D., & Jain, P. (2013). Rutting in Flexible Pavement: An approach of evaluation with Accelerated Pavement Testing Facility. *Procedia Social and Behavioral Sciences*, 149-157.
- Lotfi-Eghlim, A., & Karimi, M. S. (2016). Fatigue Behavior of Hot Mix Asphalt Modified with Nano Al₂O₃ - An Experimental Study. *Advances in Science and Technology Research Journal*, 58-63.
- Nejad, M. F., Aflaki, E., & Mohammadi, M. (2010). Fatigue behavior of SMA and HMA mixtures. *Construction and Building Materials*, 1158-1165.

- Saeidi, H., & Aghayan, I. (2016). Investigating the effects of aging and loading rate on low-temperature cracking resistance of core-based asphalt samples using semi-circular bending test. *Construction and Building Materials*, 682-690.
- Sargious, M. (1975). *Pavements and Surfacing for Highways and Airports*. Barking, Essex, England: Applied Science Publishers Ltd.
- Shafabakhsh, G., M., S., & Y., S. (2014). Case Study of Rutting Performance of HMA modified with waste rubber powder. *Case Studies in Construction Materials*, 69-76.
- Shafabakhsh, G., Sadeghnejad, M., & Chelovian, A. (2015). Experimental Study on Creep behavior of Stone Mastic Asphalt by Using of Nano Al₂O₃. *International Journal of Scientific & Engineering Research*, 903-911.
- Sibal, A., Das, A., & Pandey, B. (2000). Flexural fatigue characteristics of asphalt concrete with crumb rubber. *International Journal of Pavement Engineering*, 119-132.
- Sui, C., Farrar, M. J., Tuminello, W. H., & Turner, T. F. (2010). New technique for measuring low-temperature properties of asphalt binders with small amounts of material. *Transportation Research Record: Journal of the Transportation Research Board*, 23-28.
- Sui, C., Farrar, M., Harnsberger, P. M., Tuminello, W., & Turner, T. (2011). New low-temperature performance-grading method: Using 4-mm parallel plates on a

- dynamic shear rheometer. *Transportation Research Record: Journal of the Transportation Research Board*, 43-48.
- Tian, X., Zheng, J., & Zhang, Q. (2004). Effect of aging on viscoelastic performance of asphalt binder. *SATC 2004*, 226-232.
- Uddin, W. (2003). Viscoelastic Characterization of Polymer-Modified Asphalt Binders of Pavement Applications. *Applied Rheology*, 191-199.
- Van de Ven, M., Molenaar, A., & Besamusca, J. (2009). Nanoclay for binder modification of asphalt mixtures. *7th International RILEM Symposium on Advanced Testing and Characterization of Bituminous Materials* (pp. 133-142). Rhodes: Taylor & Francis Group.
- Wu, Z., Mohammad, L. N., Wang, L. B., & Mull, M. A. (2005). Fracture resistance characterization of superpave mixtures using the semi-circular bending test. *Journal of ASTM International*, 1-15.
- Xiao, F., Amirkhanian, S. N., & Putman, B. J. (2002). Evaluation of Rutting Resistance in Warm-Mix Asphalts Containing Moist Aggregate. *Transportation Research Record*, 75-84.
- Xiao, F., Amirkhanian, S., Wang, H., & Hao, P. (2014). Rheological property investigations for polymer and polyphosphoric acid modified asphalt binders at high temperatures. *Constructions and Building Materials*, 316-323.
- Yang, J., & Tighe, S. (2013). A review of advances of nanotechnology in asphalt mixtures. *Procedia-Social and Behavioral Sciences*, 1269-1276.

Yao, H., You, Z., Li, L., Shi, X., Goh, S. W., Mills-Beale, J., & Wingard, D. (2012).

Performance of asphalt binder blended with non-modified and polymer-modified nanoclay. *Construction and Building Materials*, 159-170.

Yoder, E. J. (1959). *Principles of Pavement Design*. New York: John Wiley & Sons, Inc.

You, Z., Mills-Beale, J., Foley, J. M., Roy, S., Odegard, G. M., Dai, Q., & Goh, S. W.

(2011). Nanoclay-modified asphalt materials: Preparation and characterization. *Construction and Building Materials*, 1072-1078.

Yusoff, N., Breem, A., Alattug, H., Hamim, A., & Ahmad, J. (2014). The effects of moisture susceptibility and ageing conditions on nano-silica/polymer-modified asphalt mixtures. *Construction and Building Materials*, 139-147

APPENDIX

HOT MIX DESIGN DATA - SUPERPAVE

<p>Lab. No. Location Project</p> <p>Distric County Date Pit Owner(s)</p> <p>Pit #1 Location Pit #2 Location Pit #3 Location</p>	<p>IM-6-029(127)126</p> <p>Grand Forks County</p> <p>Strata</p> <p>Pit 443 W1/2 SW1/4 21-156-56 Pit 218 16-149-44 Pit 441 10-155-36</p>	<p>Project Specification Type of AC (top lift) Type of AC (sub lift) Lifting Date Pign #4 (%) Minus #4 (%)</p> <p>Gyratory Compactive Effort Ninitial Ndesign Nmaximum</p>	<p>Section 410 PG 64-28</p> <p>36.3 63.7</p> <p>7 75 115</p>																																																																
<p>Mix Properties at Recommended Asphalt Content</p> <table border="0" style="width: 100%;"> <thead> <tr> <th></th> <th>Mix Design</th> <th>Specification</th> </tr> </thead> <tbody> <tr><td>Optimum AC (%)</td><td>5.8</td><td></td></tr> <tr><td>Density (pcf)</td><td>145.4</td><td></td></tr> <tr><td>Air Voids (%)</td><td>4.0</td><td>2.5 - 5.0</td></tr> <tr><td>VMA (%)</td><td>15.7</td><td>14.0 Min.</td></tr> <tr><td>VFA (%)</td><td>74.0</td><td>65 - 75%</td></tr> <tr><td>%Gmm @ Ninitial</td><td>88.3</td><td>89% Max.</td></tr> <tr><td>%Gmm @ Nmaximum</td><td>97.0</td><td>98.0% Max.</td></tr> <tr><td>AC Film Thickness (m)</td><td>9.9</td><td>7.5 - 13</td></tr> <tr><td>Dust/Effective AC Ratio</td><td>1.0</td><td>0.6 - 1.3</td></tr> <tr><td>Fine Agg Angularity (%)</td><td>45.3</td><td>45% Min.</td></tr> <tr><td>Sand Equivalent (%)</td><td>58.1</td><td>40% Min.</td></tr> <tr><td>Coarse Agg Angularity (%)</td><td>51.0</td><td>85% Min.</td></tr> <tr><td>Flake/elongated Pieces (%)</td><td>1.0</td><td>10% Max.</td></tr> </tbody> </table>			Mix Design	Specification	Optimum AC (%)	5.8		Density (pcf)	145.4		Air Voids (%)	4.0	2.5 - 5.0	VMA (%)	15.7	14.0 Min.	VFA (%)	74.0	65 - 75%	%Gmm @ Ninitial	88.3	89% Max.	%Gmm @ Nmaximum	97.0	98.0% Max.	AC Film Thickness (m)	9.9	7.5 - 13	Dust/Effective AC Ratio	1.0	0.6 - 1.3	Fine Agg Angularity (%)	45.3	45% Min.	Sand Equivalent (%)	58.1	40% Min.	Coarse Agg Angularity (%)	51.0	85% Min.	Flake/elongated Pieces (%)	1.0	10% Max.	<p>Summary of Aggregate Characteristics from Mix Design</p> <table border="0" style="width: 100%;"> <thead> <tr> <th>Gradation (% passing)</th> <th></th> </tr> </thead> <tbody> <tr><td>5/8"</td><td>100.0</td></tr> <tr><td>1/2"</td><td>96.4</td></tr> <tr><td>3/8"</td><td>84.0</td></tr> <tr><td>#4</td><td>63.7</td></tr> <tr><td>#8</td><td>51.1</td></tr> <tr><td>#16</td><td>36.3</td></tr> <tr><td>#30</td><td>24.2</td></tr> <tr><td>#50</td><td>9.9</td></tr> <tr><td>#100</td><td>6.3</td></tr> <tr><td>#200</td><td>5.0</td></tr> </tbody> </table>		Gradation (% passing)		5/8"	100.0	1/2"	96.4	3/8"	84.0	#4	63.7	#8	51.1	#16	36.3	#30	24.2	#50	9.9	#100	6.3	#200	5.0
	Mix Design	Specification																																																																	
Optimum AC (%)	5.8																																																																		
Density (pcf)	145.4																																																																		
Air Voids (%)	4.0	2.5 - 5.0																																																																	
VMA (%)	15.7	14.0 Min.																																																																	
VFA (%)	74.0	65 - 75%																																																																	
%Gmm @ Ninitial	88.3	89% Max.																																																																	
%Gmm @ Nmaximum	97.0	98.0% Max.																																																																	
AC Film Thickness (m)	9.9	7.5 - 13																																																																	
Dust/Effective AC Ratio	1.0	0.6 - 1.3																																																																	
Fine Agg Angularity (%)	45.3	45% Min.																																																																	
Sand Equivalent (%)	58.1	40% Min.																																																																	
Coarse Agg Angularity (%)	51.0	85% Min.																																																																	
Flake/elongated Pieces (%)	1.0	10% Max.																																																																	
Gradation (% passing)																																																																			
5/8"	100.0																																																																		
1/2"	96.4																																																																		
3/8"	84.0																																																																		
#4	63.7																																																																		
#8	51.1																																																																		
#16	36.3																																																																		
#30	24.2																																																																		
#50	9.9																																																																		
#100	6.3																																																																		
#200	5.0																																																																		
<p>Maximum SpG @ Ndes 2.427</p> <p>Frac. Faces Fine (%) 63.3 Frac. Faces Course (%) 92.8</p>		<p>Asphalt Absorption (%) 0.70 Water Absorption (%) 1.19 Light Wt Particles (%) 2.4 Toughness (% Loss)</p>																																																																	
<p>Final Aggregate Blend (%)</p> <table border="0" style="width: 100%;"> <tr><td>51</td><td>Crushed Rock</td><td>Pit 443</td></tr> <tr><td>26</td><td>Natural Fines</td><td>Pit 218</td></tr> <tr><td>16</td><td>Wash Frc Sand</td><td>Pit 441</td></tr> <tr><td>27</td><td>Crusher Fines</td><td>Pit 443</td></tr> </table>		51	Crushed Rock	Pit 443	26	Natural Fines	Pit 218	16	Wash Frc Sand	Pit 441	27	Crusher Fines	Pit 443	<p>Specific Gravity Information</p> <table border="0" style="width: 100%;"> <tr><td>Bulk (Gsb)</td><td>2.609</td></tr> <tr><td>Apparent (Gsa)</td><td>2.718</td></tr> <tr><td>Effective (Gme)</td><td>2.658</td></tr> </table>		Bulk (Gsb)	2.609	Apparent (Gsa)	2.718	Effective (Gme)	2.658																																														
51	Crushed Rock	Pit 443																																																																	
26	Natural Fines	Pit 218																																																																	
16	Wash Frc Sand	Pit 441																																																																	
27	Crusher Fines	Pit 443																																																																	
Bulk (Gsb)	2.609																																																																		
Apparent (Gsa)	2.718																																																																		
Effective (Gme)	2.658																																																																		
<p>Remarks:</p> <hr/> <hr/> <hr/> <hr/> <hr/> <hr/> <hr/> <hr/>																																																																			
<p>Distribution: Materials and Research 0</p>																																																																			

Figure 76. PG58-28 HMA Mix Design Summary

HOT MIX DESIGN DATA - SUPERPAVE

Department of Transportation, Materials and Research (Rev. 3/18)

5/5/15

Mix Design Company: Knife River Materials

Loc. No.	I-29 near St Thomas Rosemont	Project Specification	Section 430
Location	SIM-G-028(128)(183) PCN-20798	Type of AC (top lift)	64-28
Project	NH-G-081(085)204 PCN-21130	Type of AC (bottom)	36-28
District	Grand Forks	Testing Date	12/7/15
County	Pembina, Walsh	Plus #4 (%)	33.5
Data	5/8"10	Minus #4 (%)	68.2
PI Owner(s)	Troygeson	Gyratory Compactive Effort	
PI #1 Location	Deerwood township, Kirtson co MN	N-initial	7
PI #2 Location		N-design	75
PI #3 Location		N-maximum	115

Mix Properties at Recommended Asphalt Content

	Mix Design	Specification
Optimum AC (%)	5.4	
Density (pcf)	148.1	
Air Voids (%)	4.0	2.0-6.0
VMA (%)	14.1	14.0 min
VFA (%)	77.7	65-75
%Gmm @ Nominal	87.0	85%max
%Gmm @ Maximum	97.5	88%max
AC Film Thickness (mil)	9.5	7.5-13.0
Dist. Effective AC Ratio	0.9	0-1.3
Fine Agg Angularity (%)	45.5	45min
Sand Equivalent (%)	77.3	40min
Coarse Agg Angularity (%)	88.0	85min
Flakiness Index (%)	3.0	10max

Summary of Aggregate Characteristics from Mix Design

Gradation (% passing)	Blend	Virgin
58"	100.0	100.0
1/2"	99.6	100.0
3/8"	91.5	91.7
#4	66.2	64.7
#8	41.3	37.8
#16	28.1	25.1
#30	18.5	15.8
#60	12.0	12.5
#100	5.0	4.5
#200	4.1	2.5

Maximum SpG @ Niles

Virgin Add AC (%)
Virgin Agg. FAA (%)

Final Aggregate Blend (%)

9	N Fines	Deerwood
16	bank	Deerwood
44	washed stock	Deerwood
3	bank	Deerwood
20	RAP	

Asphalt Absorption (%)
Water Absorption (%)
Light Wt. Particles (%)
Toughness (% Loss)

Specific Gravity Information

Combined Bulk (Gsb)
No. 4 Combined Bulk (Gso)
No. 4 Virgin Bulk (Gso)
Apparent (Gsa)
Effective (Gme)

Remarks:

Also project SIM-G-028(110)(183) PCN-18961

Mix Design Technician & ID: Danny Schmiel 1306

Distribution:
Materials and Research
Grand Forks

Figure 77. PG64-28 HMA Mix Design Summary